博士論文

Development of phase change material-inserted adsorbent for the recovery of the heat of adsorption
（相変化物質内包吸着材の開発による吸着熱の制御）

崔　智慧
（Jihye Choi）

Supervisor Professor
Masaru Ogura

Department of Chemical System Engineering,
The University of Tokyo
March, 2020

Table of Contents

Chapter 1. General introduction

1.1 Adsorption

Adsorption is a phenomenon that the concentration of molecules is increased at the surface boundary of solid material in liquid or gas phase. When the attractive force between the molecule and the surface is Van der Waals force, this phenomenon is considered as a physical adsorption. When the attractive force derives from a chemical bond, involving hydrogen bond, this phenomenon is considered as a chemical adsorption. In most cases, the chemical adsorption has more strong attraction between molecules and the surface, compared with the physical adsorption. The solid material for adsorbing molecules is called adsorbent, and the adsorbed molecule is called adsorbate. The state of the adsorbed molecules is more stable than the diffusing molecules. Therefore, the molecule released the heat when adsorbed. And this heat is called the heat of adsorption. On the contrary, the detachment of the adsorbate from the surface of the adsorbent is called desorption.

In order to use adsorption in industry, a material having large surface area is preferable for the adsorbent. Therefore, porous materials are used as adsorbent. Adsorption is used in many industrial fields, such as separation process, catalytic reaction, and gas storage.

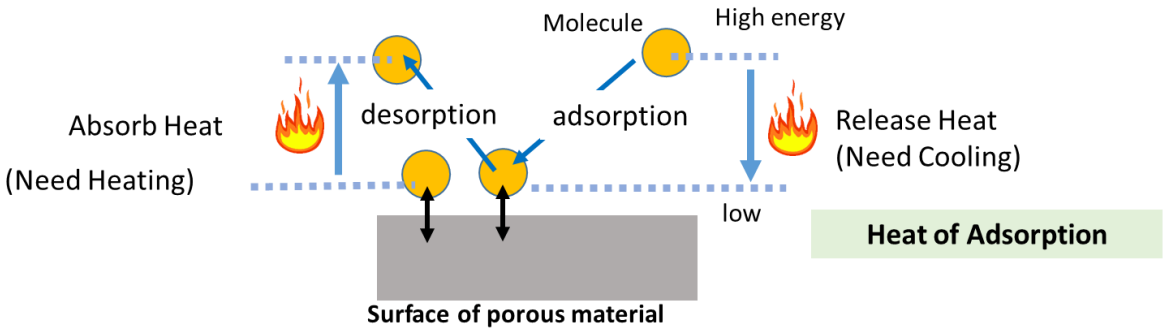

Figure 1. Schematic image of adsorption and desorption.

1.1.1 Adsorption process

Generally, a chemical engineering process using adsorption is called adsorption process. Separation of mixtures, purification of wasted water, and dehumidifying of wet air, are typical examples of the adsorption process. There are several types of reactor for the adsorption process.

Batch adsorption process is mainly used to remove or gain the particular components from the liquid solution (Figure 2). In this process, the adsorbent is placed in the reactor with stirring, so that the boundary of the solution and the adsorbent reaches to an equilibrium state of adsorption. After equilibrium, the adsorbent and the solution is recovered via filtration.

Fixed-bed adsorption is one of most widely used process in the industry. The fixed-bed process is an operation for supplying fluid, which containing adsorptive molecules, to the packed adsorbent column (Figure 3). The recovery of diluted solution, air dehumidification, and advanced waste water treatment are the typical examples of the fixed-bed adsorption process.

Fluidized-bed adsorption process was mostly used during the 1950 ~ 1960. In the process of the fluidized bed adsorption, the adsorbent is placed on the top of the metal sieve trays and the gas flow passing up through the sieves of the tray (Figure 4). The solid adsorbents also fluidize with gas flow at the same time.

Pressure swing adsorption (PSA) is an adsorption process with changing the partial pressure of a component in the bed. At the high pressure, adsorption occurs, and at the low pressure, desorption occurs (Figure 5). The most strong point of PSA process is that the operation of PSA is extremely short. Typically, one cycle of adsorption process, from the adsorption to desorption, is finished in 10 ~ 20 minutes depend on the bed volume. PSA is largely used for the separation of mixed gas, especially separation of nitrogen and oxygen in the air. Also, PSA is used for the recovery of hydrogen gas or dehumidification.

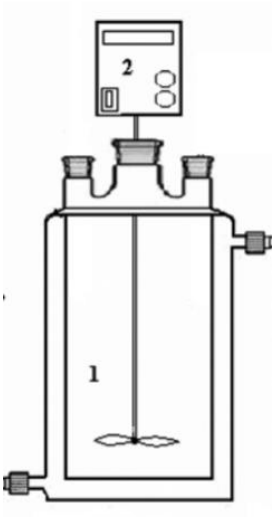

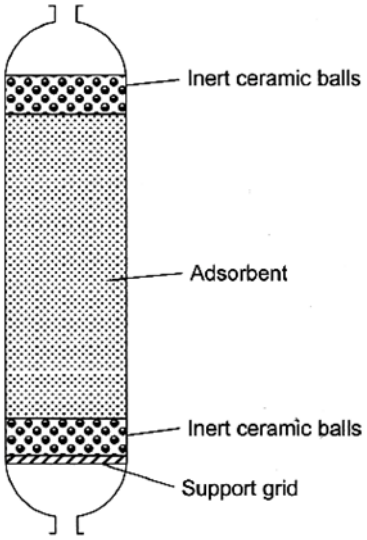

(Left) Figure 2. Schematic illustration of batch reactor [1].

(Right) Figure 3. Schematic illustration of fixed-bed reactor [91].

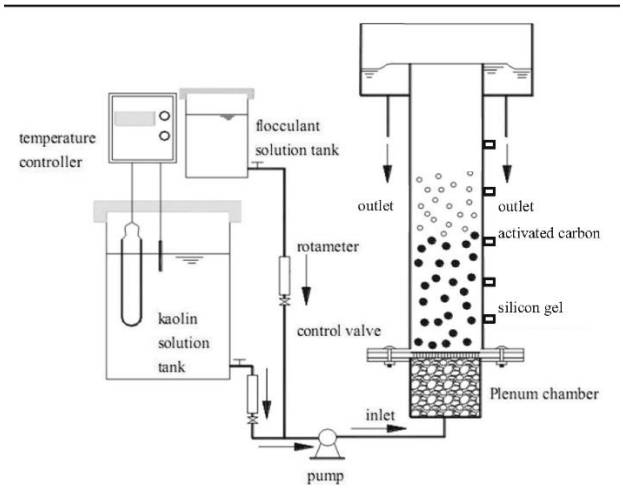

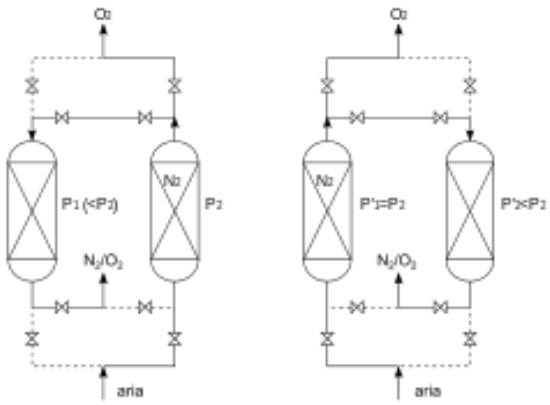

(Left) Figure 4. Schematic illustration of fluidized-bed reactor [2].

(Right) Figure 5. Schematic illustration of PSA reactor [92].

1.1.2 Removal of the heat of adsorption

1.1.2.1 Importance of removal of heat of adsorption

Adsorption and desorption is an exothermic and endothermic phenomenon respectively. Hence, the temperature of the adsorption system is remarkably increased or decreased during the adsorption or desorption[3]. Subsequently, owing to the temperature change, the equilibrium of adsorption is also changed, and the apparent rate of adsorption decreases. As a result, the performance of adsorption process is severely degraded due to the generation of the heat of adsorption. Therefore, to avoid the degradation of performance in adsorption process, the removal of released heat of adsorption is essential.

Hydrogen storage using adsorption is a good example to explain the importance of the removal of the heat of adsorption. Hydrogen is a fuel for the fuel-cell vehicles. Mostly, the hydrogen is concentrated in the loaded storage tank inside the vehicle with extremely high pressure, which is almost 35 to 70 MPa[96]. To endure the high pressure, the hydrogen storage tank is composed by strong materials, such as aluminum liner, carbon fiber, and glass fiber[96]. Recently, the vehicle company, Honda, reported a consideration for realizing smaller and lighter hydrogen storage tank by using adsorption[96]. According to this report, a large amount of heat is released during the charging step of hydrogen owing to the generated heat of adsorption (10 - 30 kJ/mol-H_2) within the short time. This released heat increase the temperature of tank and decreasing the hydrogen storage performance. To rapidly remove this released heat of adsorption in a few minutes, extremely a large amount of heat exchanger is required. This is because hydrogen charging at the hydrogen station is required to be completed in at least 5 minutes. As a result, owing to this largely increased amount of heat exchanger, the hydrogen storage tank cannot be smaller or lighter even after using adsorption technique. Therefore, to realize the hydrogen storage tank using adsorption, superior heat removal performance is absolutely essential.

There is another short-time adsorption process, which is pressure swing

adsorption (PSA) as mentioned in 1.3.2. In the PSA process, similar to the other short time adsorption process including hydrogen storage, superior performance of a heat removal system is required for removing the released heat of adsorption in a short time. Without superior performance of heat removal system, the performance of PSA will be significantly decreased. Therefore, many previous researches have been reported to improve the heat removal performance in a PSA process[4,5].

Also, adsorption heat pump (AHP) is another example for requiring high performance of heat removal[6–8]. AHP is a cooling machine by using the evaporation enthalpy of adsorbate. AHP produces the cooling energy from solar energy or wasted hot water from the industries. Therefore, AHP is an environmental friendly method. Also, AHP has an advantage that it produces the cooling energy directly from the primary energy, not from electricity. Adsorption heat pump is composed of 4 parts, i.e. condenser, evaporator, adsorption bed, and desorption bed. Mostly, in the adsorption/desorption bed, water vapor is used as an adsorbate. Hence, water vapor goes around the adsorption heat pump cycle, which is composed of 4 parts. At the evaporator, the enthalpy of evaporated water works as the cooling energy. Larger amount of water produces larger cooling energy. Therefore, the amount of circulating water in the cycle determines the performance of adsorption heat pump. In the AHP cycle, the amount of circulating water is equal to the effective amount of adsorbed water, i.e. the difference between the adsorbed amount of water vapor at the adsorption bed and at the desorption bed. The cycle time of the AHP is quite short such as several minutes. Therefore, a larger effective amount of adsorbed water is required to upgrading the performance of AHP. A larger effective amount of adsorbed water can be realized by upgrading the adsorption and desorption performances. The adsorption and desorption performance can be upgraded by achieving higher performance of heat removal at the adsorption bed. Therefore, the heat removal rate at the adsorption tower is an important key to improve the performance of AHP[93]. Consequently, it can be considered that the removal of the heat of adsorption is one of the important aspects for further development in the

adsorption process.

The removal of heat of adsorption can be largely classified into 2 groups as shown in Figure 6. One is a heat exchanger using sensible heat, and the other is a phase change material (PCM)-using methods via latent heat storage. To the best of my knowledge, all of the adsorption processes used in the industries are using the heat exchanger for the removal of the heat of adsorption. On the other hand, owing to the several advantages of latent heat storage, PCM-using method has been studied for a new heat recovery method in the adsorption process. Specific explanations about those two heat removal methods are described in following chapters.

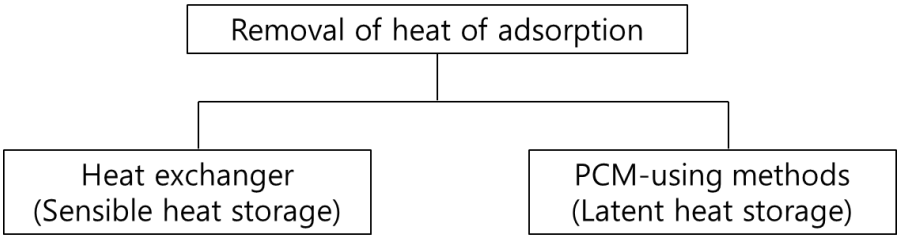

Figure 6. Classification of the removal method of the heat of adsorption

1.1.2.2 Heat exchanger for removing the heat of adsorption

In typical, the heat of adsorption is removed by using heat exchangers in industrial fields. A heat exchanger is a simple heat removal system, which is transferring the released heat to coolant fluid, such as cold water[9]. Therefore, a heat exchanger is a sensible heat removal system. The heat exchanger has some strong advantages such that simple principle, and easy to operate.

One of the key parameter for improving the heat removal performance of a heat exchanger is a thermal conductivity. During several decades, researches for realizing the high thermal conductivity of a heat exchanger were reported to improve the heat removal performance. For example, providing internal fins on the metal voids of a heat exchanger[10] or inserting metallic net in a adsorbent bed for increasing both the heat-exchange surface area and thermal conductivity was reported[6] as shown in Figure 7. Also, coating the adsorbent around the heat exchanger pipe, fin or metal foam is reported for the methods for improving the thermal conductivity as shown in Figure 8[6]. Moreover, providing expandable graphite[11] at the heat exchanger was also reported as another method for improving the thermal conductivity.

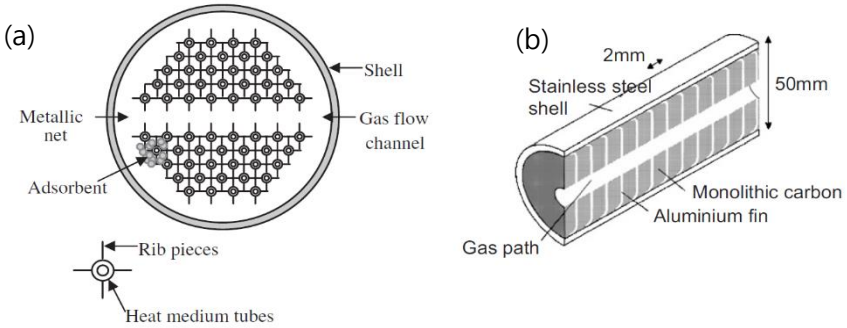

Figure 7. (a) Metallic net and (b) internal fins at a heat exchanger[6].

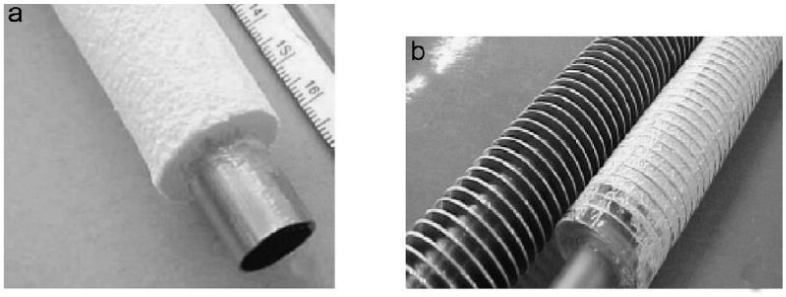

Figure 8. adsorbent coating around (a) pipe and (b) fin of a heat exchanger[6].

1.1.2.3 PCM-using methods for removing the heat of adsorption

Recently, as a new method, applying phase change materials (PCMs) in the heat removal system of adsorption process has been studied. Unlike a heat exchanger, the PCM-using method is based on latent heat storage. Latent heat storage is a method using the enthalpy change during the phase change of a material, such as melting[12]. Materials that possess especially large latent heat during phase change are adequate to be used in the latent heat storage system. These kinds of phase change materials used in the latent heat storage is abbreviated as PCMs[13]. Latent heat storage has an advantage of higher heat storage density than other heat storage systems such as a heat exchanger. In the adsorption process, applied PCMs absorb and store the released heat during adsorption, and this stored heat is expected to be re-used during desorption. Therefore, more efficient removal of heat of adsorption can be expected when using PCMs in the adsorption process compared to a heat exchanger.

For example, PCM-embedded metallic tube in a natural gas charging/discharging process was reported by Li and Li at 2015 as shown in Figure 9[14]. Height of copper tube was 350 mm and the outside diameter of copper tube was 6 mm. By inserting 6.10 % volume ratio of PCM-embedded metallic void into the adsorbent bed for natural gas charging, 21.8 ℃ of temperature was suppressed.

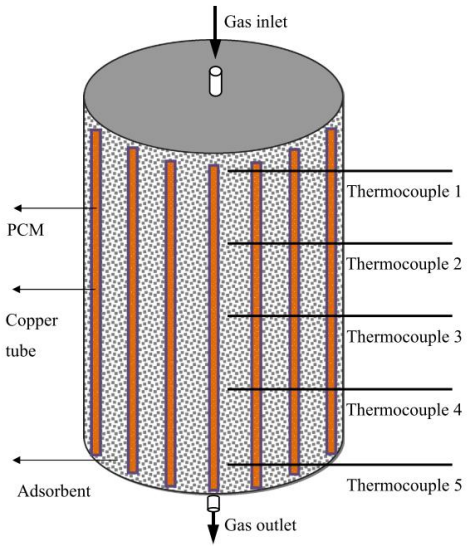

Figure 9. PCM-embedded copper tube applied on a natural gas charging process[14].

Also, to increase a thermal conductivity, PCM capsule in a dehumidifying desiccant bed was reported by Rady *et al.*[15]. In this report, the same sizes of PCM capsule and adsorbent pellet are applied in a dehumidifying desiccant bed, which are 1 mm, respectively. The released heat of adsorption is expected to be more rapidly transferred to the encapsulated PCM by shorter heat transfer distance compared to the bulk-scale metallic tube. A schematic image of a method of packing encapsulated PCM simultaneously with an adsorbent into the adsorption column is shown in Figure 10.

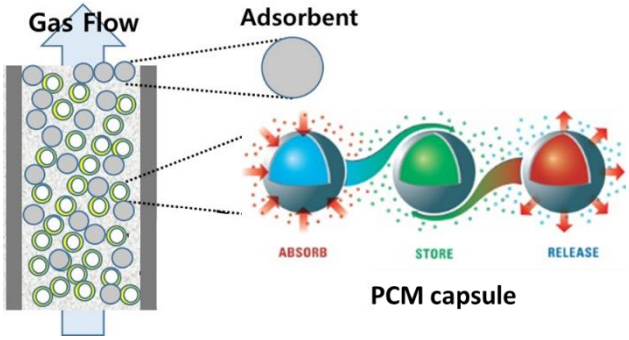

Figure 10. A schematic image of PCM capsule and adsorbent packed in an adsorption column[99].

Figure 10 serves a method of absorbing the heat of adsorption using the latent heat of PCM during melting/freezing. First, the released heat of adsorption from the adsorbent transfers to the flowing gas. Then, the heat is transferred, once again, from the gas to PCM capsule, and absorbed by the PCM capsule. By introducing the PCM capsules in the dehumidifying adsorbent bed, the drastic increase of a bed temperature at the initial stage was suppressed in the results of Rady *et al.* [15]. Also, during the initial stage, approximately during the initial 800 seconds, the dehumidification efficiency was slightly increased, with appropriate volume fraction of PCM capsules in the bed.

However, when these described PCM-using methods are applied to a rapid adsorption process such as PSA (Pressure Swing Adsorption), there could be a problem that the packed PCM capsule cannot be fully utilized due to the slow heat transfer rate between the adsorbent and the PCM capsule. This might be because the heat transfer between the adsorbent and the PCM capsule in the adsorption

column occurs in 2 steps, i.e. from the adsorbent to the gas, and from the gas to the PCM capsule. Also, small heat capacity of gas might be critical to the heat transfer.

Therefore, Horstmeier *et al.* reported a new type of PCM-integrated adsorbent for improving the performance of vacuum swing adsorption process for carbon dioxide removal[4]. They suggests an adsorbent pellet with three layers (adsorbent, metal, and PCM) was applied on a vacuum swing adsorption (VSA) process. This study evaluated one step heat transfer by modeling a pellet in the shape of a sphere with three layers as shown in Figure 11. By using this adsorbent, the heat exchange between the PCM and the adsorbent directly occurs, and does not go through the fluid. Hence, more rapid heat transfer can be expected. However, the model of the pellet was a theoretical proposal and could not be experimentally prepared.

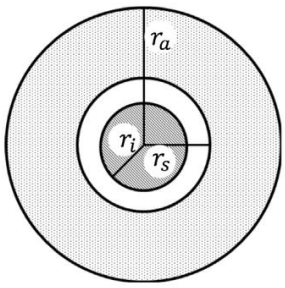

Figure 11. PCM integrated adsorbent
(r_i: PCM, $r_s - r_i$:metal, $r_a - r_s - r_i$:adsorbent) [4].

From these previous researches, it can be considered that a new PCM-using method that can rapidly remove the heat of adsorption is necessary to increase both a heat storage efficiency and the adsorption performance in the short-time adsorption process.

1.2 Latent heat storage

1.2.1 Latent heat storage using PCM

Generally, heat removal systems in the adsorption process can be classified into three groups: sensible heat storage, heat storage using chemical reaction, and latent heat storage[16]. Latent heat storage is a heat storage method using the enthalpy change during the phase change, such as melting or evaporation (Figure 12)[12]. Latent heat storage has an advantage of higher heat storage density than other heat storage systems. For the phase change, the one between liquid and gas is barely used for the latent heat storage. This is because the phase change between the liquid and the gas is very difficult to handle, due to the huge volume change during phase change. Mostly, phase change between the solid and the liquid is used for the latent heat storage, because the latter phase change is easy to handle.

Materials that possess especially large latent heat during phase change are used as the latent heat storage materials. This kind of phase change materials used in latent heat storage is abbreviated as PCMs[13]. There are various types of PCMs based on inorganic, organic, and so on. Hydrate is a representative inorganic PCM. Hydrate has an advantage that possesses high enthalpy of fusion, which is latent heat. However, the melting point of hydrate is usually high, and the degree of supercooling is also high. These are difficulties for utilizing hydrates as a latent heat storage materials in the industries. On the contrary, paraffin is a representative organic PCM. Paraffin has some advantages such that the melting point is close to room temperature and the degree of supercooling is low.

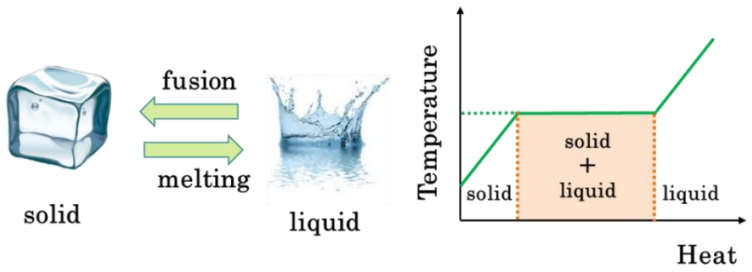

Figure 12. Solid-liquid phase change of water.

As for the several decades, PCM was used for a heat storage material in the various fields. For example, beverage bottle or food containers are using PCMs in the containers to maintain the beverage or food at the cold temperature[17]. Bottle is composed by a double-wall including a PCM (Figure 13 (a)). The food container is commercialized by SOFRIGAM with PCM melting points of 0 °C, -15 °C, and -20 °C (Figure 13 (b)) [94]. These concepts could be used for not only food but also many other products, for example, a blood transportation in a medical application[17]. Also, PCM is used for heating applications, such as hand warmers.

Figure 13. (a) isothermal water bottle (b) PCM-containing food container (c) hand warmer using PCM [17,94,95].

Also, PCMs are used in building units to upgrade a thermal performance of buildings. PCMs can be loaded in various building units such as wall board, shutter, and plate as shown in Figure 14[12].

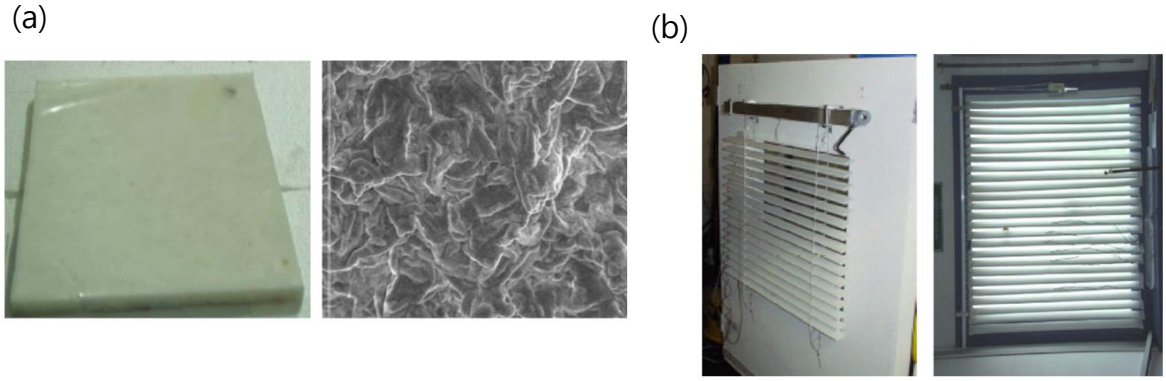

Figure 14. (a) PCM-containing plate, (b) PCM-containing shutter[12].

1.2.2 Analysis of phase change - Differential scanning calorimetry

Differential scanning calorimetry (DSC) is a thermo-analytical device. This device measures the amount of heat required to raise or lower the temperature of the sample. DSC is mostly used for observing phase changes. DSC measures the phase changing temperature and the thermal energy changing during the phase change, such as glass transition, fusion, and melting. The diagram of the device is as shown in Figure 15. Through measuring the difference of applied amount of heat between the reference sample (α-Al_2O_3) and the sample, a function of heat flow with respect to the temperature change can be detected, as shown in Figure 16. In figure 16, the contact point between the baseline and the tangent line of the peak is defined as the phase change temperature. The peak area indicates the change of enthalpy during phase change, which corresponds to the latent heat.

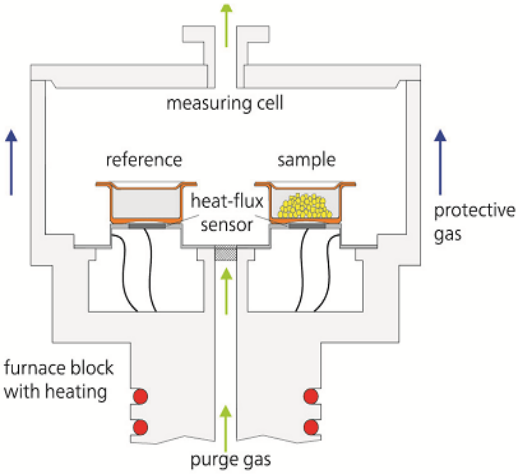

Figure 15. Differential scanning calorimetry [90].

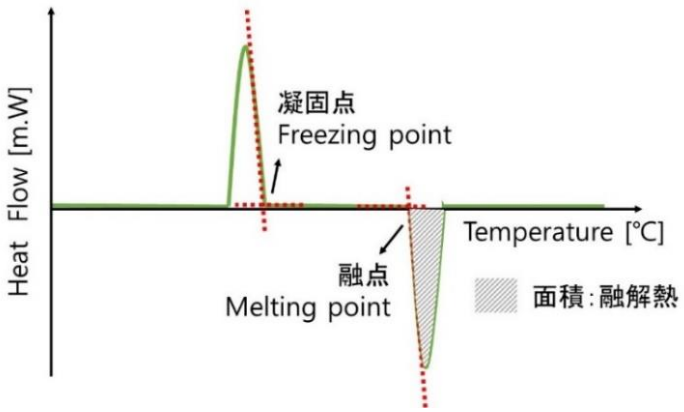

Figure 16. DSC raw data.

1.2.3 New heat storage material - Mesoporous materials

In order to utilize the solid-liquid phase change, a container for capturing the liquid PCM is required. In the previous chapter 1.1.2, the examples of utilized PCM with bulky containers for capturing PCMs are described. Among various containers for PCM, including metal void or capsules, periodic mesoporous space of porous material has been reported as a new container for confining PCM[14,18]. International union of pure and applied chemistry (IUPAC) classified pores into three groups depending on their pore size. Small pores with a pore diameter of 2 nm or less are called micropores. Pores with a size between 2 nm and 50 nm are called mesopores. Large pores with a diameter more than 50 nm are called macropores. Mesoporous material is a porous material with the size between 2 – 50 nm. There are several advantages for using mesoporous material as a PCM-container. One is that, mesoporous materials possess high thermal and structure stabilities to endure the volume change during the phase change. Also, PCM is confined in mesopores by strong surface tension, hence, a leakage problem of liquified PCM can be solved. Moreover, a thermal conductivity of the PCM-containing mesoporous materials can be improved compared to bulky containers, owing to the shorter heat transfer distance. Compared to other microporous materials with the size of pores smaller than 2 nm, mesoporous materials are more adequate material for the heat storage material. This is because, phase change cannot occur in the ultra-small micropore, since only a few molecular layers can be confined in the micropore. On the contrary, the mesoporous spaces are large enough to phase change occurs. However, the phase change behavior of the confined PCM in the meso-scale spaces is different from that of the bulk state. Compared to the bulk state, meso-scale spaces are extremely small and narrow spaces. Therefore, the phase change behavior of PCM confined in mesoporous space must be studied before utilizing PCM-confined mesoporous materials as heat storage materials.

The behavior of phase change in meso-scale spaces, such as a capillary, has been studied in academic field for a long time. The most well-known explanation about

phase change in the capillary is the Gibbs-Thomson equation (Equation 1) [19,20]. In a narrow space with the small pore radius, *r*, the melting point of confined PCM becomes lower than the bulk melting point. This difference in the melting point between the bulk state and the confined state, ΔT, can be explained by the Gibbs-Thomson equation.

$$\Delta T = \frac{2T_m V_m \gamma_{sl}}{r\Delta H_f} \quad \text{(Eq. 1)}$$

(γ_{sl}:surface tension at the interface, ΔH_f: enthalpy of fusion,
V_m: molar volume, T_m: melting point of bulk state)

In 1990, C.L. Jackson reported a phase change behavior of organic molecules in mesopores[20]. As well as this research, researches regarding the change of melting point of organic materials in porous space have been reported until now[16,21,22]. According to these previous researches, it is generally accepted that the changes of melting point of confined PCM in a confined space is fitted well to the modified Gibbs-Thomson equation (equation 2).

$$\Delta T = \frac{A}{d-2t} \quad \text{(Eq. 2)}$$

(A: Constant、d: pore diameter, t: non-freezing layer thickness)

On the other hand, there are only a few reports paying attention to the relationship between ΔH_f and pore diameter *d*. The enthalpy of fusion, ΔH_f, is an important value in latent heat storage, because ΔH_f determines the heat storage capacity. It has been experimentally reported that ΔH_f decreases with the decrease of the pore diameter. However, there are only a few previous researches that can clearly explain the decrease of ΔH_f in mesopores. Therefore, a research for understanding the changes of ΔH_f in the mesopores is required now to utilize PCM-confined mesoporous materials with a high heat storage efficiency.

1.3 Porous materials

Porous materials are materials that possessing lots of pores inside. Porous materials are possessing unique structures and high surface areas, as for the porous characteristics. For this reason, porous materials are used as an adsorbent, catalysis, membrane, or liquid/gas storage materials in various process. There are various types of porous materials with different composing materials, structure characteristics, and the size of pores in the world.

1.3.1 Zeolite

Zeolite is a crystalline microporous material with a framework built of silicate (SiO_4-) and aluminate (AlO_4-). Natural zeolite exists as a mineral in earth. On the other hand, more than 200 framework types of zeolite has been reported that was synthesized by human, as shown in Figure 17.

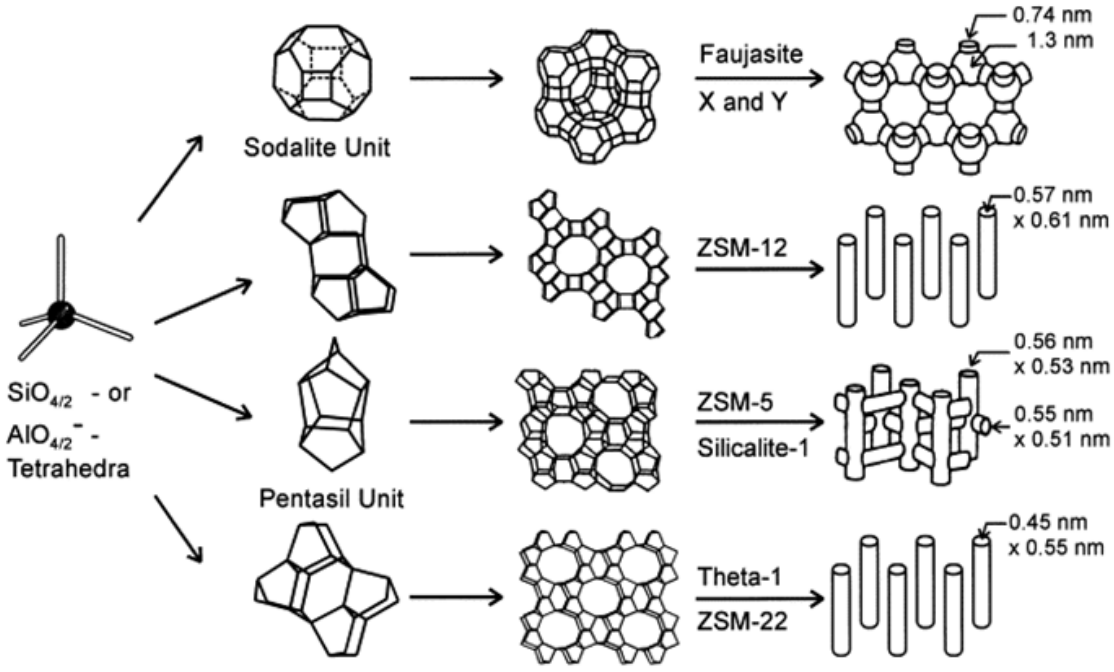

Figure 17. Various types of zeolite building units, frameworks and pore structures.[23]

Most representative synthesized zeolite is MFI, which is named ZSM-5. In 1972, ZSM-5 is first reported and patented by Mobil oil cooperation[24]. ZSM-5 was famous

for the heterogeneous catalysis used in the reactions of hydrocarbon isomerization, in the petroleum industries. The original microporous framework of zeolite is widely used as a catalyst and a gas adsorbent owing to their shape selectivity, high specific surface area, high thermal stability, high chemical stability and controllable hydrophilic/hydrophobic properties[25,26]. Despite of these strong advantages of zeolite, there are also limitations in zeolite, in which molecule diffuse slowly inside the micropores of zeolite. Owing to the extremely small size of pores of zeolite, pore blocking and active site deactivation occur and these resulted also in the diffusion limitations[27]. To avoid the diffusion limitations in zeolite, two approaches have been made. One is that, synthesis of zeolite with a small crystal size to shorten the diffusion route. The other is introduction of larger pores in crystal[28–30]. The zeolite, which contains larger pores in crystal, is called as mesoporous zeolite (Figure 18).

1.3.2 Mesoporous zeolite

Mesoporous zeolite possesses both micropores and mesopores in crystal. There are several methods to introduce the mesopores in the crystals of zeolite. Those methods are developed during recent several decades owing to the advantage of introducing mesopores in the crsytals of zeolite, as described above.

As for the mesopore introducing methods, first, there are destructive methods, such as acid leaching, alkaline leaching, and fluoride etching. Zeolite is composed of alumina and silica. Acid leaching extract Al from the zeolite framework and the extracted vacant space becomes a mesopore. On the other hand, alkaline leaching extract Si from zeolite framework to form mesopores (Figure 19). Therefore, alkaline leaching is also called as desilication. Alkaline leaching extracts only Si and acid leaching extracts only Al. Hence, alkaline leaching is effective to be applied to a zeolite with high Si/Al ratio and acid leaching is effective when it is applied to Al rich zeolite. However, leaching Si is more efficient compared to leaching Al in most zeolites, since Si is more abundant than Al. Therefore, acid leaching is a rarely used method, and alkali leaching is a popular method for

introducing mesopores in zeolite. Alkaline treatment can be applied to different types of zeolite with the various range of Si/Al ratio. Also, HF is commonly used for etching or dissolving Si-containing materials, such as silicon substrate in semiconductor field. Fluoride ion, F^-, etches selectively Al in zeolite framework. However, HF_2^- ion indiscriminately dissolves both Si and Al. Therefore, HF_2^- treatment is a powerful method to form mesopores in zeolite framework. HF_2^- treatment can be applied to any type of zeolite, including various Si/Al ratios[28].

The second method for introducing large mesopores in the zeolite crystal is using templates. Two templates are used for the formation of microporosity and mesoporosity. This method has advantages such that 1) mesopore diameter is controllable, and 2) mesopore can be formed in an ordered structure. Organosilanes, cationic polymers, dual function polymers, and dual function surfactants are examples of templates.

Finally, there is a method that generating large pores by agglomerating small size crystals of zeolite. Simple agglomeration of nano-sized zeolite with a narrow particle size distribution results in mesopore formation, as shown in Figure 20.

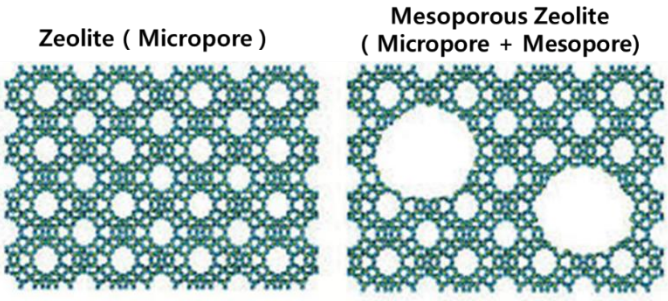

Figure 18. Framework of zeolite (left) and mesoporous zeolite (right).

Figure 19. Schematic images of alkali leaching.

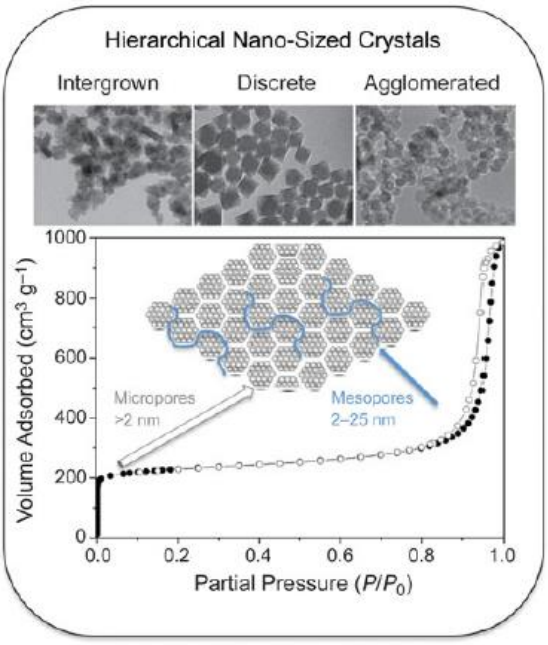

Figure 20. SEM image and nitrogen adsorption-desorption isotherms of agglomerated nano-sized zeolite crystals[27].

1.3.2 Mesoporous silica and carbon

Mesoporous silica is a material having a mesopore within a silica structure. The first report on mesoporous silica was made in 1990[31]. Kanemite, which is a layered silicate and an alkyltrimethylammonium ion was reacted and calcined to synthesize a porous silica material with a three-dimensional skeleton. From 1990 and until now, researches for developing synthesis methods of various structure type of mesoporous silica, have been conducted. Recently, there are many types of reported mesoporous silica with various three-dimensional structures and different pore sizes, such as, MCM-41, SBA-15 and MCF. Mesoporous silica SBA-15 is one of the representative examples of mesoporous silica (Figure 21)[32].

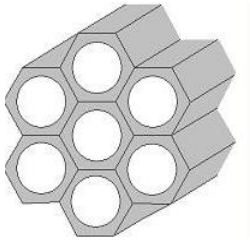

Figure 21. Structure of mesoporous silica SBA-15.

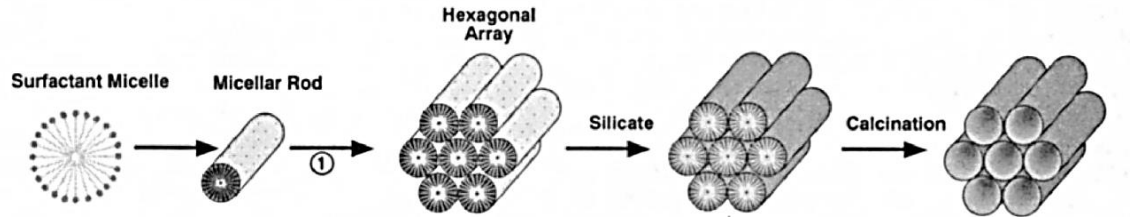

Figure 22. Schematic image of a formation mechanism of mesoporous silica[33].

The synthesis procedure of mesoporous silica is shown in Figure 22. First, surfactant, such as a triblock copolymer pluronic P123, forms a micelle in the aqueous solution. Then the crystalline structure is made through self-assembly of silicate near the micelle. From this as-synthesized hexagonal crystalline silica structure, the micelle is removed by the calcination at a high temperature, and forming mesopores. In case of SBA-15, the wall thickness of mesoporous silica is approximately around 3 nm. Also, the micelle shape of surfactant P123 is not a perfect sphere since P123 is a triblock co-polymer. Therefore, the shape of the mesopore is not a perfect cylindrical shape. There are small micropores inside of the silica wall, which connect the mesopore and the mesopore, and this micropore is called as a channel micropore (Figure 23 (a))[34].

The synthesis of mesoporous silica can be roughly divided into three steps: micelle formation, aging, and calcination. Therefore, the researches to control the pore size of mesoporous silica can be divided into three groups, focused on each step, individually. Kruk et al. reported SBA-15 with ultra-large mesopores by dissolving organic molecule, which is called as swelling agent, in micelles to expand the micelles, as shown in Figure 23 (b)[35]. As for the swelling agent, organic substances such as decane and tri-isopropylbenzene are mainly selected. This is a study that focused on the step of the micelle formation. Also, the size of micelles can be adjusted by simply changing the aging temperature, as shown in Figure 23 (a)[36]. This study focused on the step of aging. Finally, the silica structure itself can be shrunk by increasing the calcination temperature, resulting in decreasing the mesopore diameter[37]. This study focused on the step of calcination. From the methods above, the pore diameter of mesoporous silica is able to be controlled.

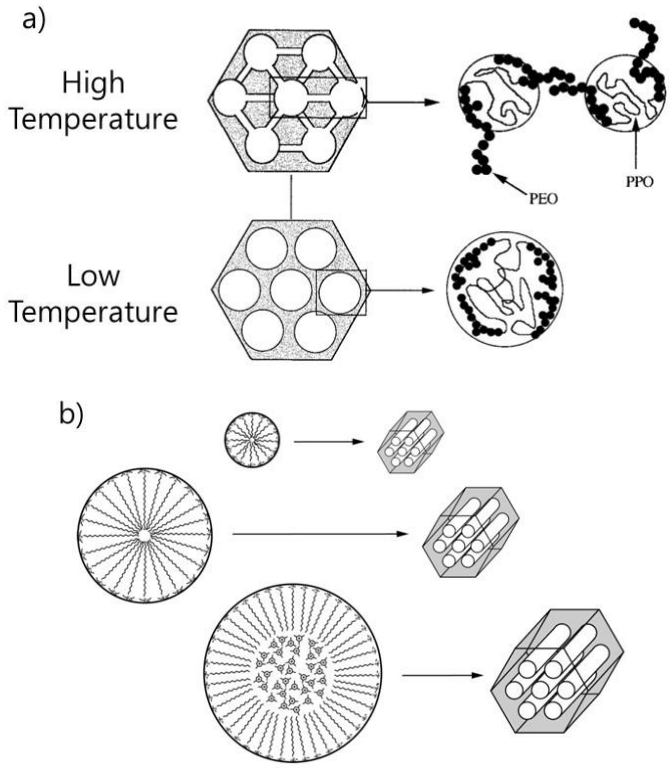

Figure 23. The control of pore diameter in SBA-15, a) using different synthesis temperature [34] and b) using swelling agent to expand the micelle[35].

Mesoporous carbon is a material made of carbon, and possessing mesopores in the framework. Synthesis of mesoporous carbon can be roughly divided into two methods: nano-casting strategy and direct synthesis method as shown in Figure 24. The nano-casting strategy is a method of synthesizing mesoporous carbon using a template of an ordered framework that is already synthesized, such as zeolite or mesoporous silica. Mesoporous carbon CMK-3 is one of the representative mesoporous carbon synthesized by the nano-casting strategy method by using mesoporous silica SBA-15 as the template. The direct synthesis is a method that mesoporous carbon is directly synthesized by using a surfactant and a carbon precursor. Representative examples of mesoporous carbon are synthesized by the direct synthesis method such as COU-1, FDU-15, and C-ORNL-1. Specific comparison of these two synthesis methods is shown in Table 1.

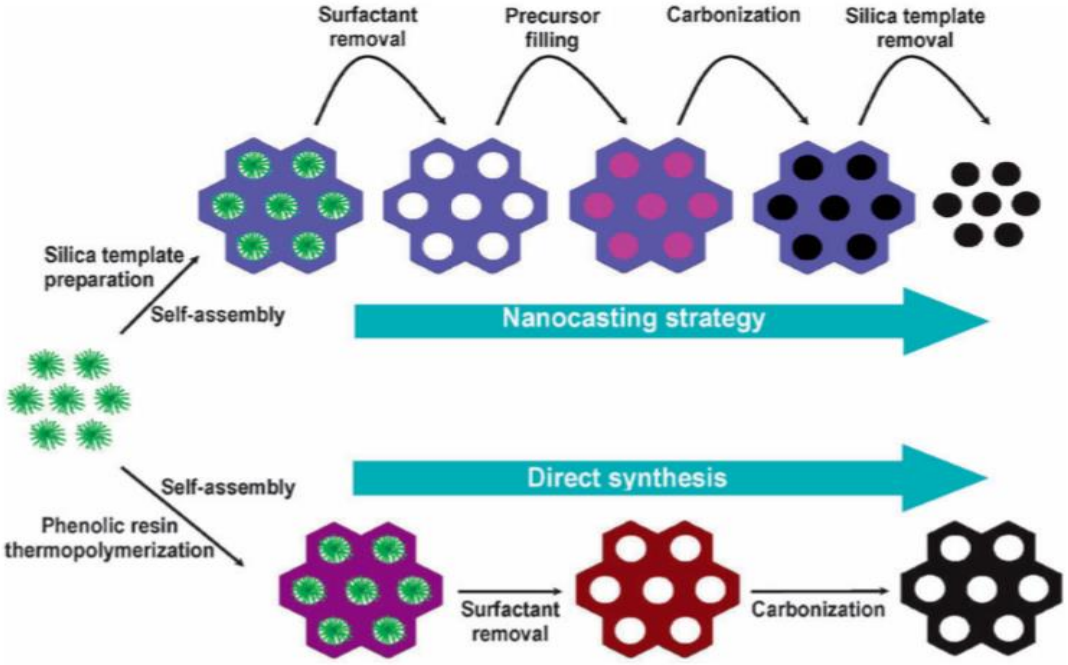

Figure 24. Two representative methods of synthesis mesoporous carbon[38].

Table 1. Comparison of synthesis methods for mesoporous carbon[38].

	Direct Synthesis	Nano-casting
Synthesis steps	Few	Many
Template	Surfactant block copolymers	Mesoporous silica Zeolite
Removing template	Calcination	Etching through HF
Mesophase control	pH, surfactant, temperature…	Silica-template
Pore size distribution	Narrow	Broad
Stability	High	Low
Others	Low cost Large-scale synthesis	High cost, Long synthesis time

Carbon materials are well-known as nonpolar and hydrophobic materials. However, the surface of the carbon material can be oxidized by using an oxidizing agent, such as oxygen, ozone or water, during the production process or in the air atmosphere. Therefore, oxygen-containing functional groups exist on the carbon surface, such as phenol, carboxylic acid and lactone[39].

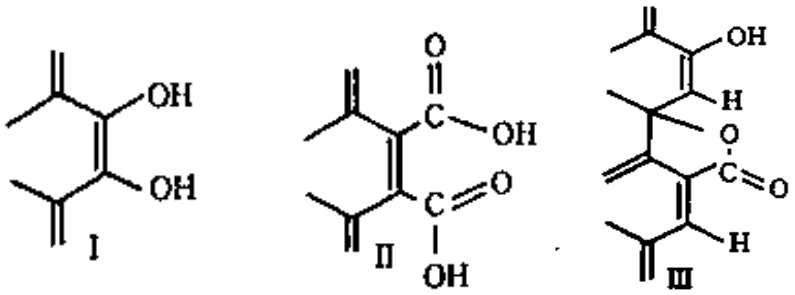

Figure 25. Surface functional group that exists on carbon surface.
(Ⅰ:phenol, Ⅱ:carboxylic acid, Ⅲ:lactone)

In addition to the analysis of the surface by using FT-IR or XPS, there is a titration proposed by Boehm as a method for examining the quantity of oxygen-containing functional groups on the carbon surface[40]. The procedure of titration is as follows. First, placing a carbon material in a solution of sodium hydroxide, sodium hydrogen carbonate, and sodium carbonate, respectively, so that each alkali solution fully react with the acidic functional groups that exist on the carbon surface for about 3 days. Then titrating the pH of this reacted solution by using hydrochloric acid solution. Through the titration, the amount of the functional group can be quantified. At this time, sodium hydroxide reacts with all oxygen-containing functional groups: phenol, carboxylic acid and lactone. Sodium hydrogen carbonate reacts only with carboxyl groups. Sodium carbonate reacts with both carboxyl groups and lactone groups. Based on these differences, the amount of each species of surface functional group can be calculated through titration.

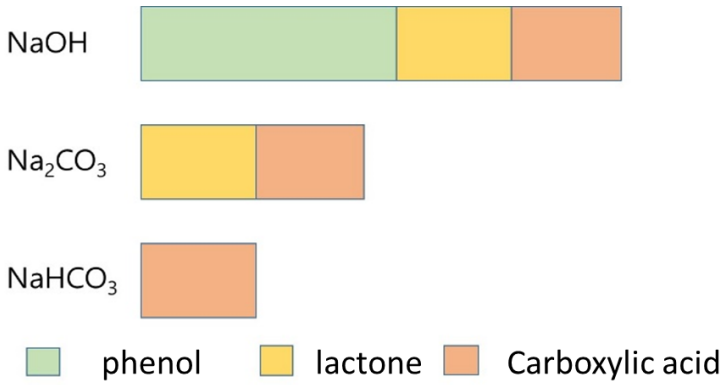

Figure 26. Types of functional groups that react to each alkali solution.

In most cases, there are only few amount of oxygen-containing functional groups that exist on carbon material. However, the amount of oxygen-containing functional groups on the carbon surface can be increased by oxidizing the carbon material, so that, even the water can be adsorbed on carbon. It has been reported that the amount of the functional group is increased when the carbon material is treated by nitric acid and sulfuric acid[41], or when the carbon material is treated by ozone[42].

1.3.3 Carbon nanotube

The first reports of carbon nanotubes (CNTs) were made in 1991 by Donald S. Bethune (IBM) and Suimo lijima (NEC). They discovered the single-wall carbon nanotubes, which are made of graphene sheets. Carbon nanotube is classified by the layer number of the graphene sheet. One layer carbon nanotube is called as single-wall carbon nanotubes (SWCNT) and carbon nanotube with more than one layer is called as multi-wall carbon nanotube (MWCNT)[43]. Moreover, rolling mode of carbon nanotube is classified into zig-zag, armchair, and chiral, according to the combined form of graphene.

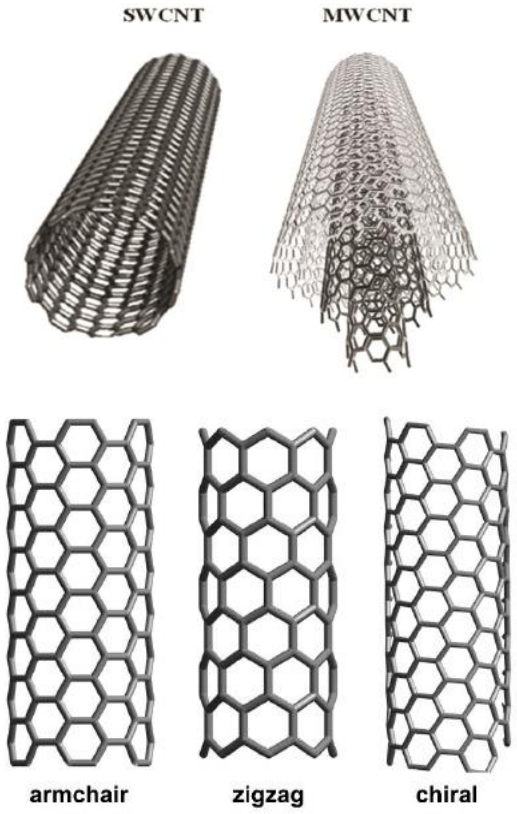

Figure 27. Classification of carbon nanotubes [88,89].

Carbon nanotubes have been widely studied, because they have various applications ranging from electrodes to transistors, films, solar cells, and hydrogen storage, due to the electrical conductivity of carbon. Also, for the hydrogen storage, modification of functional groups on the surface of carbon nanotubes is studied. In 1999, Li and K were doped on the surface of carbon and successfully stored hydrogen inside carbon nanotubes at room temperature[44]. In addition, there have been many studies about hydrogen storage using carbon nanotubes, such as development of Pd supported carbon nanotubes[45], or SWCNT with a superior hydrogen storage performance at room temperature[46]. Furthermore, not only for the hydrogen storage, but also for the various applications, many studies have been conducted for modifying the functional groups on the surface of carbon nanotubes, including carboxyl acid groups, and amino groups[41].

Another impressive characteristic of the carbon nanotubes is an excellent thermal conductivity of carbon. It is generally accepted that the thermal

conductivity of carbon materials is superior to any other carbonaceous matter. However, the superior thermal conductivity is capable only in the direction of the graphene sheet. The thermal conductivity from the carbon layer to layer, is much lower compared to that in the direction of single graphene sheet. Hence, in case of multi-layer carbon, such as MWCNT, transfer of heat in the vertical direction of the layer occurs more slowly compared to SWCNT. Since SWCNT has only single layer of graphene sheet, it has a superior thermal conductivity.

Among various techniques of synthesis carbon nanotube, chemical vapor deposition (CVD) is the most popular and widely used, due to low cost, high yield, and massive production[47] (Figure 28). The growth mechanism of CNT in CVD method is described in Figure 29.[48] The graphene sheet grows from the substrate through the catalytic reaction, which occurs at a metal site. As for the metal, transition metals are mostly used. After the growth of CNT stop, the side edge of the synthesized CNT is closed, owing to the existence of metal. To remove the metal and open the edge, further treatment is required such as acidic treatment.

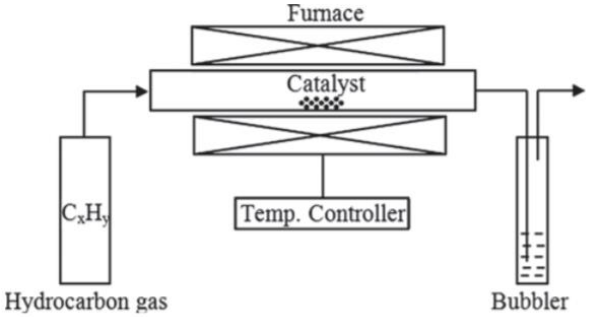

Figure 28. CVD setup diagram[48].

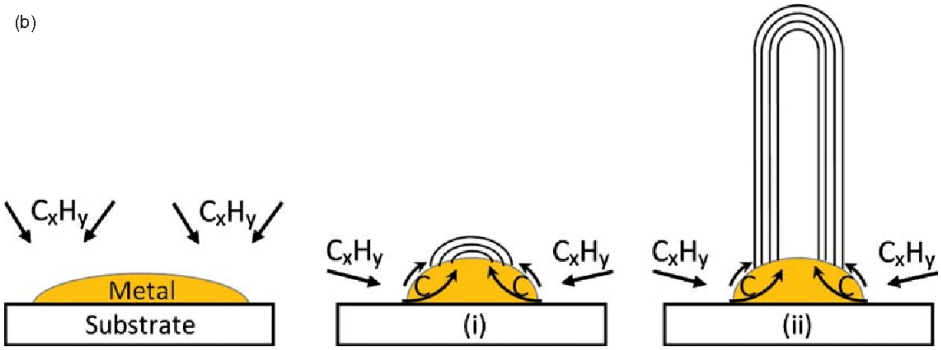

Figure 29.Growth of carbon nanotube in CVD method[48].

1.4 Research objective of this thesis

As mentioned in the previous chapter 1.1, removal of the heat of adsorption is crucial to avoid the degradation of adsorption performance. In order to remove the heat of adsorption and avoid the drastic increase of temperature in the adsorption process, there is a method where the latent heat of PCM is used as mentioned in chapter 1.2.3.3. However, in most of the previous researches that dealt with the removal of the released heat of adsorption using PCM, the heat transfer occurs in 2 steps, i.e. from the adsorption site to the flowing gas, then from the gas to the PCM. Therefore, there has been a limitation in the rate of heat transfer.

In this dissertation, for the rapid removal and storage of the heat of adsorption using latent heat, a PCM-inserted adsorbent is newly designed. By inserting PCM directly into the adsorbent, the generation and removal of the heat of adsorption can be completed inside one material as shown in Figure 30.

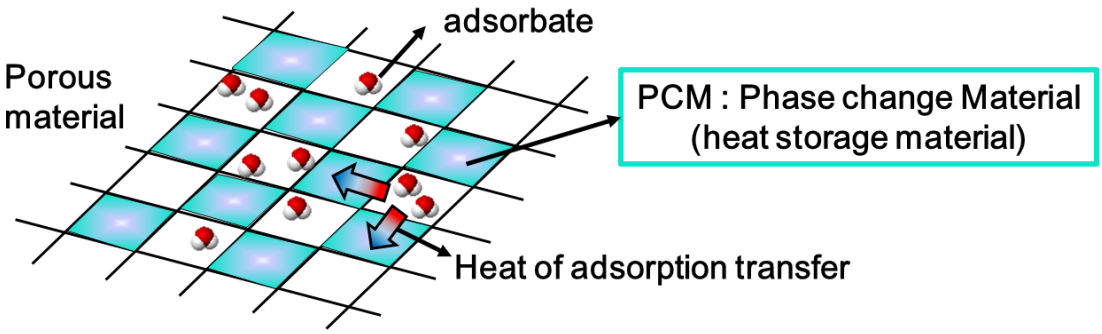

Figure 30. Schematic image of PCM-inserted adsorbent.

In the concept of PCM-inserted adsorbent, the heat of adsorption can transfer more effectively to the PCM, compared with using extra containers for PCM, such as a capsule, owing to the three reasons. First, heat transfer distance becomes extremely short. Since PCM is inserted into the pores of adsorbent itself, a heat transfer distance is expected to be from a few nanometers (porous wall thickness) to a few micrometers (crystal particle diameter). Second, heat transfers completed inside the one material, and does not go through the flowing gas. Third, due to the existence of PCM, the specific heat of adsorbent itself also increases. This indicates

that not only the latent heat storage, but also the sensible heat storage will be used with the increased capacity of heat storage. Hence, in the concept of PCM-inserted adsorbent, rapid removal of the heat of adsorption can be expected. Also, the absorbed thermal energy through PCM is expected to be re-used during the desorption process. Therefore, PCM-inserted adsorbent has an advantage that this method is an energy-saving method compared with other sensible heat storage approaches. Moreover, in case of PCM-inserted adsorbent, adsorbent also works as the container of PCM. Therefore, PCM can be homogenously distributed in the bed. In case of using alternative containers, sometimes, PCM cannot be fully utilized owing to the heterogeneous distribution. Mostly, PCM heterogeneously distributes in the column of adsorbent bed owing to the density difference between the PCM container and the adsorbent pellet. Furthermore, in the concept of PCM-inserted adsorbent, PCM does not easily leak from the pores of adsorbent, due to the surface tension of the confined PCM. On the other hand, other containers for confining PCM, such as a polymer capsule, may be cracked owing to the pressure change during the adsorption process. Therefore, the leakage problem of liquid PCM from the container can be improved when PCM is confined in the body of adsorbent. In addition, the structure and thermal stability can be also improved with using porous materials as containers.

An ultimate goal of this dissertation is realization of the apparent isothermal behavior in an adsorption process under an adiabatic condition by developing a PCM-inserted adsorbent, meaning that 100% removal of the released heat during the adsorption is attained through PCM. By realizing the isothermal-adiabatic adsorption process, the improvement of the adsorption performance through the recovery of the heat of adsorption by developing a PCM-inserted adsorbent, is another ultimate goal in this dissertation. Therefore, the improvement of the adsorption performance through the recovery of the heat of adsorption by developing a PCM-inserted adsorbent, is another ultimate goal in this dissertation. To develop PCM-inserted adsorbent, following steps are required. Following steps are intensively studied in this dissertation.

(1) Understanding of phase change behavior of PCM in the mesoporous space
(2) Proposal of specific concept for the PCM-inserted adsorbent
(3) Optimization of PCM-inserted adsorbent through simulation
(4) Evaluation of the effectiveness of the proposed system through experimental

In the step (1), by understanding the phase change behavior of PCM in the mesoporous space, the most adequate condition for using mesoporous space as heat storage space can be clarified. With the results of step (1), specific concept for the PCM-inserted adsorbent can be proposed. As for the adsorbent materials of the 'PCM-inserted adsorbent', three different porous materials described in the previous chapter 1.3, i.e. mesoporous zeolite, mesoporous silica, and carbon nanotube, are considered in this thesis. Those materials are selected from the various perspectives of advantages. For example, a facility of controlling a pore diameter in case of mesoporous silica and mesoporous zeolite, and a facility of modifying a surface functional group and high thermal conductivity in case of carbon. In the step (3), proposed PCM-inserted adsorbent can be optimized through the simulations. At the same time, in the step (4), proposed PCM-inserted adsorbent can be evaluated as an effective concept or not through experimental.

By following these steps, this dissertation is expected to be reach closer to the ultimate goal, which is the improvement of the adsorption performance through the recovery of the heat of adsorption by developing a PCM-inserted adsorbent.

1.5 Thesis outline

In chapter 1, general research backgrounds and the research objective of this dissertation are described. Specifically, PCM-inserted adsorbent is proposed as a new concept for the rapid removal of the heat of adsorption. Also, the objective and the ultimate goal of developing PCM-inserted adsorbent are described.

In the chapter 2, the melting point and the enthalpy of fusion of confined PCM were studied. Understanding of melting behavior of PCM in a mesoporous space is necessary to develop a PCM-inserted adsorbent. Mesopore diameter, functional groups of PCM, and the amount of surface functional group of the host material are studied as key parameters affecting to the melting properties of PCM.

Then, proposal of a specific concept for the PCM-inserted adsorbent is required. Specifically, the concept is required, that inserted PCM and the adsorbate can separately coexist in the host adsorbent. In the chapter 3, three different types of the concept are proposed, i.e. PCM-inserted mesoporous silica SBA-15, PCM-inserted carbon nanotube, and PCM-inserted mesoporous zeolite SSZ-13. The proposed concept is experimentally prepared and theoretically evaluated. As a result, among three concepts, mesoporous silica SBA-15 showed the most enhanced performance of dehumidifying fixed-bed adsorption process with inserting PCM.

Therefore, understanding of key parameters is necessary to make the inserted PCM works more efficiently. Hence, in the chapter 4, parametric studies for the optimization of PCM-inserted SBA-15 was done by simulation. The enthalpy of fusion of inserted PCM, the amount of inserted PCM, and the inlet temperature are studied as key parameters.

In chapter 5, an experiment of dehumidifying fixed-bed adsorption process is carried out to demonstrate the effectiveness of the PCM-inserted SBA-15. Due to the limitation in the experimental conditions, the optimized condition selected in chapter 4, could not be demonstrated. However, the temperature of adsorption system was successfully suppressed through the latent heat storage of PCM. PCM-inserted SBA-15 is proved as effective concept for the PCM-inserted adsorbent.

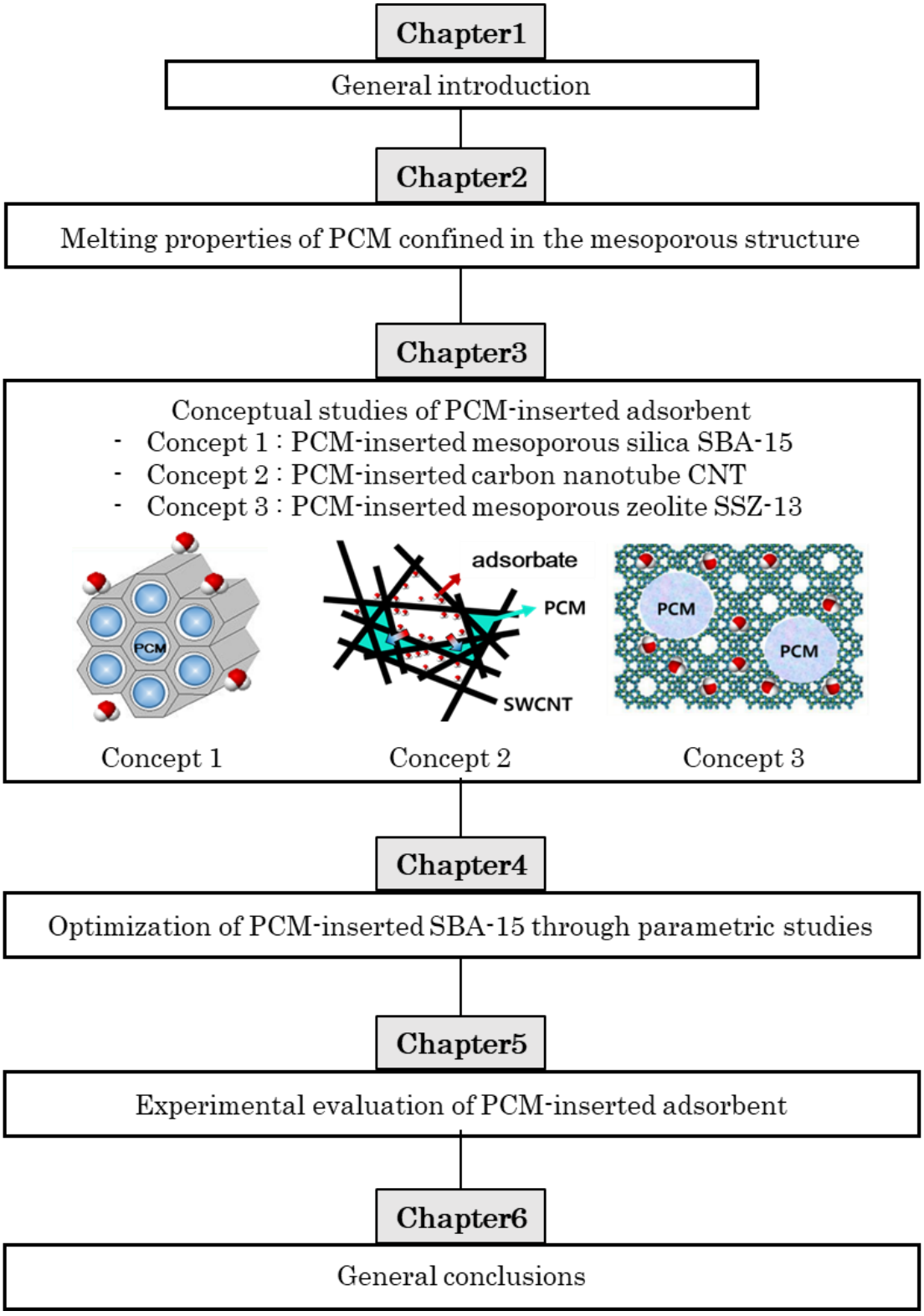

Figure 31. Doctoral dissertation structure.

Chapter 2. Melting properties of PCM confined in the mesoporous structure

2.1 Introduction

Conservation of energy is becoming more important due to the depletion of fossil fuels and increased energy consumption, accompanied with developing new green energy. Especially, efficient use of wasted energy such as thermal energy recovery and heat storage are important issues for conserving energy. Thermal energy can be classified into three different types: sensible heat[49], latent heat[16], and the heat generated during reactions[50]. Among them, thermal energy conservation using latent heat has an advantage that it can store high density level of thermal energy within a sharp temperature range.

Utilization of a phase change material(PCM) in latent heat storage system is applied in various heat storage field such as building materials[12], solar energy harvesting[51], and performance upgrading of the adsorption process[4,52]. Solid-liquid phase change is mostly used in latent heat storage. This is because solid-liquid phase change is easier to handle owing to the small volume change compared to other types of phase change such as gas-liquid or gas-solid PCMs[53]. Mostly, PCMs are classified as organic PCM such as paraffin, fatty acid and inorganic PCM such as metals, and hydrates[13]. Polymer[54], metallic voids[52], and micro-capsule[55], etc., were reported as the containers to capture PCMs inside.

Recently, porous materials have been reported as a new host material for containing PCM owing to their high specific surface area, high structural stability. Most importantly, leakage problem of liquefied PCMs from the container can be improved when porous materials are used as host material owing to high surface tension derived from nanopores[16,22,56]. Previously, melting and freezing properties in a restricted narrow space such as a capillary have mainly been researched by using small model molecules, for example, water[57], methane[58], and benzene[20]. However, small model molecules are not suitable for PCMs. In case of water, the

degree of super cooling is significantly high. In case of small organic molecules such as methane of benzene, the melting point of each molecules are extremely low or high to utilize.

Hence, the melting and freezing properties of confined, long-chain organic PCM molecules which show less degrees of super cooling and melting points near room temperature such as polyethylene glycol(PEG)[59], paraffin[60], and fatty acid[16] are under discussion. Specifically, the decrease of melting point of confined PCM molecules is being intensively investigated. In addition to the melting point, the enthalpy of fusion is also an important property for the practical application of PCMs in heat storage. However, only very few previous works dealt with the change of enthalpy of fusion even though the enthalpy of fusion determines the capacity of stored heat. According to the best of my knowledge, almost all of the previously reported PCM-confined materials are prepared by method called liquid impregnation[20,22,56]. In this method, PCM confined into mesopores of host material via evaporation of volatile liquid solvent from a mixture of dissolved PCM and host material by heating or evacuation. In the step of impregnate dissolved PCM, the dissolved liquid phase PCM confined not only inside mesopore, but also left at the outside mesopore, such as on the external surface and intergranular space. This is because liquid PCM directly contact with the host material comes in liquid impregnation method. This indicates that the accurate amount of PCM existing inside the mesopores and the exact pore filling ratio of PCM were unknown. Therefore, the enthalpy of fusion of confined PCM prepared by liquid impregnation was discussed in terms of the units of J/g-sample or approximately J/g-PCM [20,22,56].

This study aim to confine PCMs only inside the mesopores. In this study, PCM confined into only mesopores using vapor transportation method. Therefore, the exact pore filling ratio was calculated. Also, the change of enthalpy of fusion could be accurately discussed with the unit of J/g-PCM, and the adequate and effective conditions for obtaining a high value of the latent heat of PCMs were determined.

In this study, as the organic PCMs, paraffin, fatty acid, and fatty alcohol were selected. As the host materials for confining PCMs, mesoporous silica SBA-15 and soft-templated mesoporous carbon(MC), which possesses a same hexagonal

structure of SBA-15, were prepared. The effect of confining method on melting properties of confined PCM is studied in this research. Also, as a key parameters to affect melting properties, pore diameters of the host materials, functional groups of PCMs, and quantity of functional groups of host materials are investigated. Based on the key parameters, the condition the achieving high value of enthalpy of fusion is determined.

2.2 Experimental

2.2.1 Preparation of mesoporous silica SBA-15s

SBA-15 was synthesized by templating a cylindrical mesoporous structure made via micelle. Triblock copolymer $EO_{20}PO_{70}EO_{20}$ (pluronic P123, Sigma-Aldrich) is used as the surfactant, and tetraethyl orthosilicate(TEOS) is employed as the silica precursor. Three different pore sizes of SBA-15 was synthesized. Each of SBA-15 sample was named after their pore size, i.e. SBA-15-5.6nm, SBA-15-7.6nm and SBA-15-12.5nm.

SBA-15-7.6nm was synthesized by following the procedure of literature written by Zhao et al.[32]. 4.0 g of pluronic P123 was added in the mixture of 120 g of 2 M HCl and 30 g of water. After dissolving P123, 8.50 g of TEOS was added into solution, and the mixture was stirred at 35 °C for 20 h. Subsequently, the mixture was aged at 100 °C without stirring. Then, filtered the solution and washed with deionized water and dried at 100 °C for 12 h. The obtained solid product was calcined under air flow for 6 h at 773 K to remove the micelle. The temperature was increased by 1 K/min. SBA-15-5.6nm was synthesized with same procedure of SBA-15-7.6nm. However, the condition of aging temperature is changed[61]. The aging temperature for SBA-15-5.6nm was 40 °C. SBA-15-12.5 nm was synthesized by following the procedure proposed by Kruk et al.[35]. In this procedure, triisopropylbenzene(TIPB) was added as a swelling agent in the step of mixing P123 and HCl solution to expand the cylindrical micelle. The synthesize temperature was 17 °C with stirring and aging temperature was 120 °C without stirring.

2.2.2 Preparation of mesoporous carbons

Mesoporous carbon (MC) was synthesized by templating a cylindrical mesoporous structure made via micelle. As the surfactant, pluronic triblock copolymers $EO_{100}PO_{65}EO_{100}$ (F127, Sigma-Aldrich) was used. As a carbon source, resorcinol was used. The synthesis procedure was followed by Libbrecht et al.[62]. Specifically, 2.2 g of resorcinol, 2.2 g of F127, 9 mL of ethanol, and 9 mL of 3M HCl was added in a vial. The mixed solution was fully stirred to totally dissolved F127 in the closed vial. Then, 2.6 g of 37 wt% formaldehyde was added. Subsequently, the solution was stirred at 100 rpm for 15 min. Then, the solution changed into high viscosity solution. The sticky solution was poured into a 10 cm-diameter petri dish. Next, ethanol was evaporated from the solution at 25 °C for 6 h and subsequently cured at 60 °C in an oven for 18 h. Then, the formed resorcinol/formaldehyde resin was scratched off from the petri-dish. The resin was calcined under nitrogen flow. The calcined temperature was increased to 350 °C with a heating rate of 1 K/min, then maintained for 2 h. In addition, to carbonize the resin, the calcined temperature was increased to 800 °C with a rate of 2 K/min, then maintained at 800 °C for 3 h.

Some of the synthesized mesoporous carbon, MC, was oxidized under ozone flow to modify the surface of carbon. The amount oxygen-containing functional groups exist on the MC can be increased through oxidization. The obtained oxidized-mesoporous carbon was denoted as OMC.

2.2.3 Characterization of SBA-15s and mesoporous carbons

Nitrogen adsorption (Quantachrome, QUADRSORB evo™) was performed to analyze the porous properties of synthesized mesoporous silica and carbon. Total pore volume V_t, BET surface area S_{BET}, pore diameter d, and pore size distribution of the mesoporous silica and carbon was measured. Pre-treatment of nitrogen adsorption of mesoporous samples was carried out at 300 °C for 3 h. Also, pre-treatment of nitrogen adsorption of PCM-confined mesoporous samples was carried out at 25 °C for 3 h to avoid the desorption of PCM. The total pore volume of mesoporous samples was calculated by the saturated amount of adsorbed nitrogen when the relative pressure was 0.95. The pore size distribution was calculated using the NLDFT method. X-Ray diffraction (XRD, Rigaku, Rint-2100) patterns of mesoporous silica and carbon were measured. Operating condition was 40 kV and 40 mA using Cu Kα radiation. SEM image of SBA-15-7.6 nm is measured to identify the morphology of the SBA-15.

Boehm titration was performed[40] to characterize the amount of surface oxygen-containing groups on mesoporous carbon. 0.1 g of MC or OMC was added to 0.1 M NaOH solution and 0.1 M $NaHCO_3$ solution, respectively. The mixture of solution and carbon was stirred at 300 rpm for 3 days at 30 °C. Then, filtered the solution and titrated by 0.1 M HCl solution. The quantity of oxygen-containing functional groups exist on MC and OCM were calculated by titration[63].

The thermal properties of the confined PCM in the mesoporous space of SBA-15 were measured by thermogravimetric analysis (TGA; Rigaku, Thermoplus TG8120). The analyzed temperature range was from 298 K to 523 K and the heating rate was 1 K/min.

2.2.4 Confinement of PCM molecules to mesoporous materials

A host mesoporous material, i.e. SBA-15 or MC dried at 130 °C for more than 1-2 h to remove the adsorbed water. Then, the weight of dried material, m_b, was measured. On the other hand, PCM was placed at the bottom of the corked vacuum desiccator. Then, the dried host material was separately placed in the upper side of a desiccator. Subsequently, the desiccator was evacuated. After that, the desiccator was put in a 100 – 130 °C oven (depend on the species of PCM) for a few hours, until the adsorption of PCM reach to the equilibrium state. The vapor pressure of each PCM was approximately 1 mmHg at the 100 – 130 °C. During this step, the vaporized PCM adsorbed and condensed inside the mesopores of host materials. The weight of recovered resultant solid, m_a, was measured. By weighting the sample before and after confining PCM, the ratio of the volume of confined PCM to the total pore volume of SBA-15, was calculated as follows:

$$w = \frac{100(m_a - m_b)}{\rho m_b V_t} \quad \text{(Eq. 3)}$$

where m_a represents the weight of PCM-confined SBA-15, m_b represents the weight of SBA-15, ρ represents the density of PCM, and V_t represents the total pore volume of SBA-15 measured from nitrogen adsorption. The value w can be considered as a pore filling ratio of PCM inside mesopores. In this study, six different species of PCMs, i.e. paraffins (octadecane, tetradecane), fatty acids (dodecanoic acid, decanoic acid), and fatty alcohols (tetradecanol, and dodecanol), were confined in each SBA-15 sample. Two species of PCM, i.e. octadecane and tetradecanol, were confined in MC and OMC.

In addition, to investigate the effect of confinement method on the melting properties of PCM, octadecane-confined SBA-15 was prepared with different method, which called liquid impregnation. Liquid impregnation is a conventional method for confining PCM. The procedure of liquid impregnation was followed that described in literature[22].

2.2.5 Analysis of the melting properties of confined PCM

The melting properties, i.e. melting point and the enthalpy of fusion, of confined PCM in mesopores were measured by using differential scanning calorimetry (DSC, Shimadzu DSC-60). 2–3 mg of PCM-confined sample was used for each analysis. The heating/cooling rate of samples was 10 K/min.

2.3 Results and discussion

2.3.1 Preparation of PCMs-confined SBA-15

Mesoporous silica SBA-15 with different pore diameter, i.e. SBA-15-5.6 nm, SBA-15-7.6 nm, and SBA-15-12.5 nm was synthesized. Figure 32 depict the nitrogen adsorption-desorption isotherms and the pore size distributions of synthesized SBA-15. The porous characteristics of each SBA-15 sample, calculated from nitrogen adsorption-desorption, is listed on Table 2.

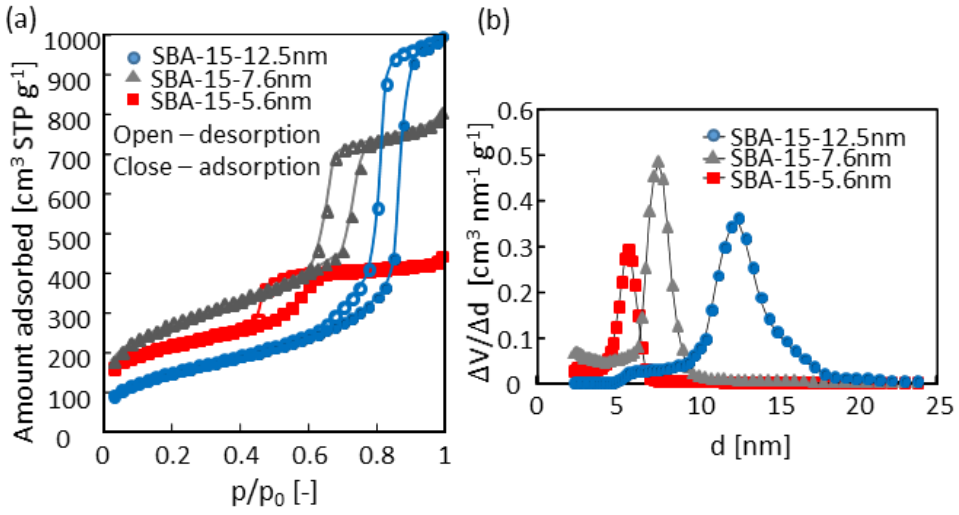

Figure 32. (a) Nitrogen adsorption-desorption isotherms of SBA-15s (b) Pore size distribution of SBA-15.

Table 2. Porous characteristics of synthesized SBA-15.

Sample	S_{BET} [m^2/g]	V_t [cm^3/g]	V_{micro} [cm^3/g]	V_{meso} [cm^3/g]	d [nm]
SBA-15-5.6 nm	492	0.444	0.148	0.296	5.6
SBA-15-7.6 nm	941	1.093	0.115	0.978	7.6
SBA-15-12.5 nm	533	1.534	0.000	1.534	12.5

The micropore volume, V_{micro}, of each SBA-15 was calculated using the t-plot method. The mesopore volume, V_{meso}, was calculated as the difference between V_t and V_t, i.e. $V_t - V_{micro}$. Three SBA-15 samples with cylinder-shaped mesopores but different pore diatmeter were successfully obtained. The pore diameters of each SBA-15 calculated using the NLDFT method, which were 5.6 nm, 7.6 nm, and 12.5 nm, respectively. SBA-15-12.5 nm showed relatively broad pore size distribution as compared to those of SBA-15-5.6 nm and SBA-15-7.6 nm. This is because triisopropylbenzene(TIPB), which works as a swelling agent, was heterogeneously solved in the micelle. Figure 33 depict the low-angle XRD patterns of synthesized SBA-15. The XRD patterns of all the SBA-15 samples showed a two-dimensional hexagonal periodicity originating from SBA-15. Consequently, it can be confirmed that host mesoporous silica SBA-15 with different pore size were successfully prepared.

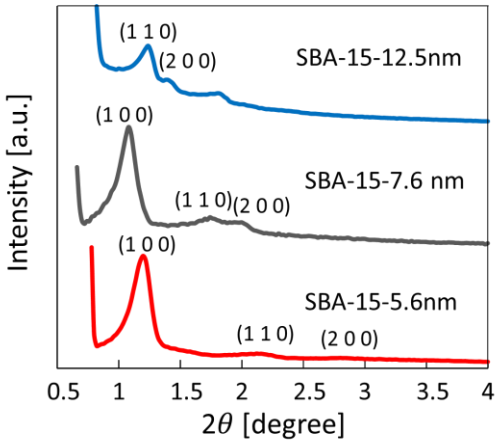

Figure 33. Low angle XRD patterns of SBA-15s.

Also, the SEM images of prepared SBA-15-7.6 nm is measured as shown in Figure 34. The prepared SBA-15 showed a typical morphology of previously reported SBA-15, which is 'sausage-like' morphology[64].

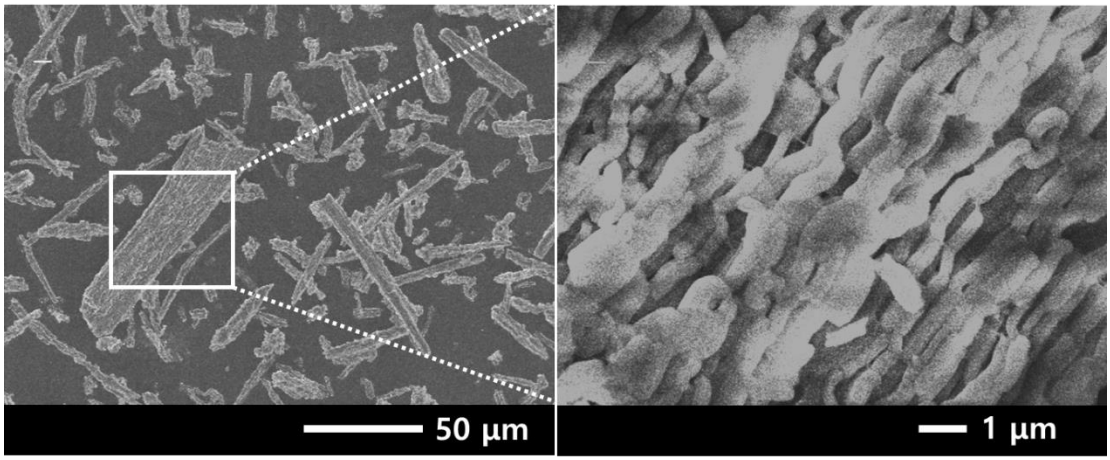

Figure 34. SEM images of SBA-15-7.6 nm.

The nitrogen adsorption-desorption isotherms of octadecane-confined SBA-15 are presented in Figure 35. Subsequently, Figure 36 depict the pore filling ratio, *w*, of confined PCMs in the mesopores of SBA-15 with different pore size. The pore filling ratio was calculated by using Equation 3.

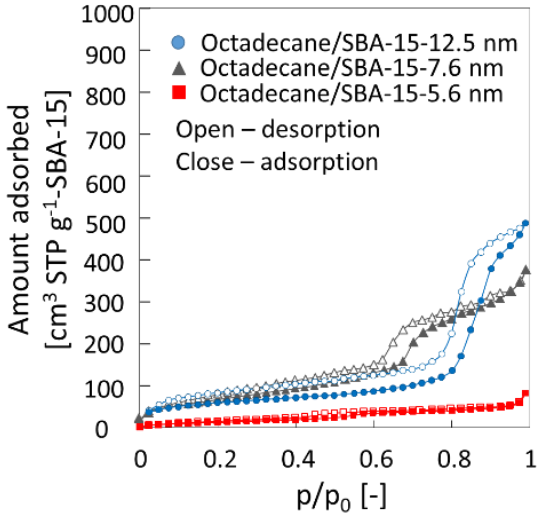

Figure 35. Nitrogen adsorption-desorption isotherms of octadecane/SBA-15.

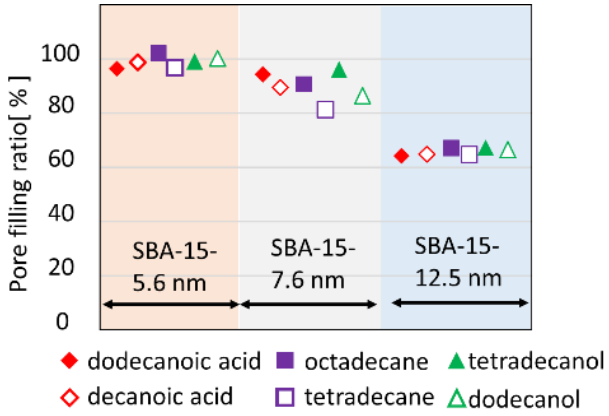

Figure 36. Pore filling ratio of PCMs confined in SBA-15s.

The adsorbed volume of nitrogen in Figure 35 is calculated as 'per weight of host SBA-15', not 'per weight of sample (PCM+SBA-15)' by using results of pore filling ratio, w shown in Figure 36. Figure 35 depicted that the amount of nitrogen adsorbed on each octadecane-confined SBA-15 was significantly decreased, when compared to the amount of nitrogen adsorbed on pure SBA-15 (Figure 32). This suggests that PCMs were filled inside the mesopore. However, the decrease of the amount of adsorbed nitrogen on octadecane-confined SBA-15 compared to pure SBA-15 was depend on the pore diameter of each sample. The volume of nitrogen adsorbed on SBA-15 sample decreased more when the pore diameter of sample is smaller. This refers that pore filling ratio of PCM inside mesopores is decrease with increase of a pore diameter. The decrease of pore filling ratio is also noticed in Figure 36. Almost 100% of the pores of SBA-15-5.6 nm and SBA-15-7.6 nm were filled with PCMs. However, the pore filling ratio of SBA-15-12.5 nm was only 65%. From these results, it can be considered that the confining PCM into 100% of mesoporous space getting difficult with the increase in pore diameter. To fully confining PCM into mesopores, a condensation of adsorbed PCMs is necessary. The PCM adsorbed inside mesopores condense at higher relative pressure with larger pore diameter. Since I confined PCM in the low vapor pressure during confining step, which was approximately 1 mmHg, the relative pressure of PCM might be not high enough to condense and to fulfill the PCM inside mesopores at large pore diameter.

2.3.2 Effect of confining methods on melting properties

Octadecane-confined SBA-15 samples was prepared using liquid impregnation or vapor transportation methods to compare their effects on the melting properties of PCM. The melting properties of prepared octadecane-confined SBA-15 samples are measured using DSC. The DSC curves of each samples are depicted in Figure 37.

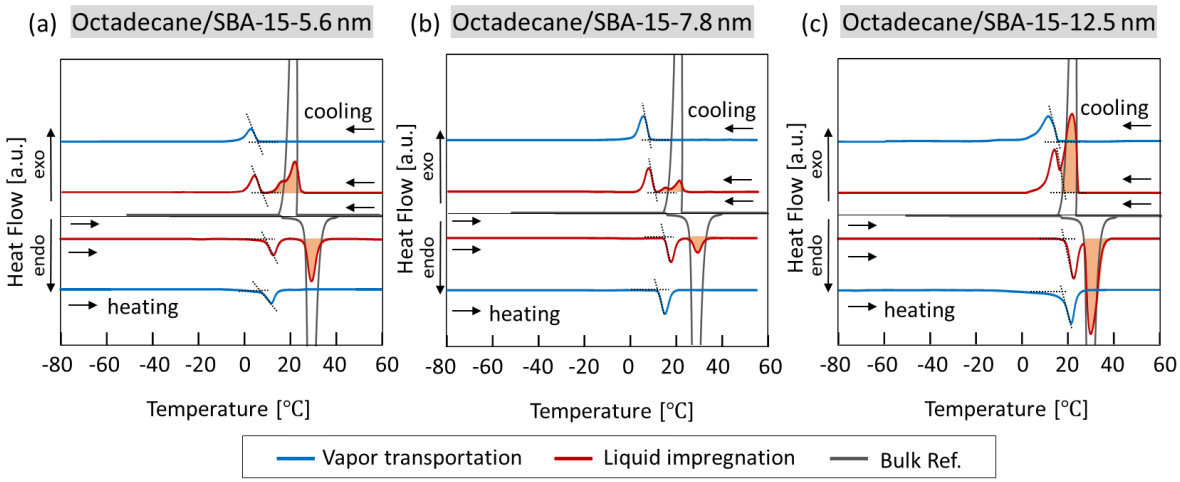

Figure 37. DSC curves of octadecane-confined SBA-15 using different confining methods: liquid impregnation and vapor transportation. (a)octadecane/SBA-15-5.6 nm, (b)octadecane/SBA-15-7.6 nm, (c)octadecane/SBA-15-12.5 nm.

The phase change peak of bulk octadecane is shown as reference in Figure 37. All octadecane-confined SBA-15 samples prepared using vapor transportation demonstrated only one endothermic peak and one exothermic peak, respectively. However, all samples prepared using liquid impregnation depicted 2-3 peaks: One near the peak obtained from the samples prepared using vapor transportation, and 1-2 more peak near the bulk reference. This 1-2 phase change peak of samples prepared by liquid impregnation, was observed near peak of the bulk reference, thereby, these peaks can be considered as originated from a bulk state of PCM such as an external surface of SBA-15 or intergranular space of SBA-15 grains. This is because, in the method of liquid impregnation, the host material first mixed with dissolved liquid PCM so host material directly contact to the bulk PCM. On

the other hand, DSC peaks that observed at a lower temperature can be considered as originated from nano-confined PCM inside the mesopore of SBA-15.

Figure 38 depict the weight loss of octadecane/SBA-15 samples prepared by liquid impregnation or vapor transportation.

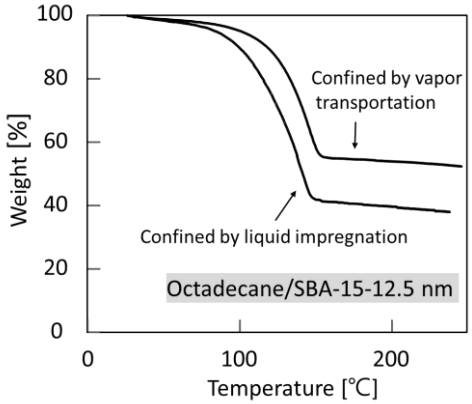

Figure 38. TGA curves of octadecane/SBA-15 prepared using different methods.

The weight loss of octadecane in SBA-15 using vapor transportation was 66%, which shows good agreement with the pore filling ratio result shown in Figure 36. On the other hand, the calculated weight loss of octadecane in SBA-15 using liquid impregnation was 109%, which is more than 100%. Hence, this result also suggest that PCM confined using liquid impregnation is heterogeneously distributed on SBA-15, not only inside mesopores but also bulky space such as the external surface or in the intergranular space. Further, the weight loss of the sample prepared using liquid impregnation started at lower temperature compared to the sample prepared using vapor impregnation. This is because heterogeneously distribute octadecane molecules prepared using liquid impregnation have weaker interaction than confined octadecane due to strong surface tension, thereby, the vaporization of bulk-derived octadecane began in a lower temperature range.

As depicted in Figure 37, when bulk-derived PCM exists in the sample prepared using liquid impregnation, the nano-confined peaks shifted closer to bulk-derived peak at a high temperature. Since there was no difference between the two samples except for their confining methods, the shift of both melting and freezing points was concluded as an effect of PCM confining method. Specifically, the shift of the freezing point might have been affected by the nucleation of bulk PCMs[21].

The shift of the melting point might have been affected by the changes of the meniscus of the confined PCM [65] owing to the PCMs exist on the external surface and in the intergranular space of host SBA-15. Consequently, confining PCM using vapor transportation is an effective method to prevent the effect of excessive bulk PCM residue on its melting and freezing properties. Moreover, the pore filling ratio can be exactly calculated by using vapor transportation as shown in Figure 36. This is an important advantage for discussing melting properties because the exact value of the enthalpy of fusion with the unit of J/g-PCM can be elucidated using the accurate pore filling ratio.

2.3.3 Changes in enthalpy of fusion and melting point of PCMs confined in mesoporous silica SBA-15

DSC curves of 6 different species of organic PCMs, i.e. octadecane, tetradecane, dodecanoic acid, decanoic acid, tetradecanol, and dodecanol, confined in SBA-15 with different pore diameters during heating are depicted in Figure 39. The enthalpy of fusion ΔH_f with the unit of J/g-PCM, and the melting point $T_{melting}$ are listed in Table 3. ΔH_f was calculated from J/g-sample to J/g-PCM by using the result of pore filling ratio. The enthalpy of fusion and melting points of the confined PCMs in all samples showed lower when compared with that of the bulk PCMs. The value of enthalpy of fusion and melting point was increased and getting closer to the corresponding values of the bulk PCMs with the increase of pore diameter. In case of fatty alcohols, no phase change was observed when those were confined in SBA-15-5.6 nm in Figure 39. This is because the phase change of the confined fatty alcohols difficult to occur due to a strong interaction between the fatty alcohol molecules and the host silica-wall. Or, there is a possibility that the enthalpy change of the phase change is not enough high to be detected by DSC machine. In case of tetradecanol/SBA-15-12.5 nm, two endothermic peaks were demonstrated. This suggest that phase transition of tetradecanol occurred in 2 step, i.e. solid-solid and solid-liquid[66]. Therefore, in Table 2, the enthalpy of fusion of tetradecanol/SBA-15-12.5 nm was calculated by sum of the enthalpy of both two peaks.

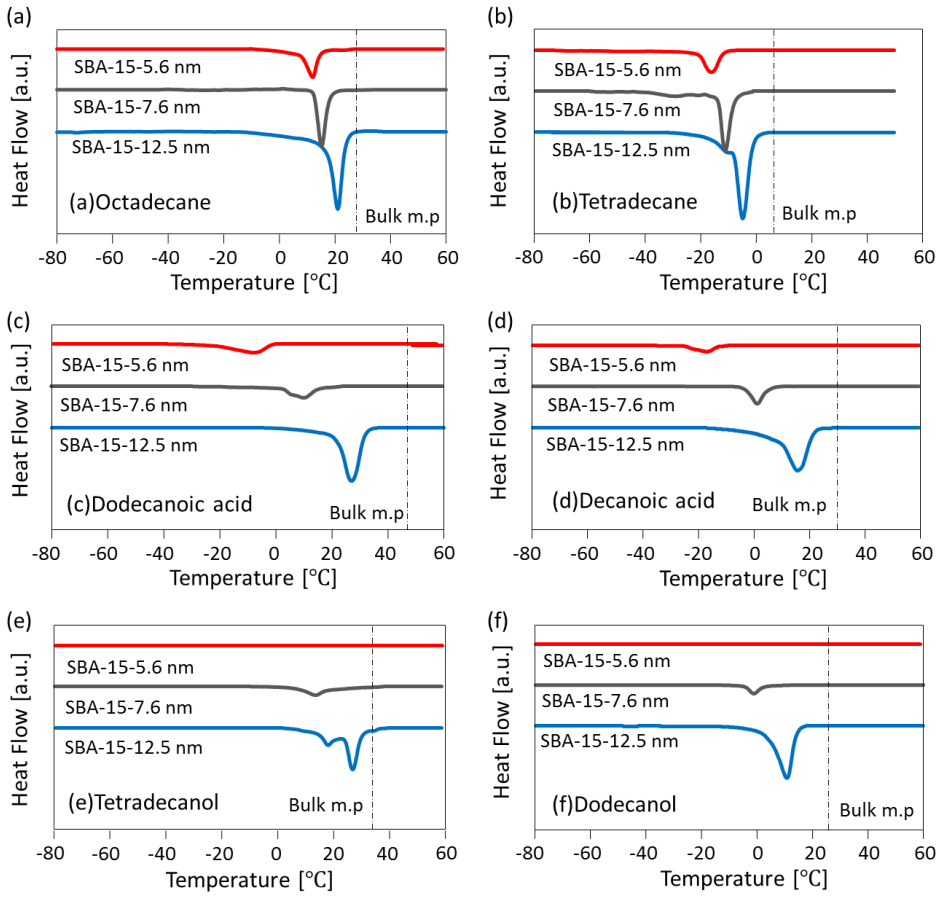

Figure 39. DSC curves of (a)octadecane, (b)tetradecane, (c)dodecanoic acid, (d)decanoic acid, (e)tetradecanol, and (f)dodecanol confined in SBA-15s with different pore diameter.

Table 3. The enthalpy of fusion and the melting point of confined PCMs in SBA-15s with different pore diameter.

	SBA-15	Octadecane	Dodecanoic acid	Tetradecanol	Tetradecane	Decanoic acid	Dodecanol
ΔH_f [J/g-PCM]	5.6 nm	39.1	19.1	-	54.6	9.0	-
	7.6 nm	53.3	30.8	6.4	82.2	33.9	10.3
	12.5 nm	103.3	65.9	48.4	124.2	64.3	69.5
	Bulk	230	169	198	216	163	196
$T_{melting}$ [℃]	5.6 nm	9.3	-8.86	-	-20.4	-26.0	-
	7.6 nm	11.7	3.6	6.4	-12.4	-4.1	-4.1
	12.5 nm	17.4	22.32	11.4	-7.4	11.1	0.2
	Bulk	26.5	44.6	36.0	6.2	30.0	24.0

Conventionally, the difference in the melting points between the confined and the bulk (ΔT) is expressed by the Gibbs-Thomson equation[19] as below.

$$\Delta T = \frac{T_{bulk} V_m \gamma_{sl} \cos\theta}{d \Delta H_f} \qquad \text{(Equation 3)}$$

In this equation, γ_{sl} indicates the surface tension of confined, ΔH_f is the enthalpy of fusion, V_m is the molar volume, T_{bulk} is the melting point of bulk, θ refers the contact angle at interface, and d is pore diameter. The Gibbs-Thomson equation is a remarkable work, and was generally used in many preceding researches to understand melting properties of confined materials[19,22]. This equation suggest that an inverse of pore diameter (d^{-1}) and the gap of melting point between the bulk and the confined (ΔT) have a linear relationship. Also, as you can notice from Eq.2, the extrapolation of linear relationship between ΔT and d^{-1} is converged to zero. The experimental ΔT_m values obtained from DSC results is plotted as a function of pore diameter d^{-1} in Figure 40 (a). Also, relative enthalpy of fusion of confined to bulk is plotted as a function of d in Figure 40 (b).

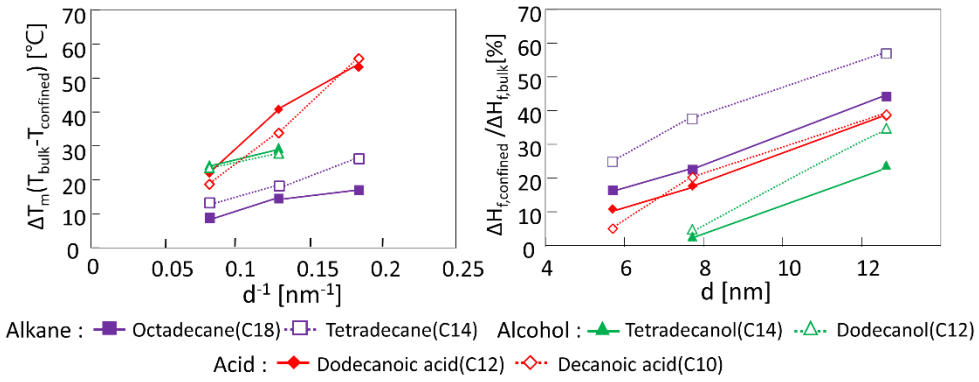

Figure 40. (a) Experimental ΔT_m values plotted as a function of pore diameter d^{-1}, and (b) the relative enthalpy of fusion of each PCM to bulk as a function of d.

As depicted in Figure 40 (a), d^{-1} and ΔT of confined organic PCM have a linear relationship, which shows good agreement with the Gibbs-Thomson equation. However, the extrapolation of d^{-1} and ΔT was not converged to zero. The plotted range of pore diameters was under approximately 13 nm in Figure 40. Therefore, the extrapolation of d^{-1} and ΔT was not converged to zero suggests that another effecting parameter should be additionally considered in extremely restricted

space to evaluate the changes in melting point by using the Gibbs-Thomson equation. Additional parameters, for example, non-melting layer[19,67] or surface roughness[68], required to be considered in a nanoscale phase change.

Also, the relative enthalpy of fusion of the confined to the bulk has a linear relationship with the pore diameter (see Figure 40 (b)). This suggest that the enthalpy of fusion of confined PCM approaches to the original value of the bulk PCM with increase of the pore diameter. A non-melting layer can be considered as the reason for this. The non-melting layer is a few molecular layers exists near the wall of the host that does not freeze or melt. It is generally accepted that phase change does not occur due to the strong interaction between molecular layers and the surrounding wall of the host[69]. With the decrease of the pore diameter, subsequently, the relative occupied volume of the non-melting layer inside the pore increases. As a result, the influence of the non-melting layer becomes more significant and the value of the enthalpy of fusion lowered with the decrease of the pore diameter. Furthermore, the state of liquid phase inside the pore can be considered as not exactly the same as that of the bulk liquid phase. Possibly, this can be another reason for the reduction of the enthalpy of fusion. As depicted in Figure 40 (b), the relative value of the enthalpy of fusion was observed as nearly more than 40 % when pore diameter of SBA-15 was larger than 10 nm. The value of enthalpy of fusion of tetradecane/SBA-15-12.5 nm was almost 60% of that of the bulk PCM. According to the previous study done by Jackson[20], the enthalpy of fusion sharply increases when the pore diameter d is in the range of approximately under 10 nm. When pore diameter is ranged between approximately 10 to 25 nm, the enthalpy of fusion moderately increases. When pore diameter becomes larger than 25 nm, the apparent enthalpy of fusion is saturated, and does not increase with increase of pore diameter. Based on this reported result, it can be predicted that the enthalpy of fusion of the confined organic PCMs will be saturated after d increases more than 12.5 nm. In addition, as discussed above, confining PCM in the mesopore with 100 % is getting more difficult to realize with the increase in pore diameter owing to the low vapor pressure of organic PCMs, in the method of vapor transportation. Hence, 10 – 20 nm can be considered as a preferable pore

diameter for confining PCM to achieve high enthalpy of fusion with high pore filling ratio inside the mesopore.

Generally, SBA-15 possess cylindrical mesopores, but also possess micropores at the same time. However, the enthalpy of fusion derived from the PCM inside micropores can be neglected since phase change at micropore is difficult to occur due to the extremely small pore diameter. Hence, there is a possibility that the enthalpy of fusion with the unit of J/g-PCM calculated from the weight of PCM existing only mesopores, not from the weight of PCM existing both mesopores and micropores, can be increased, and further investigation is required.

All the PCMs in Figure 40 depicted a linear relationship with the pore diameter of SBA-15, except fatty alcohols/SBA-15-5.6 nm. However, there is a difference in the linear relationship with the functional groups of confined PCM, i.e. paraffin, fatty acids, and fatty alcohol. At the wall of SBA-15, silanol groups (Si-OH) exist. Hydroxyl group of fatty alcohol and carboxylic acid group of fatty acid actively interact with silanol group of SBA-15 via hydrogen bonding. In case of an alkane group of paraffin, interaction between the confined PCM and the wall of host is relatively weak. Thereby, the melting point and enthalpy of fusion of confined fatty acids and fatty alcohol, were more significantly changes in SBA-15 than that of paraffin. This suggest that the pore diameter affect more dominantly on the melting properties when the interaction between PCM molecules and the porous wall is stronger. Consequently, to achieve high enthalpy of fusion inside mesopores composed by hydrophilic materials e.g. silica, PCMs should be selected as weakly interact hydrophobic molecules such as paraffin.

2.3.4 Characterization of synthesized mesoporous carbons

Nitrogen adsorption and desorption isotherms, and pore size distribution of synthesized mesoporous carbons MC and OMC are demonstrated in Figure 41 (a) and (b) respectively. The shape of adsorption-desorption branch, the total amount of adsorbed nitrogen, and distribution of the pore size of MC and OMC was perfectly overlapped. This suggests the physical properties of OMC are maintained in the step of oxidizing MC with ozone to forming OMC.

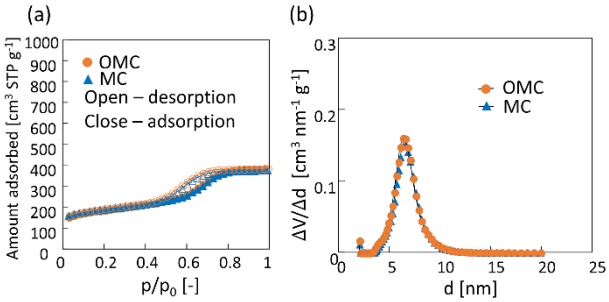

Figure 41. (a)Nitrogen adsorption-desorption isotherms of MC and OMC (b) pore size distribution of MC and OMC.

The amount of oxygen-containing groups exist on the surface of MC and OMC was measured using the Boehm titration method, and the results are listed in Table 4.

Table 4. Amount of the oxygen-containing groups exist on carbon surface.

	Phenolic hydroxyl [mmol/g]	Carboxylic acid [mmol/g]
MC	0.047	1.086
OMC	0.846	4.568

The amount of phenolic hydroxyl group and carboxylic acid group on the surface of OMC is more abundant, which is 5 – 6 times larger amount, compared to MC. From this result, it can be confirmed that the surface of OMC is successfully oxidized through ozone without changing any physical properties such as pore shape, total pore volume, pore diameter, and pore size distribution (See Figure 41). The pore filling ratios of PCM (octadecane and tetradecanol) confined in the mesopores of MC and OMC, respectively, are depicted in Figure 42. Each of PCM was successfully confined into MC and OMC.

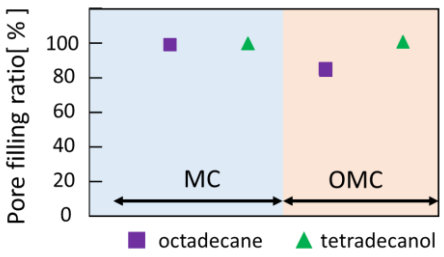

Figure 42. Pore filling ratios of PCMs confined in MC and OMC.

2.3.5 Changes in enthalpy of fusion and melting point of PCMs confined in mesoporous carbons

The DSC curves of PCMs confined in MC and OMC, respectively, are demonstrated in Figure 43. Octadecane and tetradecanol was selected as PCM.

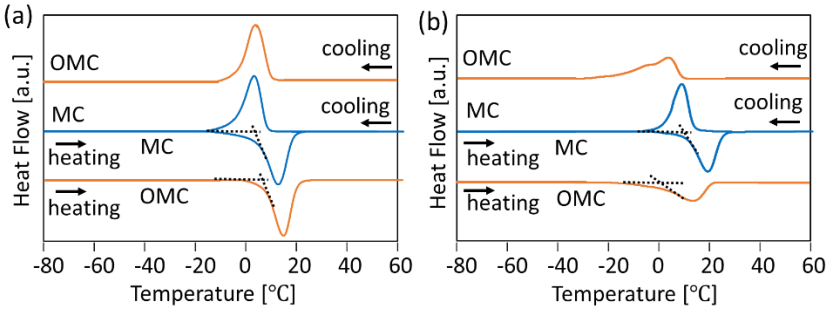

Figure 43. DSC curves of (a)octadecane and (b)tetradecanol confined in mesoporous carbons.

The enthalpy of fusion is calculated from to the area of the thermal peak. The melting point is the point where the base line and a tangential line of the thermal peak cross over. In case of octadecane, the melting properties, i.e. the enthalpy of fusion and melting point showed small change when it confined in MC or OMC. However, in case of tetradecanol, a significant changes was observed on the enthalpy of fusion and the melting point when it confined in MC or OMC. When tetradecanol confined in OMC, the amount of surface oxygen-containing groups is much larger compared to MC, resulted in significant reduction of the enthalpy of fusion. The specific enthalpies of confined PCMs with the unit of J/g-PCM are listed in Table 5.

Table 5. The enthalpies of fusion of PCMs confined in mesoporous carbons.

PCM	Host material	ΔH_f[J/g-PCM]	$\Delta H_{f,MC} - \Delta H_{f,OMC}$[J/g-PCM]
octadecane	MC	46.1	1.4
	OMC	44.7	
tetradecanol	MC	30.0	18.5
	OMC	11.5	

$\Delta H_{f,MC} - \Delta H_{f,OMC}$ indicates the enthalpies differences of confined PCM in MC and OMC. The oxygen-containing functional groups existing on the surface of OMC was 5–6 times larger than that on MC. The enthalpy of fusion of confined octadecane was lower only by 1.4 J/g-PCM with changes of the surface oxygen-containing group. On the other hand, in case of tetradecanol, the enthalpy of fusion was lower by 18.5 J/g-PCM, which is almost 50% of the enthalpy of fusion decreased. The hydroxyl group of tetradecanol is hydrophilic functional group, thereby storngly interacts with the oxygen-containing groups (phenolic hydroxyl and carboxylic acid) exist on surrounding carbon wall. Owing to this strong interaction, tetradecanol molecules are restricted from moving freely and having difficulty to be arranged orderly, i.e., arranged in solid structure, especially near the carbon wall. Therefore, owing to the strong interaction in the restricted narrow space, the thickness of the non-melting layer can increase, and subsequently, the enthalpy of fusion can decrease. On the contrary, octadecane has alkane group which is hydrophobic, thereby, the enthalpy of fusion did not significantly changed due to a small interaction between the octadecane molecules and the oxygen-containing group.

In conclude, the interaction between a functional group on the PCM molecules and a functional group on the surface of the host material strongly affects the melting properties of the confined PCM. If the functional group of PCM molecules strongly interact with a surrounding surface functional group of the host, two approaches can be considered to achieve a high enthalpy of fusion, i.e. high latent-heat storage capacity. One is that decreasing the quantity of interacting surface functional groups exist on the wall of the host. Second is that substitution of PCM into the molecules with weakly interacting functional group. Specifically, PCM such as paraffin is preferable to achieve a high latent-heat storage capacity under most conditions because paraffin is composed by only hydrocarbons.

2.4 Conclusions

The changes in the enthalpy of fusion and melting point of confined long-chain organic PCMs in a cylindrical mesopore of silica and carbon is investigated. PCM confining method, mesopore diameter, functional groups of PCM molecules, and functional groups of the wall of the host material were investigated as effecting parameters on the melting behavior of confined PCMs. First, PCM confining method 'vapor transportation' enables to confining PCM only inside the mesopore. Also, when the pore diameter decreases, the mesoporous space containing PCM is getting narrow and more restricted. Hence, the non-melting layer influence more significantly to the melting behavior, and leads to the decrease in the value of the enthalpy of fusion and melting point of PCM. In addition, when the interaction between PCM molecules and the surrounding wall of the host is strong interaction such as hydrogen bonding, the confined PCM molecules cannot be aligned in order and their motion is strictly limited. This resulted in the decrease in the enthalpy of fusion. In conclude, by selecting the host materials with large mesopores (e.g. 10–20 nm) and PCM molecules with a functional group that having weak interaction with the host material such as paraffin, the high enthalpy of fusion of confined PCM, which is greater than 50% of the value of the bulk, can be achieved.

Chapter 3. Conceptual studies of PCM-inserted adsorbent

3.1 Introduction

The released heat of adsorption increases the temperature of an adsorption system, which result in degrading the adsorption performance. Especially, in case of a short-time adsorption process e.g. PSA, adsorption performance is highly affected by temperature increase due to non-isothermal[3] and apparently adiabatic conditions[70]. Accordingly, removal of the released heat of adsorption is essential to achieve higher adsorption performance[71,72]. Among various methods of recovering the heat of adsorption, there is a method using the latent-heat of phase change materials (PCMs). Solid-liquid phase change is mostly used for the latent-heat storage using PCM. Hydrates, metals, organic compounds such as paraffin, and polyethylene glycol are examples of PCMs. Heat storage using latent-heat of PCM has an advantage that it can store high density of thermal energy within a small temperature range compared to sensible-heat storage method. In the previously reported studies, PCM was embedded in a fixed-bed adsorption process for the recovery of the heat of adsorption[14,15,73]. The released heat of adsorption transfer, then adsorbed by PCM, subsequently PCM changes from solid to liquid. To embed PCM in the adsorbent bed, various sizes of containers for capturing PCM have been studied from a large scale to small scale. For example, 40 mm rubber sphere[73], 6 mm metal void[14], and 1 mm polymer capsule[15] are reported as PCM-containing materials. When these PCM-containing materials are embedded in a fixed-bed adsorption process, the released heat of adsorption transfer from an adsorbent pellet to the fluid, then fluid to PCM-containing materials. Hence, there might be problems that embedded PCMs cannot effectively used as heat-storage materials due to the slow heat transfer. Therefore, a shorter heat transfer distance from adsorption site to PCM is required to improve the heat-recovery efficiency of the PCM.

For this reason, as already described in chapter 1.4, a new concept for applying PCM to an adsorption process with extremely short heat-transfer distance is

proposed by inserting the PCM directly into the adsorbent, i.e. PCM-inserted adsorbent. Again, the schematic image of PCM-inserted adsorbent is illustrated in Figure 44. By inserting PCM directly into the pores of adsorbent, the adsorption and the recovery of the heat of adsorption via PCM simultaneously occurs. The inserted PCM is strongly confined by surface tension, thereby, PCM is barely leaked from the adsorbent.

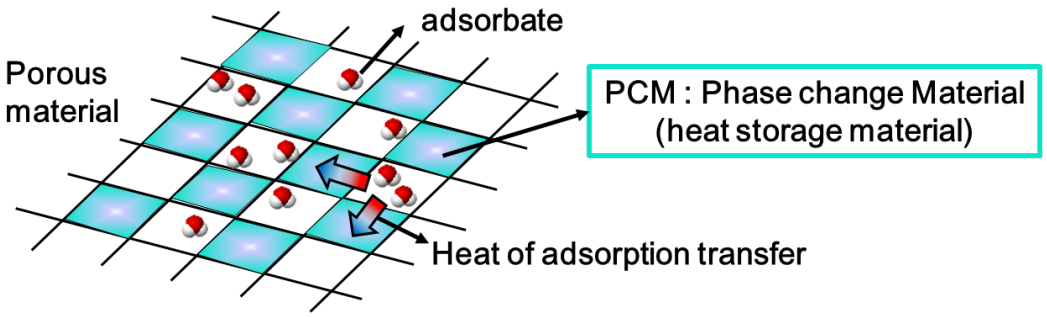

Figure 44. Schematic image of PCM-inserted adsorbent.

Most impressive advantage of this PCM-inserted adsorbent is that heat-transfer completed inside the adsorbent, not passing through the fluid. Therefore, in the concept of PCM-inserted adsorbent, rapid heat exchange between the inserted PCM and adsorption site ca be realized. Similarly, in the literature of Horstmeir, an adsorbent pellet with three layers (adsorbent, metal, and PCM) was proposed and numerically applied on a vacuum swing adsorption (VSA) process[74]. This study evaluated direct heat transfer by modeling a pellet in the shape of a sphere with three layers. However, this modeled pellet was a theoretical proposal and could not be experimentally prepared at least until now.

In this study, to experimentally prepare the PCM-inserted adsorbent, the adsorbent should possess a large vacant space where phase change can occur, such as a mesopore. Also, to realize the concept of PCM-inserted adsorbent, separation of the space for existing adsorbate and the PCM inside the adsorbent is necessary. Hence, as for the adsorbent material for satisfying both conditions, three different materials are selected for the preparation of PCM-inserted adsorbent, i.e. mesoporous silica SBA-15, carbon nanotube (CNT), and mesoporous zeolite SSZ-13. Specific explanations about each concept of PCM-

inserted adsorbent will be discussed in the chapter 3.2, 3.3, and 3.3 respectively.

Moreover, in this chapter, the heat recovery efficiency of the proposed each concept of PCM-inserted adsorbent was theoretically evaluated through a dehumidifying fixed-bed adsorption process. The heat-recovery efficiency of each concept is evaluated by improvement of adsorption performance, which is the amount of adsorbed water-vapor at the same period of time during the initial stage. This is because, as mentioned above, PCM-inserted adsorbent is proposed in order to increasing adsorption performance, which is highly affected by temperature increase such as short-times adsorption process, PSA.

In general, PCM containers such as polymer capsule, spheres, metal voids were separately added into the adsorbent bed, thereby, PCM containers and adsorbent pellets are mixed in the bed. In this case, the PCM containers and the adsorbent pellets are mostly distributed heterogeneously in the bed, owing to their density difference. On the contrary, in case of PCM-inserted adsorbent, adsorbent itself works as containers for PCM, thereby, only PCM-inserted adsorbent pellet packed in the adsorbent bed. Accordingly, PCMs can be homogenously distributed in the adsorbent bed since there is no density difference among the PCM-inserted adsorbent pellets. This is another advantage of PCM-inserted adsorbent. In this study, to clarify this advantage of PCM-inserted adsorbent, a dehumidifying fixed-bed adsorption process with different distributions of PCM capsules is also studied.

3.2 Concept 1 – Mesoporous silica SBA-15

3.2.1 Proposal of the concept

Mesoporous silica SBA-15 is a material that possessing crystalline hexagonal structure with cylindrical pores. In this chapter, SBA-15 is used as an adsorbent of PCM-inserted adsorbent. In the concept of SBA-15, PCM is fully inserted in the mesoporous space of SBA-15. The schematic image of PCM-inserted SBA-15 is illustrated in Figure 45 below.

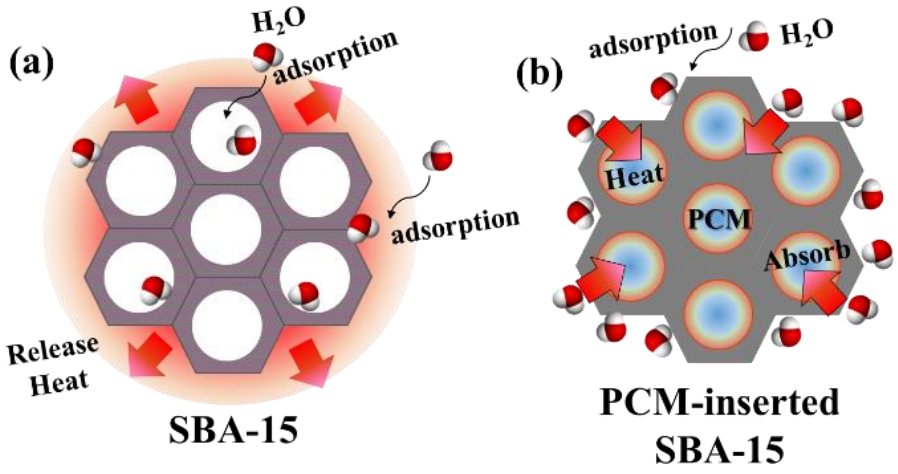

Figure 45. Schematic image of (a) SBA-15, and (b) PCM-inserted SBA-15.

As you can notice from Figure 45, if there is no PCM exist, the mesoporous space and the external surface of SBA-15 is both used as adsorption site. On the contrary, in case of PCM-inserted SBA-15, mesoporous space is fully occupied by PCM. Therefore, the major adsorption site can be considered as an external space or intergranular space of SBA-15. The released heat from the adsorption site, transfers to the silica wall of SBA-15, then transfers to PCM, subsequently absorbed by the PCM. In this concept, heat-transfer distance can be considered as appx. 3 nm (thickness of silica wall of SBA-15) ~ 0.5 um (radius of the particle of SBA-15).

3.2.2 Experimental - Preparation of PCM-inserted SBA-15

As for the PCM, paraffin(C22, Docosane) was inserted in mesopore of SBA-15 via vapor transportation. The method 'vapor transportation' is already confirmed as PCM confining method that only into the mesoporous space in chapter 2.3.2. The detail procedure of vapor transportation is described in chapter 2.2.4. The porous structure properties of prepared paraffin (As for PCM)-inserted SBA-15 is characterized by nitrogen adsorption. In addition, a water-vapor adsorption isotherm is measured to identify that adsorption site is still remained after inserting PCM. The water-vapor adsorption is measured at 6 different temperature to investigate a temperature dependence on the water-vapor adsorption isotherm of PCM-inserted SBA-15 whether PCM exists as liquid or solid. Also, isosteric heat of adsorption is calculated. Moreover, the melting properties of inserted paraffin, i.e. phase change temperature and the enthalpy of fusion, is characterized by DSC. DSC measurement is repeat for 5 times to investigate that inserted PCM is leaked or not from the mesopores with repeated thermal treatment.

3.2.3 Theoretical evaluation

To evaluate the performance of PCM-inserted SBA-15, a fixed-bed dehumidifying adsorption process was simulated under adiabatic conditions with three different adsorbents, i.e., SBA-15, SBA-15 with PCM capsules, and PCM-inserted SBA-15, was carried out. Specifically, SBA-15 without PCM was simulated as a reference. SBA-15 with PCM capsules was also simulated as a comparative method of inserting PCM. In case of SBA-15 with PCM capsules, the distribution of capsules in the adsorbent bed must be considered. Hence, SBA-15 with different distributions of PCM capsules in the bed, are also simulated.

In the calculation, assumption that the adsorption system is under adiabatic condition was necessary to investigate the effect of heat recovery through PCM on the adsorption performance. The enthalpy of fusion of inserted PCM was considered as a function of temperature, according to the literature of Karthikeyan[75]. Moreover, water-vapor adsorption isotherms of SBA-15 and PCM-inserted SBA-15, were considered as function of relative pressure, i.e. $q^* = f(p/p_0)$. Here, p_0 is a function of temperature, hence, the equilibrium amount of water vapor can also be considered a function of temperature.

In detail, for establishing the mathematical models, the following 15 assumptions were made:

1. Adiabatic condition
2. The effect of the wall of the column neglected
3. Ideal-gas behavior (i.e., PV = nRT)
4. 1D-model. Axial-direction profiles considered. Radial-direction profiles neglected.
5. Axial dispersion neglected
6. Adsorption mass balance followed the linear driving force (LDF) model
7. Radial-temperature profile inside the pellet neglected
8. Inert gas used: Nitrogen
9. Adsorption of nitrogen is neglected
10. All the physical properties are independent of the temperature

11. Constant bed void fraction

12. Constant concentration and temperature at the inlet

13. Enthalpy of melting, H, linearly increases with increase in temperature T

$H(T) = bT + c,\ T_{start} \leq \mathrm{T} \leq T_{end}$

14. Water-vapor-adsorption isotherm is considered a function of the relative pressure.

15. Diffusion inside the mesopore is neglected in case of the PCM-inserted adsorbent because the mesopore is completely filled with the PCM.

3.2.3.1 Governing equation

Basically, the mathematical model of fixed-bed adsorption is based on a set of partial differential equations along the axial direction, referenced from several previous works[4,76–78]. The energy balance and mass balance equations of 3 types of adsorbent, i.e. SBA-15, SBA-15 with PCM capsule and PCM-inserted adsorbent, are governed as follows:

<u>Type 1. SBA-15</u>

Overall mass balance : $\frac{\partial C}{\partial t} + u\frac{\partial C}{\partial x} + \frac{\rho_B}{\varepsilon}\frac{dq}{dt} = 0$ (Eq.4)

Adsorption rate : $\rho_B \frac{dq}{dt} = K_{LDF}\,(q^* - q)$ (Eq.5)

Energy balances for fluid : $c_{p,F}\rho_F \frac{\partial T_F}{\partial t} + c_{p,F}\rho_F u\frac{\partial T_F}{\partial x} - h_1 a_1 \frac{(1-\varepsilon)}{\varepsilon}(T_p - T_F) = 0$ (Eq.6)

Energy balances for pellet : $c_{p,p}\rho_p \frac{\partial T_p}{\partial t} + h_1 a_1 (T_p - T_F) - Q_{st}\rho_p \frac{dq}{dt} = 0$ (Eq.7)

<u>Type 2. SBA-15 with PCM capsule</u>

Component ratio : $\varepsilon + \varepsilon_p + \varepsilon_{cap} = 1$ (Eq.8)

Overall mass balance : $\frac{\partial C}{\partial t} + u\frac{\partial C}{\partial x} + \frac{\rho_B}{\varepsilon}\frac{dq}{dt} = 0$ (Eq.9)

Adsorption rate : $\rho_B \frac{dq}{dt} = K_{LDF}\,(q^* - \mathrm{q})$ (Eq.10)

Energy balances for fluid :

$c_{p,F}\rho_F \frac{\partial T_F}{\partial t} + c_{p,F}\rho_f u\frac{\partial T_F}{\partial x} + h_1 a_1 \frac{\varepsilon_p}{\varepsilon}(T_F - T_p) + h_2 a_2 \frac{\varepsilon_{cap}}{\varepsilon}(T_F - T_{cap}) = 0$ (Eq.11)

Energy balances for pellet : $c_{p,p}\rho_p \frac{\partial T_p}{\partial t} + h_1 a_1 (T_p - T_F) - Q_{st}\rho_p \frac{dq}{dt} = 0$ (Eq.12)

Energy balances for PCM capsule:

$$h_2 a_2\left(T_F - T_{cap}\right) + \rho_{pcm}\frac{\partial H(T)}{\partial t} = c_{p,cap}\rho_{cap}\frac{\partial T_{cap}}{\partial t} \quad \text{(Eq.13)}$$

Type 3. PCM-inserted SBA-15

Overall mass balance: $\frac{\partial C}{\partial t} + u\frac{\partial C}{\partial x} + \frac{\rho_B}{\varepsilon}\frac{dq}{dt} = 0$ (Eq.14)

Adsorption rate : $\rho_B\frac{dq}{dt} = K_{LDF}\,(\,q^* - \mathrm{q})$ (Eq.15)

Energy balances for fluid :

$$c_{p,F}\rho_F\frac{\partial T_F}{\partial t} + c_{p,F}\rho_f u\frac{\partial T_F}{\partial x} - h_1 a_1\frac{(1-\varepsilon)}{\varepsilon}\left(T_p - T_F\right) = 0 \quad \text{(Eq.16)}$$

Energy balances for pellet :

$$c_{p,p}\rho_p\frac{\partial T_p}{\partial t} + h_1 a_1\left(T_p - T_F\right) - Q_{st}\rho_p\frac{dq}{dt} + \rho_{pcm}\frac{\partial H(T)}{\partial t} = 0 \quad \text{(Eq.17)}$$

Initial condition

For $0 \le x \le L$

$T_F = T_{F,in}, T_p = T_{F,in}, T_{cap} = T_{F,in}$

$\frac{dq}{dt} = 0,\ \frac{dC}{dt} = 0,\ \frac{dC}{dx} = 0$

Boundary condition

at $x = 0,\ \ T_F = T_{F,in},\ \mathrm{C} = C_0$

at $x = L,\ \frac{dT_F}{dx} = 0\ ,\ \frac{dC}{dx} = 0$

In the calculation, all equations are changed in form of dimensionless parameters defined as follow:

$$\bar{u} = u/u_0$$

$$\overline{T_F} = T_F/T_{F,in},\ \overline{T_p} = T_p/T_{F,in},\ \overline{T_{pcm}} = T_{pcm}/T_{F,in}$$

$$\bar{X} = x/L$$

$$\bar{t} = u_0 t/L$$

The equations are discretized by the explicit method for the calculations. And equations are solve computationally using Excel/VBA.

3.2.3.2 Estimation of model parameters

Calculation of saturation pressure of water vapor, P_0

P_0 was calculated from antoine equation:

$$log_{10}P_0 = A - \frac{B}{C+T} \quad \text{(Eq.18)}$$

Calculation of LDF overall mass transfer coefficient, K_{LDF}

Basically, K_{LDF} is calculated by the equation from the work of Gorbach as follows:

$$\frac{1}{K_{LDF}} = \frac{R_p}{3k_F}\frac{q^*\rho_s}{C} + \frac{{R_p}^2}{15\varepsilon_s D_{eff}}\frac{q^*\rho_s}{C} + \frac{{R_s}^2}{15D_s} \quad \text{(Eq.19)}$$

Here, the first term represents mass transfer at boundary film, the second term represents diffusion in macroporous media in pellet and the last term is derived from the diffusion in particle of adsorbent. However, in case of PCM-inserted SBA-15, mesoporous space is fully occupied with PCM. Therefore, in case of PCM-inserted SBA-15, the last term at SEq.18, which represents diffusion in the mesopores, can be neglected and K_{LDF} is calculated by the equation as follows:

$$\frac{1}{K_{LDF}} = \frac{R_p}{3k_F}\frac{q^*\rho_s}{C} + \frac{{R_p}^2}{15\varepsilon_s D_{eff}}\frac{q^*\rho_s}{C} \quad \text{(Eq.20)}$$

k_F is mass transfer coefficient at boundary film. k_F is calculated from Carberry equation:

$$\frac{k_F\varepsilon}{u}\left(\frac{\mu_F}{\rho_F D}\right)^{2/3} = 1.15\left(\frac{d_p u \rho_F}{\mu_F \varepsilon}\right)^{-1/2} \quad \text{(Eq.21)}$$

Calculation of diffusion coefficients

A molecular diffusion coefficient D was calculated from stokes-einstein equation:

$$D = \frac{k_B T}{6\pi\mu a} \quad \text{(Eq.22)}$$

Effective diffusion coefficient D_{eff} can be obtained from tortuosity τ and porosity ε_{macro}. In the mesopores of SBA-15, diffusion coefficient D_s was calculated from knudsen diffusion coefficient D_k.

$$D_{eff} = \frac{\varepsilon_{macro}}{\tau} D$$

$$D_k = \frac{2}{3} r_{pore}\sqrt{\frac{8RT}{\pi M}}\ , D_0 = \frac{1}{D} + \frac{1}{D_k}\ ,\ D_s = \frac{\varepsilon_{meso}}{\tau} D_0 \ \text{(Assume } \tau = 3)$$

Calculation of Heat transfer coefficient

Heat transfer coefficient between fluid-pellet and fluid-PCM capsule was calculated by equations that used in literature of Rady as below[15]:

$$h = J_h c_{p,F} G/Pr^{2/3} \ ,Pr = \ c_p\mu/k, \ G = \ \rho_F u/\varepsilon \ ,J_h = \ 0.052Re^{-0.3} \ ,Re = \ \rho uD/\mu$$

Specific parameters used in study

The Specific value of parameters used in the calculations used in the simulation of dehumidifying fixed-bed adsorption is shown in Table 6. In addition to the estimated parameters described above, basic parameters related to the column, such as column length, column diameter, void fraction, inlet temperature, concentration of water vapor at the inlet, and superficial flow velocity are assumed parameters in this study. As for the PCM capsule, melamine resin capsule with 70wt% of PCM loading is assumed as the material of capsule. The sizes of adsorbent pellet and the PCM capsule are also assumed values.

On the other hand, heat capacity and density of pellet is calculated values from the bulk mesoporous silica or paraffin parameters. Those bulk parameter values are referenced from the data sheets[97]. For example, pellet density ρ_p is calculated from bulk density ρ_{bulk} as follows:

$$\rho_p = \rho_{bulk} \times (1 - \varepsilon_{macro})$$

Also, the value of void fraction inside the pellet, ε_{macro}, is reference from previous work[79].

Finally, the ratio of PCM inserted in adsorbent, the phase change temperature of PCM inside the mesopores, and the enthalpy of fusion of PCM are measured values during experimentally prepared.

Table 6. Parameters used in the simulation.

column	
Column length, L	0.6 m
Column diameter, d_c	0.06 m
Void fraction, ε	0.4
Inlet temperature, $T_{F,in}$	303 K
Relative concentration of water vapor at the inlet	50 %
Concentration of water vapor at the inlet, C_{in}	0.842 mol/m^3
Superficial flow velocity, u_0	0.6 m/s
Adsorbent (Type1. SBA-15)	
Pellet density, ρ_p	333 kg/m^3
Diameter of a pellet, d_p	0.002 m
Heat capacity of a pellet, $C_{p,p}$	730 J/kg·K
Isosteric heat of adsorption, Q_{st}	42.0 KJ/mol
Pellet porosity, ε_s	0.845
Mesopore porosity of a particle, ε_{meso}	0.648
Macropore porosity of a particle, ε_{macro}	0.476
Adsorbent (Type2. PCM-inserted SBA-15)	
Pellet density, ρ_p	551 kg/m^3
Diameter of a pellet, d_p	0.002 m
Heat capacity of a pellet, $C_{p,p}$	1037 J/kg·K
Isosteric heat of adsorption, Q_{st}	43.6 KJ/mol
Pellet porosity, ε_s	0.476
Macropore porosity of a particle, ε_{macro}	0.476
Mesopore porosity of a particle, ε_{meso}	0
Ratio of PCM in the adsorbent, w_1	0.655 g-PCM/g-SBA-15
Phase change start temperature, T_{start}	304 K
Phase change end temperature, T_{end}	317 K
Enthalpy of fusion, H	53.3 J/g-PCM
PCM capsule	
Capsule fraction in the bed, ε_{cap}	0.267
Pellet fraction in the bed, ε_p	0.333
Capsule density, ρ_{cap}	995 kg/m^3
Pellet density, ρ_p	333 kg/m^3
Diameter of a capsule, d_{cap}	0.002 m
Heat capacity of a capsule, $C_{p,cap}$	0.002 m
Ratio of PCM in a capsule, w_2	0.7
Phase change start temperature, T_{start}	316 K
Phase change end temperature, T_{end}	328 K
Enthalpy of fusion, H	236.5 J/g-PCM

Packed amount of SBA-15 and PCM in bed

In the fixed-bed, packed amount of SBA-15 and PCM in fixed-bed with 3 types of adsorbents were calculated from the parameters used in this study (See Table 1), and listed in Table 7. Also, the equilibrium amount of water-vapor adsorbed q^* on each type of adsorbent, calculated from the result of the water vapor adsorption isotherm when inlet humidity is 50 %, is also listed in Table 7.

Table 7. Packed amount of SBA-15 and PCM in bed.

	Amount of SBA-15 [kg / m^3]	Amount of PCM [kg / m^3]	q^* [mg-H_2O/g-silica]
SBA-15	200	0	213
SBA-15 + PCM capsule	111	185	213
PCM-inserted SBA-15	200	131	157

In case of SBA-15 with PCM capsule, packed amount of SBA-15 was the smallest in bed, owing to the dead volume, resulted from the occupied volume of PCM capsules. Correspond to the decrease of the amount of SBA-15, the amount of adsorbed water-vapor in the bed will decrease. In case of PCM-inserted SBA-15, q^* is decreased owing to the existence of PCM inserted in SBA-15. However, same amount of SBA-15 was packed in bed. Whether in case of PCM capsule or PCM-inserted SBA-15, eventually, existence of PCM decrease the saturated amount of adsorption.

3.2.4 Results and Discussion

3.2.4.1 Preparation of PCM-inserted SBA-15

As a PCM-inserted adsorbent, paraffin-inserted SBA-15 is prepared and characterized by nitrogen adsorption. The specific characterization results of SBA-15 is described in previous chapter, which is characterization results of SBA-15-7.6 nm in chapter 2.3.1. The nitrogen adsorption-desorption isotherm of both SBA-15 and the PCM-inserted SBA-15 are depicted in Figure 46. In Figure 46, the amount of adsorbed nitrogen on the PCM-inserted SBA-15 was extremely smaller than that of SBA-15 in the range of middle-high relative pressure. This suggests that paraffin is successfully occupying the mesoporous space of SBA-15. The amount of adsorbed nitrogen was also extremely decreased in the range of low relative pressure with inserting PCM. This indicates that microporous space is filled with PCM or becoming non-accessible space by inserting PCM. The porous properties before and after inserted PCM into SBA-15 is summarized in Table 8. According to the results in Table 8, the microporous volume decreased to 0 after inserting PCM, and mesoporous volume becomes appx. 70 % decreased after inserting PCM. This results suggests that PCM is inserted into both microporous and mesoporous space. Therefore, it can be confirmed that nearly 70 % of mesoporous space is filled with PCM, and 30 % of mesoporous space is left as vacant space.

Then, the water-vapor adsorption isotherm was measured (See Fig. 47). As you can notice from Figure 47, the amount of adsorbed water decreased with existence of PCM. This suggests that the adsorption sites exist on the PCM-inserted SBA-15 decreased owing to the decreased of mesopore volume, which occupied by PCM. However, considerable amount of the adsorption sites of the PCM-inserted SBA-15 remained after inserting PCM. The amount of adsorbed water vapor on PCM-inserted SBA-15 when the relative pressure P/P_0 was 0.75 was 300 mg-H_2O/g-silica. When the P/P_0 is higher than 0.75, condensation was observed in Figure 47. Hence, this amount of adsorbed water is considered as the amount correspond to the adsorbed on the external surface and the vacant mesoporous space. This 300

mg-H_2O/g-silica of adsorbed water vapor shows good agreement with the vacant mesoporous space after inserting PCM, which is 0.305 cc/g, in Table 8. Therefore, adsorption site is suggested that not only external surface but also vacant mesoporous space. Also, since condensation of water molecules was observed after PCM inserted into SBA-15 in the high relative pressure range, intergranular spaces can be also utilized as adsorption site.

In the concept of PCM-inserted SBA-15 which described in chapter 3.2.1, the mesoporous space of SBA-15 is fulfilled with PCM and only external surface or intergranular space is works as adsorption site. However, in the prepared PCM-inserted SBA-15 in this study, PCM was occupied appx. 70 % of the mesoporous space, not 100%. Subsequently, left 30 % of mesoporous space is added to the adsorption site. However, as depicted in the Figure 48, the amount of adsorbed water vapor did not change with repeated measurement of adsorption isotherm. Also, the paraffin is a hydrophobic molecule and the water is a hydrophilic molecules. Both molecules does not dissolve to each other. Therefore, it can be considered that paraffin and water molecules are separated inside the mesoporous space.

Based on these results, a schematic image of paraffin (PCM) and water molecules (adsorbate) inside the PCM-inserted SBA-15 can be illustrated as Figure 49. Paraffin is a hydrophobic molecule and the surface of mesoporous silica SBA-15 is slightly hydrophilic owing to the existence of silanol group (Si-OH). This can be also noticeable from the water vapor adsorption isotherm of SBA-15. Therefore, in terms of hydrophobic/hydrophilic, PCM is expected to be exist with convex meniscus as shown in Figure 49. Also, since the microporous volume of PCM-inserted SBA-15 was 0 in the Table 8, the microporus space is expected to be non-accessible or fully occupied, as shown in Figure 49.

Consequently, from these results of nitrogen adsorption and water vapor adsorption isotherms depicted in Figure 46 and Figure 47, it can be conclude that paraffin is successfully inserted into SBA-15, and prepared PCM-inserted SBA-15 can work as adsorbent for capturing water.

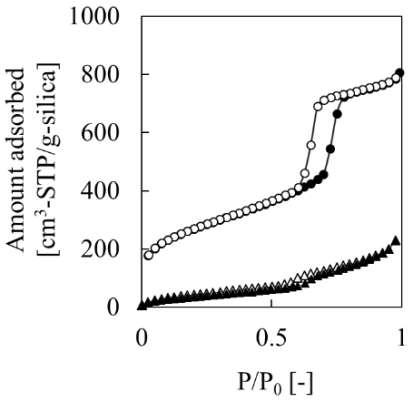

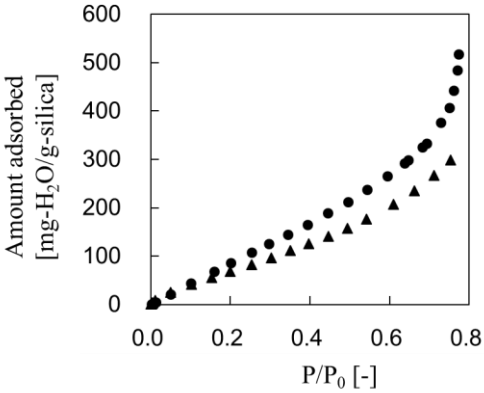

(Left) Figure 46. Nitrogen adsorption/desorption isotherm of SBA-15(○, ●) and the PCM-inserted SBA-15 (△,▲), open: adsorption, closed: desorption.

(Right) Figure 47. Water vapor adsorption isotherm of SBA-15(●) and the PCM-inserted SBA-15 (▲).

Table 8. Porous characteristics of SBA-15 and PCM-inserted SBA-15

Sample	S_{BET} [m²/g-silica]	V_{total} [cc/g-silica]	V_{micro}* [cc/g-silica]	V_{meso} [cc/g-silica]	D_{pore} [nm]	A [nm]	Wall thickness [nm]
SBA-15	941	1.093	0.115	0.978	7.6	11.4	3.8
PCM/SBA-15	132	0.305	0.000	0.305			

* calculated by t-plot method.

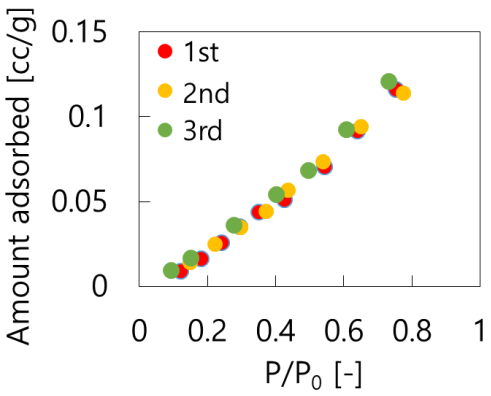

Figure 48. Repeatability of a water vapor adsorption isotherm of PCM-inserted SBA-15.

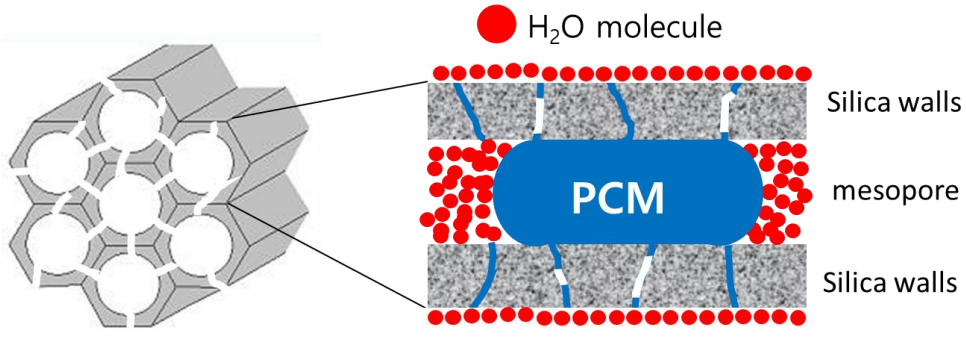

Figure 49. Schematic image of prepared PCM-inserted SBA-15.

In addition, to investigate the temperature dependence of water vapor adsorption isotherm and calculate isosteric heat of adsorption, Q_{st}, water-vapor adsorption at different temperature was measured. Figure 50 (a) depict water-vapor adsorption isotherm of SBA-15 at 20 ℃, 30 ℃, 40 ℃. Figure 50 (b) and (c) depict water-vapor adsorption isotherm of PCM-inserted SBA-15 at 20 ℃, 25 ℃, 30 ℃, 35 ℃, 40 ℃, and 45 ℃. Inserted PCM exists solid state at 20 – 30 ℃ and liquid state at 35 – 45 ℃. There was no temperature dependence of water vapor adsorption isotherms when the adsorption isotherm is a function of relative pressure P/P_0 in both SBA-15 and PCM-inserted SBA-15. The isosteric heat of adsorption of water vapor on SBA-15 and PCM-inserted SBA-15 was 42.0 kJ/mol and 43.6 kJ/mol, respectively. Also, there was no difference in the isosteric heat of adsorption where PCM exist as the solid state or the liquid state.

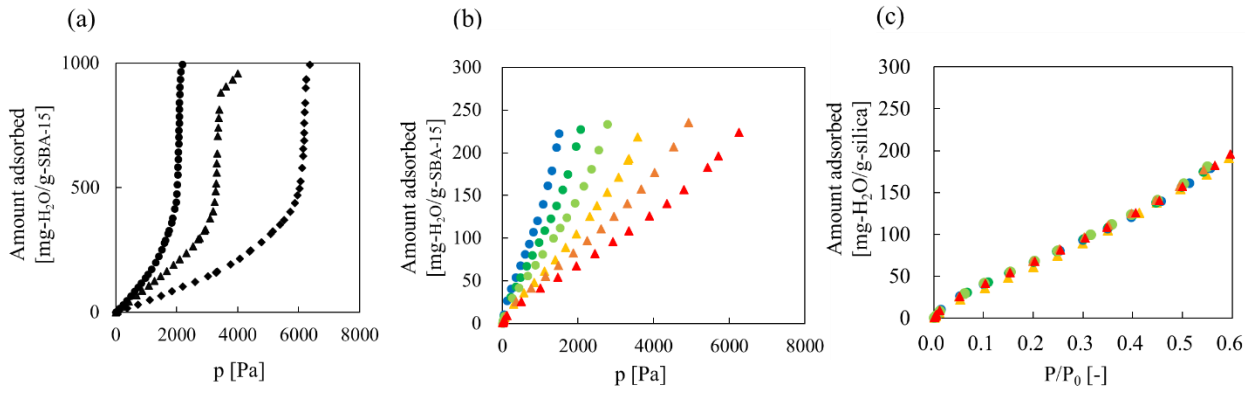

Figure 50. (a) water vapor adsorption isotherm of SBA-15 at 20 ℃ (●), 30 ℃ (▲), 40 ℃ (◆). (b), (c) water vapor adsorption isotherms of PCM-inserted SBA-15 with different pressure unit at 20 ℃ (●, blue), 25 ℃ (●, green) , 30 ℃ (●, yellowgreen), 35 ℃ (▲, yellow), 40 ℃ (▲, orange), and 45 ℃ (▲, red) with different pressure unit.

The melting properties of PCM-inserted SBA-15 was characterized by DSC. Figure 51 (a) depict the repeated DSC curves of the paraffin inserted into the mesopores of SBA-15. During the operation, the temperature was raised in the speed of 10 K/min. As for a reference, the DSC curves of original, not inserted paraffin is demonstrated in Figure 51 (b). First, phase-change peak of inserted paraffin, observed in Figure 51 (a), did not change during the repeated heating and cooling. This indicates that the inserted PCM did not leak from the mesopore during repeated thermal treatment, possibly due to strong surface tension. Also, as depicted in Figure 51 (b), melting point of inserted paraffin was 31 ℃, and the enthalpy of fusion was 53.3 J/g-PCM. This value of enthalpy of fusion is only 23 % of the value of the original value, i.e. 236.5 J/g-PCM. The melting point of inserted paraffin is also lower than that of the original value, i.e. 43 ℃. The reason why melting properties of inserted PCM is lowered than bulk state is already discussed in previous chapter 2.3.3. Although the melting properties are changed, but from the results of Figure 51, phase change of paraffin occurred inside of the mesopores of SBA-15, which suggests that inserted paraffin can be work as latent-heat-storage material.

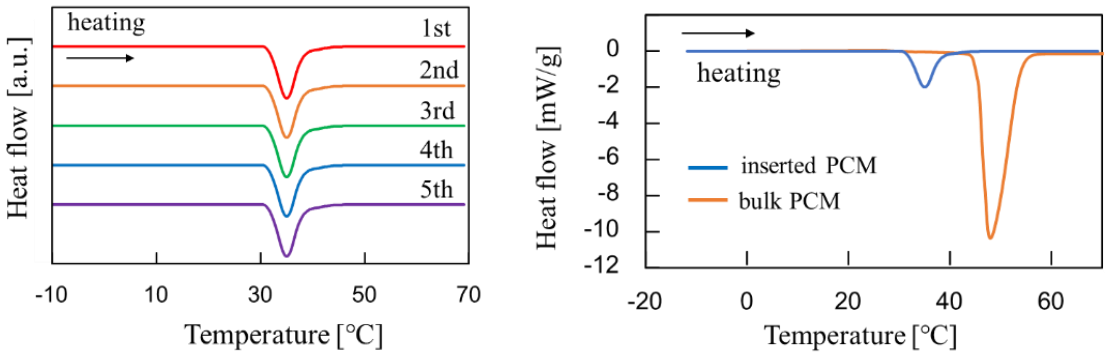

Figure 51. (a) DSC curves of the PCM-inserted SBA-15 with repeated measurements, and (b) DSC curves of inserted PCM and bulk PCM.

According to the results of water-vapor adsorption isotherm and DSC measurement, it can be concluded that PCM-inserted SBA-15, which possess both adsorption site and heat-storage site, is successfully prepared.

3.2.4.2 Theoretical evaluation

The objective of this theoretical study is an evaluation of the effectiveness of the proposed new concept, PCM-inserted SBA-15, by comparing the effectiveness of conventional SBA-15 or SBA-15 with PCM capsules in the dehumidifying fixed-bed adsorption. However, in case of SBA-15 with PCM capsules, the distribution of PCM capsules in fixed-bed should be considered. This is because, there is a density difference between the PCM capsules and the SBA-15 pellet. On the contrary, PCM-inserted adsorbent has an advantage that those pellets can homogeneously distribute in the bed. Hence, first, to clarify this advantage of PCM-inserted adsorbent, a dehumidifying fixed-bed adsorption process with different distributions of PCM capsules is also studied. Paraffin (C22, Docosane) was also used for the PCM capsule. The melting behavior of the encapsulated PCM was assumed to follow that of the bulk state, which is shown in Figure 51 (b). Various heterogeneous capsule distribution was calculated. To simply reflect the various distributions of PCM capsules in the simulation, fixed-bed was layered by 9 layer. Each layer is packed by SBA-15 or PCM capsule respectively, which demonstrated in Figure 52. Basically, specific parameters used in simulation were same to Table 6, except fluid temperature at inlet, $T_{f,in}$ and the concentration at inlet C_{in}. The value of $T_{f,in}$ was changed to 313 K, and the value of C_{in} was changed to 1.417 mol/m^3. Higher inlet temperature and concentration of fluid was chosen to achieve more noticeable difference under various capsule distribution.

The changes of temperature of fluid at the outlet is depicted in Figure 53 (a). The changes of adsorbed amount of water-vapor in total fixed-bed of SBA-15 with various capsule distribution during 5 min is shown in Figure 53 (b). Finally, a ratio of amount of stored heat by PCM to the enthalpy of fusion in the bed with time changes is depicted in Figure 53 (c).

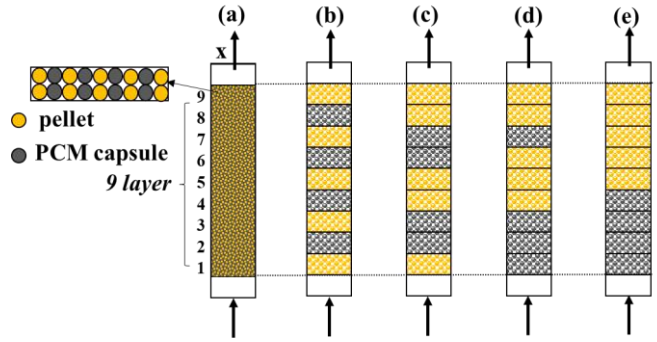

Figure 52. Various PCM capsule distribution in bed used in the simulation (a) capsule homogenously distribute in bed, (b) SBA-15: layer 1,3,5,7,9 and PCM capsule: layer 2,4,6,8 (c) SBA-15: layer 1,4,5,8,9 and PCM capsule: layer 2,3,6,7, (c) SBA-15: layer 4,5,6,8,9 and PCM capsule: layer 1,2,3,7, and (d) SBA-15: layer 5,6,7,8,9 and PCM capsule: layer 1,2,3,4.

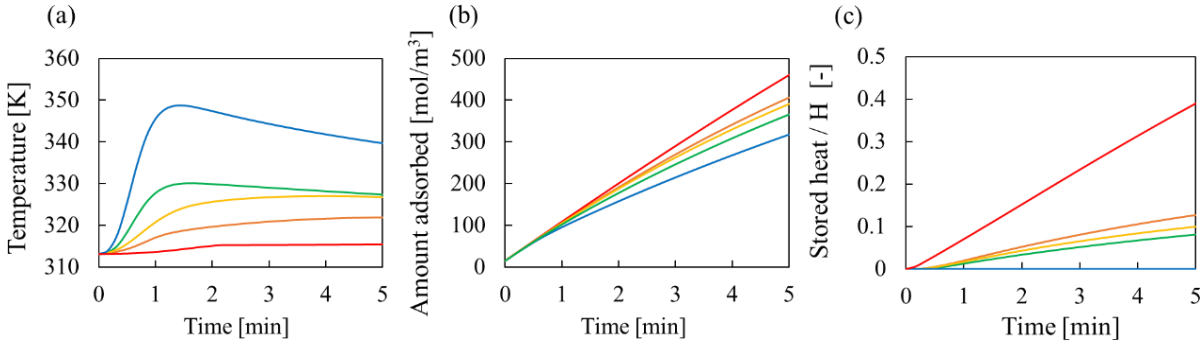

Figure 53. (a) Temperature of fluid at outlet, (b) amount of water-vapor adsorbed, and (c) ratio of amount of stored heat through PCM to the enthalpy of fusion in bed with time changes, under various conditions of PCM capsule distribution as a function of time. Red line (Fig.52 (a)), orange line (Fig.52 (b)), yellow line (Fig.52 (c)), green line (Fig.52 (d)), and blue line (Fig.52 (e)).

Among various distribution, homogeneous distribution of PCM capsule (See Fig.52 (a)) showed most high adsorption performance, as depicted in Figure 53 (b). When PCM capsules distribute more heterogeneously in the fixed-bed (See, from Fig.52 (a) to Fig.52 (e)), the temperature of fluid at outlet increased more, and the amount of adsorbed water vapor gradually decreased. Also, as you can notice from Figure 53 (c), the stored heat through PCM decreased when encapsulated PCM distribute heterogeneously. Especially, in case of Figure 52 (e), the stored heat through PCM was 0, which indicates that encapsulated PCM could not works as

heat storage material. From these results, the distribution of PCM capsule affect the efficiency of heat-storage, and subsequently affect to the performance of adsorption process.

Then, a simulation of dehumidifying fixed-bed adsorption process with three different adsorbents, i.e., SBA-15, SBA-15 with a PCM capsule, and PCM-inserted SBA-15, was performed under entirely adiabatic condition. As already mentioned, in case of SBA-15 with PCM capsule, the phase change behavior of encapsulated PCM is assumed as same to that of bulk PCM. Hence, the phase-change starting temperature was different when PCM is encapsulated or inserted. For considering this difference in phase-change starting temperature, 3 different types of SBA-15 with PCM is simulated, i.e. SBA-15 with homogenously distribute PCM capsules, and SBA-15 with the heterogeneously distributed PCM capsule, and SBA-15 with homogenously distribute PCM capsule where phase change occurs at same temperature of inserted PCM. For each adsorbent, the fluid temperature at the outlet (See Fig. 54 (a)), the ratio of the absorbed heat through the PCM to the enthalpy of fusion, χ, (See Fig. 54 (b)), the amount of water-vapor adsorbed in total fixed-bed (See Fig.54 (c)), and the ratio of the amount adsorbed q to the equilibrium amount adsorbed q^* (See Fig. 54 (d)) were calculated in the initial 5 min. The reason why showing only the results during initial 5 min is because the target for employing PCM-inserted adsorbent is a non-isothermal and apparently adiabatic adsorption process such as short-time-scale adsorption process. Parameter χ in Figure 54 (b) indicates that how much percentage of latent heat is used to store the generated heat of adsorption. As depicted in Fig. 54 (a), both encapsulated PCM system (green line) and inserted PCM system (red line) showed isothermal behaviors during the initial 5 min adsorption process. Isothermal behavior during adsorption under adiabatic condition suggested that PCM in the fixed-bed, successfully stored the thermal energy of the released heat of adsorption. This can be also confirmed from the results of Fig. 54 (b). In Fig.54 (b), at 5 min, the value χ was 93% for the PCM-inserted SBA-15 and 25% for SBA-15 with the PCM capsule that was assumed to have the same phase change temperature of the inserted PCM (green line). Here, the heat-storage capacity of inserted PCM is

smaller than encapsulated PCM, due to the smaller packed amount and the lower value of the enthalpy of fusion, thereby, the PCM-inserted SBA-15 showed higher χ value. In case of encapsulated PCM system with original phase change temperature (blue line), after the temperature reached the phase change temperature, 316 K, then the isothermal behavior was observed. Owing to this high phase changing temperature, the χ value reached to only 8 %, at 5 min (Fig. 54 (b)). As described already, unlike other encapsulated system, when the encapsulated PCM heterogeneous distribute (yellow line), encapsulated PCM could not work as heat-storage material for recovering released heat of adsorption. Hence, the temperature of fluid is increased dramatically (See Fig.54 (a)).

Accordingly, owing to the heat storage through PCM, the inserted PCM system and encapsulated PCM system showed increased amount of adsorbed water vapor, compared to the system without PCM (Fig. 54 (c)), despite of small q^*. As described in chapter 3.2.2.2, the decrease in the equilibrium amount of water vapor adsorbed q^* with existence of PCM is a weakness of using PCM in adsorption process. Therefore, the increase in the amount of adsorbed water-vapor in Fig.54 (c) suggests that, once again, heat recovery through PCM is highly important to achieve high performance. Among the various types of adsorbents, the PCM-inserted SBA-15 showed the highest amount of adsorbed water vapor in 5 min. Conversely, SBA-15 with a heterogeneously distributed PCM capsule (yellow line) showed the smallest amount of adsorbed water.

In addition, from Fig. 54 (d), the value of q/q^* increased with the existence of PCM, except encapsulated PCM system with a heterogeneous distribution. Figure 55 depicts the changes of the value q/q^*, from the inlet to the outlet, at various time, which were 0 min, 0.5 min, 1 min, 3 min and 5 min. As you can notice form Figure 55 (a), during initial 5 minute, the adsorption mainly occurred near the inlet, in the case of SBA-15. However, with existence of PCM, whether the encapsulated PCM or the inserted PCM, the adsorption of water vapor occurred from the inlet, then moved to the middle of the bed during initial 5 minutes (See Figs. 52 (b)–(e)). This suggest that the increase of adsorption performance with

the PCM was achieved owing to the rapid apparent adsorption rate by the heat recovery effect of the PCM.

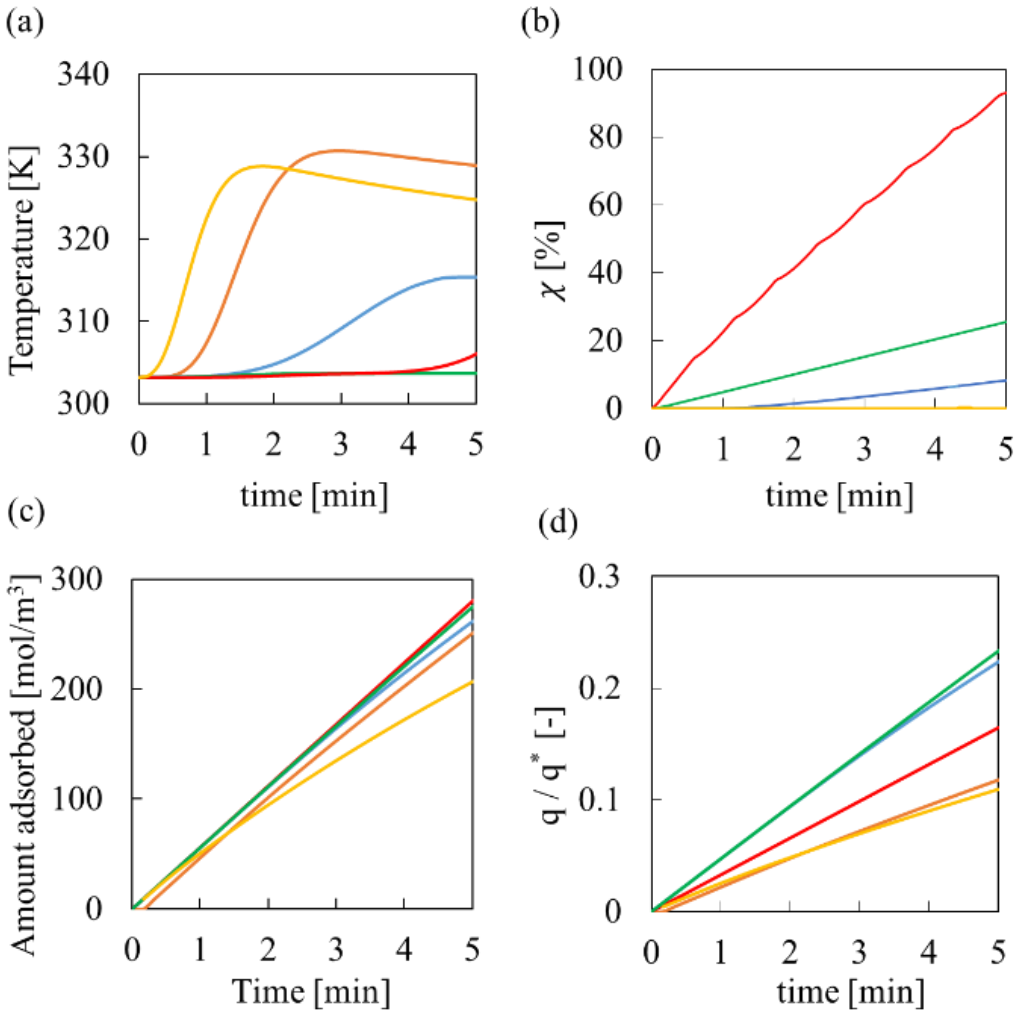

Figure 54. (a) Temperature changes of the fluid at the outlet, (b) the ratio of amount of stored heat through PCM to the enthalpy of fusion, (c) the amount of adsorbed water vapor, and (d) the ratio of the amount adsorbed to the equilibrium amount adsorbed in the bed with time changing when the packed adsorbent is SBA-15(orange), PCM-inserted SBA-15(red), SBA-15 with the PCM capsule (blue), SBA-15 with the PCM capsule that assumed to have same phase-change temperature of the inserted PCM (green), and SBA-15 with the heterogeneously distributed PCM capsule (yellow).

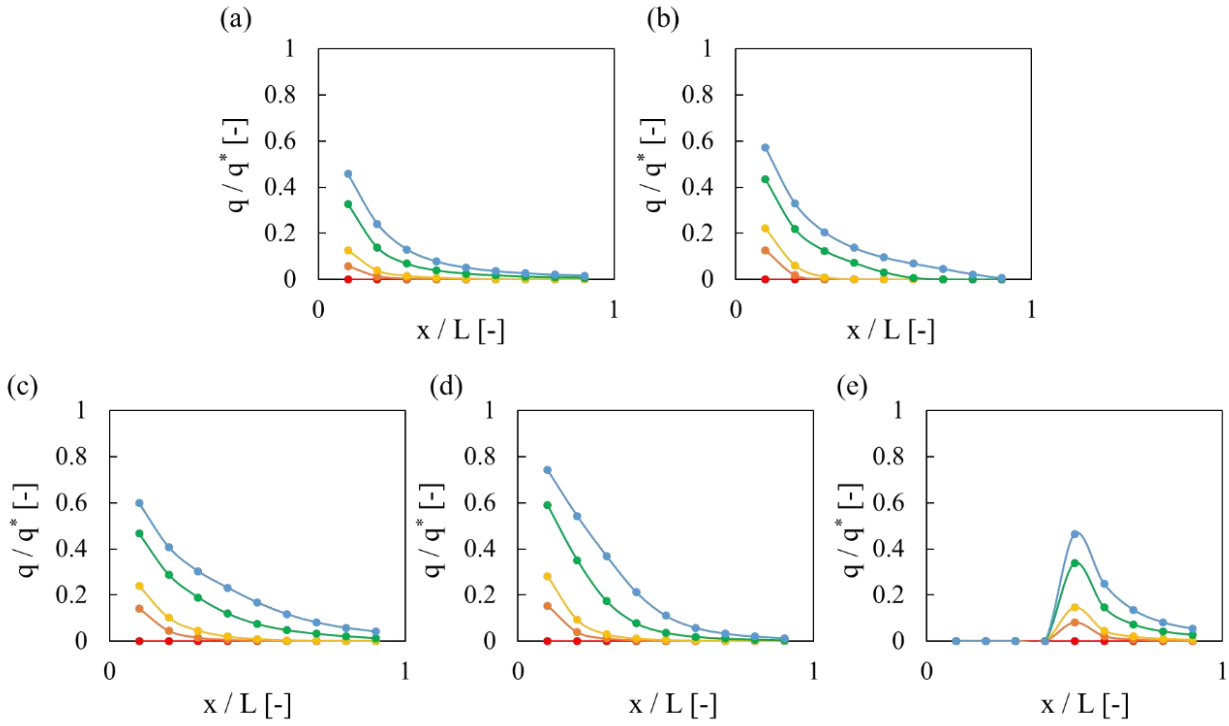

Figure 55. the ratio between the amount of adsorbed water vapor and saturated amount of adsorbed water vapor from inlet to outlet when packed adsorbent is (a) SBA-15, (b) PCM-inserted SBA-15, (c) SBA-15 with PCM capsule, and (d) SBA-15 with PCM capsule which assumed as same phase change temperature of the inserted PCM, (e) SBA-15 with heterogeneously distribute PCM capsule at various time. Red : 0 min, orange : 0.5 min, yellow: 1 min, green : 3 min, and blue : 5 min.

Furthermore, how much percentage of the released thermal energy during adsorption was transferred to the PCM or to the fluid at 5 min, was calculated. In the solo SBA-15 system, 46 % of the released amount of heat of adsorption was transferred to the fluid, and eliminated from the system. On the other hand, in the PCM-inserted system, 99 % of the released heat was absorbed by PCM, and only 1 % of the released heat transferred to the fluid, then eliminated from the system. Within 99 % of adsorbed heat by PCM, 79 % was used for latent-heat storage, and the other was used for sensible-heat storage. This heat recovered by the PCM, is expected to be re-used during the desorption process. In the encapsulated PCM system assumed to have the same phase change temperature of the inserted PCM, much larger amount of heat adsorbed by PCM, i.e. 99 % of the released heat of adsorption was adsorbed, and only 1 % of the heat transferred to the fluid. However, in case of encapsulating PCM, the heat-storage efficiency is dramatically decrease with changes in distribution. Also, for the fixed-bed adsorption under a high flow rate and high adsorption rate, the PCM-inserted adsorbent is expected to be a more effective method for recovering the heat of adsorption than the other PCM methods including PCM capsule, because the heat transfers through one step, i.e. directly from the adsorbent to the PCM in a short heat transfer distance because the PCM and adsorbate are in the same unit.

In summary, a PCM-inserted adsorbent is proposed for a new containing method of a PCM in an adsorption process. The dehumidifying fixed-bed adsorption process was simulated under adiabatic conditions with 3 types of adsorbents. The PCM-inserted adsorbent showed most high performance owing to the heat recovery effect of the PCM during initial 5 min. At 5 min, approximately 98 % of the released heat during adsorption, was recovered by the inserted PCM. PCM capsule also showed a high ability to recover the heat of adsorption. However, the heat-recovery efficiency of the PCM capsule was significantly decreased when it was distributed heterogeneously in the bed. On the contrary, PCM-inserted adsorbent always homogenously distribute in the bed. In conclusion, the PCM-inserted adsorbent is considered an effective method for recovering the heat of adsorption to achieve higher performance in the adsorption process.

3.3 concept 2 – carbon nanotube(CNT)

3.3.1 Proposal of the concept

Single wall carbon nanotube, SWCNT, is a cylindrical tube composed by one graphite sheet, with a pore size of approx.1-2 nm. The secondary structure of the SWCNT is looks like fibers, as depicted in Figure 56. Therefore, the size of secondary structure is widely distribute in the range of mesoporous- and macroporous- region. In this chapter, I focused on the secondary structure of SWCNT as a space for PCM, and propose CTN as an adsorbent of PCM-inserted adsorbent. In the step of inserted PCM into SWCTN using vapor transportation method, condensation of PCM occurs when the size of secondary structure is smaller than in some range. And, when the size of secondary structure is larger than this range, only surface adsorption of PCM occurs. The condensation of PCM indicates that the space is fully occupied by PCM, and the surface adsorption of PCM indicates that some spaces are remained for the adsorption. Therefore, in this concept, the separation of existing cites of PCM and adsorbate can be achieved by the size difference of secondary structure. The schematic image of PCM-inserted CNT is illustrated in Figure 57 below.

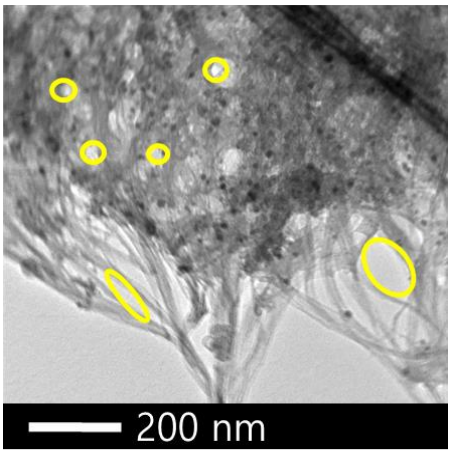

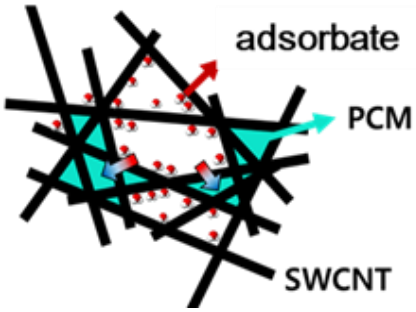

(Left) Figure 56. TEM image of SWCNT

(Right) Figure 57. Schematic image of PCM-inserted CNT

If there is no PCM exist, the porous space inside SWCNT, and also the secondary structural space of SWCNT are vacant, so these spaces can be used as an adsorption site. If PCM inserted in SWCNT using vapor transportation method, the porous space inside SWCNT and some small-size of secondary structure are occupied by PCM. Hence, the left spaces, which is large-size secondary structure, can be considered as the major adsorption site. And, the released heat from the adsorption site, i.e. some external surface and secondary structure space of SWCNT, transfers to the carbon wall, then transfers to PCM, and subsequently absorbed by the PCM.

3.3.2 Experimental – preparation of PCM-inserted CNT

As for the water-capturing adsorbent, carboxylic-acid functionalized SWCNT is purchased from Sigma-Aldrich(Carbon nanotube, single-walled, carboxylic acid functionalized). As for PCM, paraffin(C22, Docosane) was inserted into carboxylic-acid functionalized SWCNT via vapor transportation. The detail procedure of vapor transportation is described in chapter 2.2.4. The porous structure of purchased CNT, and the prepared paraffin-inserted CNT are characterized by nitrogen adsorption. In addition, a water-vapor adsorption isotherms of both samples are measured to identify that adsorption site is exist, before and after inserting PCM. The water-vapor adsorption is measured at 3 different temperature to investigate the temperature dependence on the isotherms of both CNT, and PCM-inserted CNT. Also, the isosteric heat of adsorption of water on CNT is calculated. Moreover, the melting properties of inserted paraffin, i.e. phase change temperature and the enthalpy of fusion, is characterized by DSC. DSC measurement is repeat for 5 times to investigate that inserted PCM leaks or not, from the secondary structures, with repeated thermal treatment.

3.3.3 Theoretical evaluation of PCM-inserted SBA-15

To evaluate the effectiveness of PCM-inserted CNT, a fixed-bed dehumidifying adsorption process was simulated under adiabatic conditions with two different adsorbents, i.e., CNT, and PCM-inserted CNT. Pure CNT was simulated as a reference. The enthalpy of fusion of inserted PCM was considered as a function of temperature. The water-vapor adsorption isotherm of CNT was considered as function of relative pressure, i.e. $q^* = f(p/p_0)$. The water-vapor adsorption isotherm of PCM-inserted CNT was followed by the Henry equation.

In detail, for establishing the mathematical models, the following 15 assumptions were made:

1. Adiabatic condition
2. The effect of the wall of the column neglected
3. Ideal-gas behavior (i.e., PV = nRT)
4. 1D-model. Axial-direction profiles considered. Radial-direction profiles neglected.
5. Axial dispersion neglected
6. Adsorption mass balance followed the linear driving force (LDF) model
7. Radial-temperature profile inside the pellet neglected
8. Inert gas used: Nitrogen
9. Adsorption of nitrogen is neglected
10. All the physical properties are independent of the temperature
11. Constant bed void fraction
12. Constant concentration and temperature at the inlet
13. Enthalpy of melting, H, linearly increases with increase in temperature T

    $H(T) = bT + c,\ T_{start} \leq \mathrm{T} \leq T_{end}$
14. Water-vapor-adsorption isotherm is considered a function of the relative pressure.
15. Diffusion inside the pore of CNT is neglected in case of the PCM-inserted CNT.

3.3.3.1 Governing equation

In the theoretical study, I assumed to neglect the temperature profiles in the PCM-inserted adsorbent pellet. Hence, since there are no differences in the mass- and energy- balances, the mathematical model of fixed-bed adsorption between PCM-inserted SBA-15 and PCM-inserted CNT, equations are basically equal to that used in chapter 3.2.2.1, which referenced from several previous works[4,76–78]. The energy- balance and mass- balances of two types of adsorbent, i.e. CNT, and PCM-inserted CNT, are governed as follows:

<u>Type 1. CNT</u>

Overall mass balance : $\frac{\partial C}{\partial t} + u\frac{\partial C}{\partial x} + \frac{\rho_B}{\varepsilon}\frac{dq}{dt} = 0$ (Eq.23)

Adsorption rate : $\rho_B \frac{dq}{dt} = K_{LDF}\,(q^* - q)$ (Eq.24)

Energy balances for fluid : $c_{p,F}\rho_F \frac{\partial T_F}{\partial t} + c_{p,F}\rho_F u\frac{\partial T_F}{\partial x} - h_1 a_1 \frac{(1-\varepsilon)}{\varepsilon}(T_p - T_F) = 0$ (Eq.25)

Energy balances for pellet : $c_{p,p}\rho_p \frac{\partial T_p}{\partial t} + h_1 a_1 (T_p - T_F) - Q_{st}\rho_p \frac{dq}{dt} = 0$ (Eq.26)

<u>Type 2. PCM-inserted CNT</u>

Overall mass balance: $\frac{\partial C}{\partial t} + u\frac{\partial C}{\partial x} + \frac{\rho_B}{\varepsilon}\frac{dq}{dt} = 0$ (Eq.27)

Adsorption rate : $\rho_B \frac{dq}{dt} = K_{LDF}\,(q^* - \mathrm{q})$ (Eq.28)

Energy balances for fluid : $c_{p,F}\rho_F \frac{\partial T_F}{\partial t} + c_{p,F}\rho_f u\frac{\partial T_F}{\partial x} - h_1 a_1 \frac{(1-\varepsilon)}{\varepsilon}(T_p - T_F) = 0$ (Eq.29)

Energy balances for pellet :

$$c_{p,p}\rho_p \frac{\partial T_p}{\partial t} + h_1 a_1 (T_p - T_F) - Q_{st}\rho_p \frac{dq}{dt} + \rho_{pcm}\frac{\partial H(T)}{\partial t} = 0 \quad \text{(Eq.30)}$$

The initial conditions, boundary conditions are also same to that used in chapter 3.2.2.1. In the calculation, all equations are changed in form of dimensionless parameters. The equations are discretized by the explicit method for the calculations. And equations are solve computationally using Excel/VBA.

3.3.3.2 Estimation of model parameters

Most of estimated parameters used in this study, such as saturation pressure of water vapor, diffusion coefficients, and heat transfer coefficient, were calculated as same method used in chapter 3.2.2.2.

The LDF overall mass transfer coefficient for CNT, K_{LDF}, was also calculated from the same equation, Eq.19, in chapter 3.2.2.2.

$$\frac{1}{K_{LDF}} = \frac{R_p}{3k_F}\frac{q^*\rho_s}{C} + \frac{{R_p}^2}{15\varepsilon_s D_{eff}}\frac{q^*\rho_s}{C} + \frac{{R_s}^2}{15D_s} \quad \text{(Eq.31)}$$

However, in case of CNT, the last term of this equation was calculated from the diffusion in the pores of carbon nanotube in the simulation. Also, in case of PCM-inserted CNT, K_{LDF} is calculated by also same the equation used in chapter 3.2.2.2, which is Eq.20, because the major adsorption site exist the external surface or the secondary structure, thereby, diffusion inside pore can be neglected.

The Specific value of parameters used in the calculations used in the simulation of dehumidifying fixed-bed adsorption is shown in Table 9. In addition to the estimated parameters described above, basic parameters related to the column, such as column length, column diameter, void fraction, inlet temperature, concentration of water vapor at the inlet, and superficial flow velocity are assumed parameters in this study. The size of adsorbent pellet and the value of void fraction inside the pellet, ε_{macro}, are also assumed values.

On the other hand, heat capacity and density of pellet is calculated values from the bulk mesoporous silica or paraffin parameters. Those bulk parameter values are referenced from the various previous works or data sheets[80,98].

Finally, the ratio of PCM inserted in adsorbent, the phase change temperature of PCM inside the mesopores, and the enthalpy of fusion of PCM are measured values during experimentally prepared.

Table 9. Parameters used in the simulation.

column	
Column length, L	0.6 m
Column diameter, d_c	0.06 m
Void fraction, ε	0.4
Inlet temperature, $T_{F,in}$	313 K
Relative concentration of water vapor at the inlet	70 %
Concentration of water vapor at the inlet, C_{in}	1.984 mol/m^3
Superficial flow velocity, u_0	0.6 m/s
Adsorbent (Type1. CNT)	
Pellet density, ρ_p	784 kg/m^3
Diameter of a pellet, d_p	0.002 m
Heat capacity of a pellet, $C_{p,p}$	600 J/kg·K
Isosteric heat of adsorption, Q_{st}	41 KJ/mol
Macropore porosity of a particle, ε_{macro}	0.4
Adsorbent (Type2. PCM-inserted CNT)	
Pellet density, ρ_p	1060 kg/m^3
Diameter of a pellet, d_p	0.002 m
Heat capacity of a pellet, $C_{p,p}$	836 J/kg·K
Isosteric heat of adsorption, Q_{st}	42 KJ/mol
Macropore porosity of a particle, ε_{macro}	0.4
Ratio of PCM in the adsorbent, w_1	0.353 g-PCM/g-SBA-15
Phase change start temperature, T_{start}	314 K
Phase change end temperature, T_{end}	319 K
Enthalpy of fusion, H	164.6 J/g-PCM

3.3.4 Results and Discussion

3.3.4.1 Preparation of PCM-inserted CNT

As a PCM-inserted adsorbent, paraffin-inserted CNT is prepared and characterized by nitrogen adsorption. The nitrogen adsorption-desorption isotherm of both SBA-15 and the PCM-inserted CNT are depicted in Figure 58. In Figure 58, the amount of adsorbed nitrogen on the PCM-inserted CNT was significantly decreased compared to that of CNT in all the range of P/P_0. This suggests that paraffin is successfully inserted in both inside of CNT and secondary space of CNT. Then, the water-vapor adsorption isotherm was measured and depicted in Figure 59. The amount of adsorbed water decreased with existence of PCM. However, considerable amount of the adsorption sites of the PCM-inserted CNT was still remained after inserting PCM. This remained adsorption site is deduced to exist on large secondary-structure space of CNT where the PCM was not present. From these results of Figure 58 and Figure 59, it can be conclude that paraffin is successfully inserted into CNT, and PCM-inserted CNT can work as adsorbent for capturing water. Also, there was no temperature dependency on the water-vapor isotherm of CNT (See Fig.60), and the temperature dependency on the water-vapor isotherm of PCM-inserted CNT (See Fig.60) was expressed by henry equation.

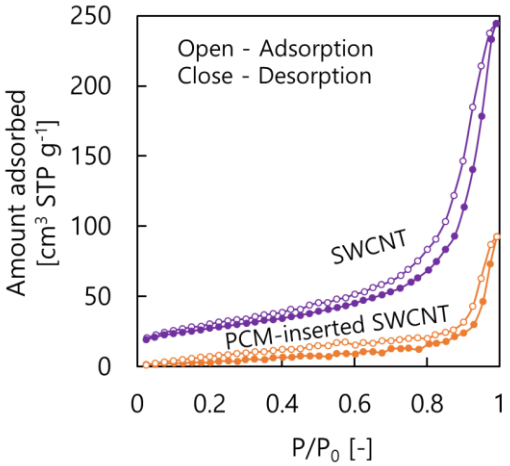

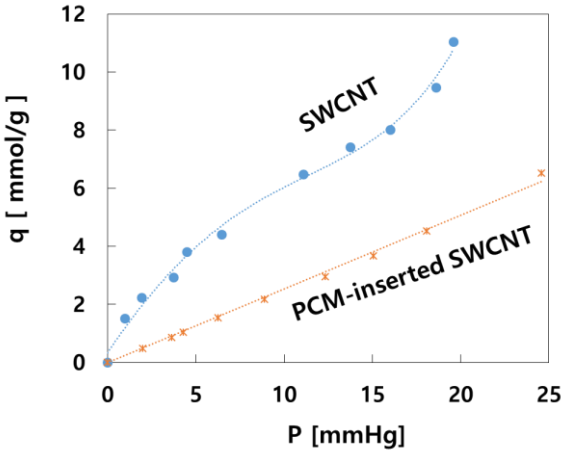

(Left) Figure 58. N_2 adsorption/desorption isotherms of CNT and PCM-inserted CNT.
(Right) Figure 59. Water adsorption isotherms of CNT and PCM-inserted CNT.

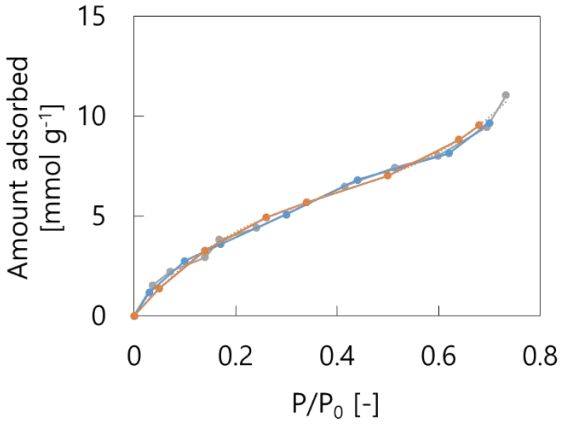

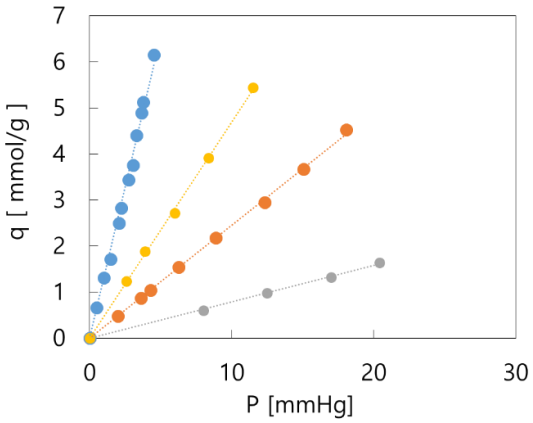

(Left) Figure 60. Water adsorption isotherms of CNT at the different temperatures (gray line : 27 ℃, blue line : 30 ℃, and orange line : 33 ℃).

(Right) Figure 61. Water adsorption isotherms of PCM-inserted CNT at the different temperatures (blue line : 0 ℃, yellow line : 16 ℃, orange line : 27 ℃, and gray line : 50 ℃).

The melting property and the thermal stability of PCM inserted in CNT was characterized by repeated DSC measurement, as shown in Figure 62. The phase-change peak of inserted paraffin in CNT was observed, and did not change during the repeated measurement. This indicates that the inserted PCM did not leak from the secondary structure of CNT during the repeated thermal treatments. In Figure 62, melting point of inserted paraffin was 41 ℃, and the enthalpy of fusion was 164.6 J/g-PCM. These value of the melting point and the enthalpy of fusion are lower than that of bulk PCM, i.e. 43 ℃ and 236.5 J/g-PCM, respectively.

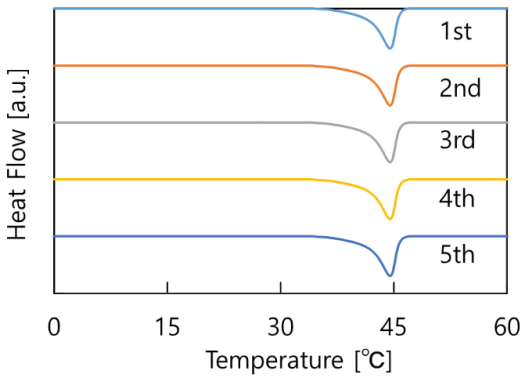

Figure 62. Repeated DSC curves of PCM-inserted CNT.

Although the melting properties are changed by inserted in CNT, phase change of paraffin occurred inside of the secondary structure, without leakage problem.

Hence, according to the results of water-vapor adsorption isotherm and DSC measurement, it can be concluded that PCM-inserted CNT, which possess both adsorption site and heat-storage site, is successfully prepared.

3.3.4.2 Theoretical evaluation of PCM-inserted CNT

The simulations of dehumidifying fixed-bed adsorption process with CNT and PCM-inserted CNT were carried out under adiabatic condition. For each adsorbent, the fluid temperature at the outlet (See Fig. 63 (a)) and the amount of water-vapor adsorbed in whole fixed-bed (See Fig.63 (b)), were calculated during the initial 10 min.

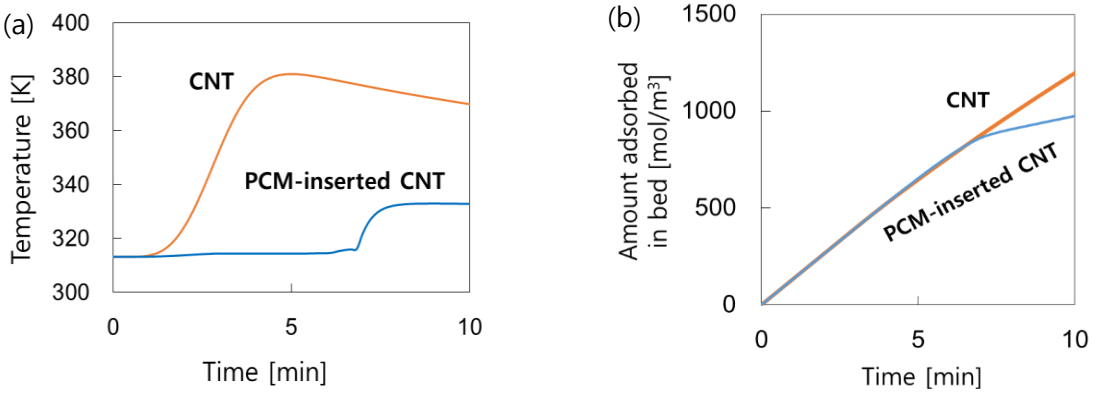

Figure 63. Time course of (a) temperature of fluid at outlet (b) the amount of adsorbed water-vapor with and without PCM.

As shown in Figure 63 (a), PMC-inserted CNT showed isothermal behaviors during the initial 7 minutes of adsorption process, due to the latent-heat storage through PCM. In Figure 63 (b), through this latent-heat storage effect of PCM, the amount of adsorbed water vapor on PCM-inserted CNT, was almost same or slightly larger, compared to on CNT during initial 7 minutes, despite of a smaller amount of q^*, which is shown in Figure 59. After 7 minutes, where the latent-heat storage through PCM is ended, the amount of adsorbed water on PCM-inserted CNT is decreased compare to on CNT, due to the smaller amount of q^*.

Figure 65 shows the changes of the value q/q^*, along with axial direction, at various time, i.e. 0 min, 0.5 min, 1 min, 3 min, 5 min and 10 min. Also, the changes of the amount of adsorbed water, along with axial direction, at various time is shown in Figure 65.

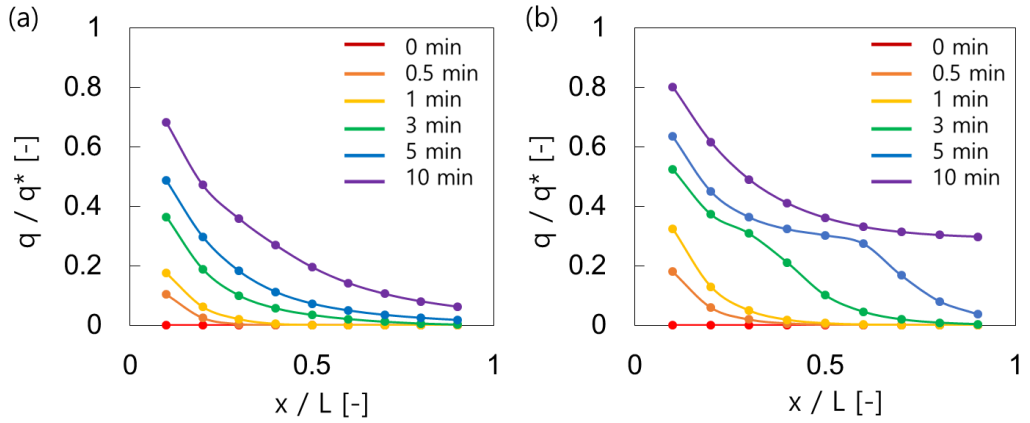

Figure 64. The changes of the value q/q^* along with axial direction at various time with (a) CNT, and (b) PCM-inserted CNT.

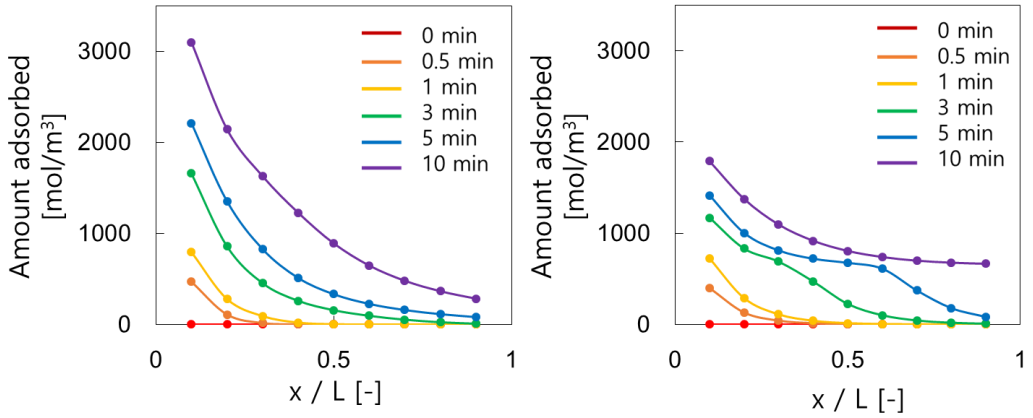

Figure 65. The amount of adsorbed water along with axial direction at various time with (a) CNT, and (b) PCM-inserted CNT.

During initial 10 minute, the value of q/q^* was increased with the existence of PCM (See Fig.64 (a) and Fig.64 (b)). In case of CNT, the adsorption mainly occurred near the inlet. In case of PCM-inserted CNT, the adsorption of water-vapor started from the inlet, then moved to the outlet. Especially, in case of PCM-

inserted CNT, the movement of adsorption band with time passing, was observed. This suggest that the increase of adsorption performance in PCM-inserted CNT was achieved due to the rapid apparent adsorption rate by the heat storage through PCM. Also, same tendency was observed in the results of Figure 65 (a) and Figure 65 (b). The amount of adsorbed water on PCM-inserted CNT was increased in both near the inlet and near the outlet. On the other hand, the amount of adsorbed water on CNT majorly increased near the inlet. However, owing to the smaller amount of q* of PCM-inserted CNT compared to that of CNT, the total amount of water adsorbed in the whole fixed-bed is not increased much, as shown in Figure 63 (b).

Furthermore, how much percentages of the released thermal energy of adsorption, was transferred to the PCM or to the fluid at 5 min, 7min and 10 min, were calculated, as shown in Table 10.

Table 10. The percentages of transferred heat of adsorption to fluid, to adsorbent (PCM+CNT), and to PCM.

Time	Adsorbent	to fluid	to adsorbent (Sensible heat)	to PCM (latent heat)
5 min	CNT	46 %	54 %	-
	PCM-inserted CNT	1%	20 %	79 %
7 min	CNT	65 %	35 %	-
	PCM-inserted CNT	2 %	22 %	77 %
10 min	CNT	78 %	22 %	-
	PCM-inserted CNT	12 %	19 %	69 %

In the solo CNT system, at the 5 min, half of the released heat of adsorption was transferred to the fluid and left half of the released heat was transferred to adsorbent. With increase of time, most of the released heat of adsorption was transferred to the fluid, and eliminated from the adsorption system. On the other hand, in the PCM-inserted system, until initial 7 min, almost 98 % of the released

heat was transferred to adsorbent, and only 2 % of the released heat transferred to the fluid. Within 98 %, 77 % of heat was stored by latent heat of PCM. Once again, this recovered heat by inserted PCM, is expected to be re-used during the desorption process. After 7 min, since the released amount of heat of adsorption is greater than the latent-heat capacity of PCM, most of the heat transferred to the fluid. This result agree with the degradation of the amount of adsorbed water after 7 min, in Figure 63 (b).

In summary, a PCM-inserted CNT is proposed for a new containing method of a PCM in an adsorption process. However, unlike PCM-inserted SBA-15 (See Fig.54 (c)), the adsorption performance did not significantly increased by using PCM-inserted CNT (See Fig.63). This might be because, severe decrease of q* in CNT with inserting PCM, compared to SBA-15.

Hence, to optimize the adsorption performance, packing fixed-bed with both CNT and PCM-inserted CNT with various ratio was studied. In the simulation, x % of CNT was packed in adsorbent bed, in same time, (100-x) % of PCM-inserted was packed in adsorbent bed. As for the value of x, 0, 10, 20, 30, 40, 50, 60, 70, 80, 90 and 100 was calculated. The value of q/q^* along axial direction, at initial 5 minutes, is shown in Figure 59. Also, the amount of adsorbed water-vapor, in the whole fixed-bed during initial 10 minutes, is shown in Figure 67.

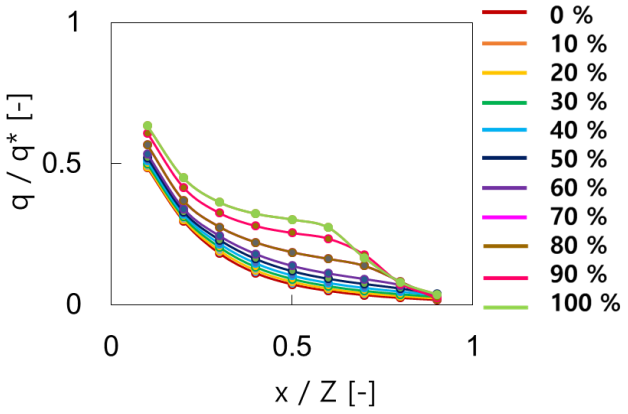

Figure 66. The changes of the value of q/q^* along axial direction with various packing percentage of CNT and PCM-inserted CNT.

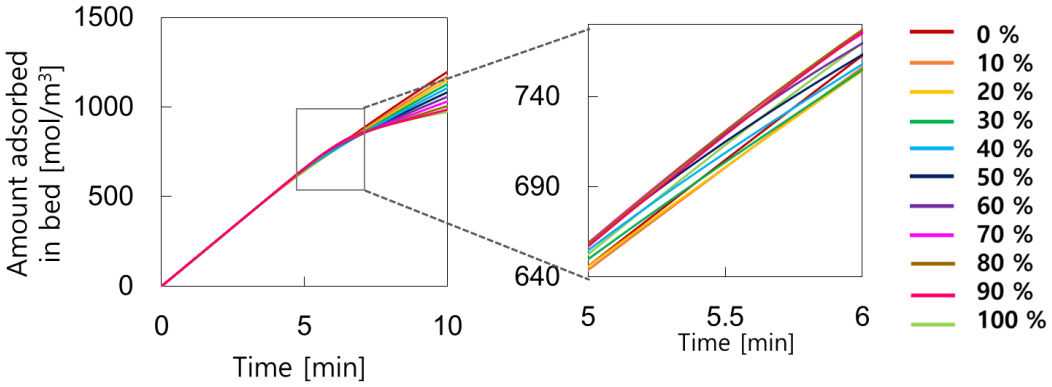

Figure 67. The amount of adsorbed water vapor with various packing percentage of CNT and PCM-inserted CNT during initial 10 minutes.

As shown in Figure 66, with increase of the packing amount of PCM-inserted CNT, the value of q/q^* at X min was increased, due to the increase of the latent-heat storage capacity. On the other hand, as shown in Figure 67, the amount of adsorbed water-vapor in the whole fixed-bed was slightly increased during initial 5 - 6 minutes by packing both CNT and PCM-inserted CNT. After 7 minutes, the amount of adsorbed water was totally depend on the packing ratio, owing to the decrease of q^* with increase of the packing percentage of PCM-inserted CNT. Figure 68 shows the amount of adsorbed water at initial 5 minute, with different packing percentages of PCM-inserted CNT. As you can notice from Figure 68, at initial 5 minutes, packing 70 % of PCM-inserted CNT and 30 % of CNT, showed best performance. Also, these results suggest that adsorption performance can be improved by packing adsorbent and PCM-inserted adsorbent at the same time with adequate ratio.

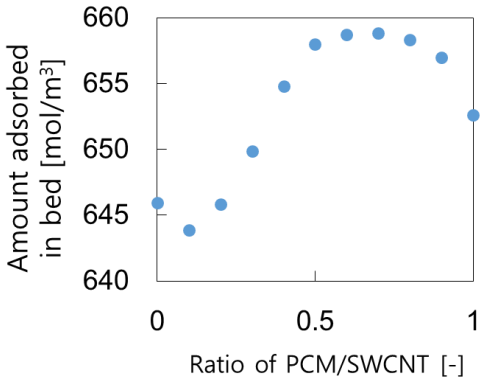

Figure 68. The amount of adsorbed water at different packing ratio of PCM-inserted CNT in the bed at 5 minute.

Consequently, a PCM-inserted CNT is proposed for a new concept of PCM-inserted adsorbent. PCM-inserted CNT was successfully prepared. To evaluate the effectiveness of PCM-inserted CNT, the dehumidifying fixed-bed adsorption process was simulated. The PCM-inserted CNT showed slightly enhanced performance owing to the heat recovery effect of the PCM during initial 6 min. Also, with packing both CNT and PCM-inserted CNT simultaneously with adequate ratio during initial 6 minutes, slight improvement on adsorption performance was achieved. Specifically, at 5 min, packing 70 % of PCM-inserted CNT and 30 % of CNT, showed best performance. The reason why the performance improvement of PCM-inserted CNT was not significant than that of PCM-inserted SBA-15, is because, the decrease of q^* by inserting PCM was more significant in case of CNT compared to SBA-15, at P/P_0=0.5. In conclusion, the PCM-inserted CNT successfully worked as a heat storage material, and, the performance of adsorption process was slightly improved.

3.4 Concept 3 – Mesoporous zeolite SSZ-13

3.4.1 Proposal of the concept

Zeolite is a crystalline, microporous material composed of silica and alumina. Since zeolite is made by silica and alumina, dissolving small part of silica or alumina in the crystal of zeolite, is possible. This dissolved space become mesopore, or sometimes macropore, inside the zeolite crystal. By partially dissolving the zeolite crystal, ‘mesoporous zeolite’ which possess both micropore and mesopore at the same time, can be prepared. Mostly, mesoporous zeolite is used in catalyst reaction owing to the fast diffusion rate in the crystal derived from large pore size. On the other hand, in this chapter, mesoporous zeolite is focused as a host material for preparing the PCM-inserted adsorbent. In this concept of PCM-inserted mesoporous zeolite, the microporous space is used for an adsorption site and the mesoporous space is used for heat-storage site. The separation of PCM and

adsorbate in the zeolite crystal can be achieved owing to the size-difference. In this concept, PCM is inserted only into the mesopores of zeolite crystal, by selecting the PCM molecule with adjust size, which is larger than the size of micropore. Hence, PCM cannot access to the microporous space, and microporous space will remain as adsorption space. At the same time, mesopore which is occupied by PCM works as heat storage site. Once again, to realize this concept, PCM molecule must be larger than the micropore diameter of zeolite. However, as for the PCM, paraffin is mostly used in this study owing to their several advantages, such as melting point near room temperature, low degree of super cooling, high enthalpy of fusion, and low vapor pressure. Therefore, to prevent the access of paraffin molecule to the micropore, among the various types of zeolite, zeolite SSZ-13 is chosen in this study. SSZ-13 has an extremely small size of micropore inside which is known as nearly 0.4 ~ 0.5 nm from the data of IZA. Also, mesoporous SSZ-13 is denoted as MSSZ-13 in this study. The schematic image of PCM-inserted MSSZ-13 is illustrated in Figure 69 below.

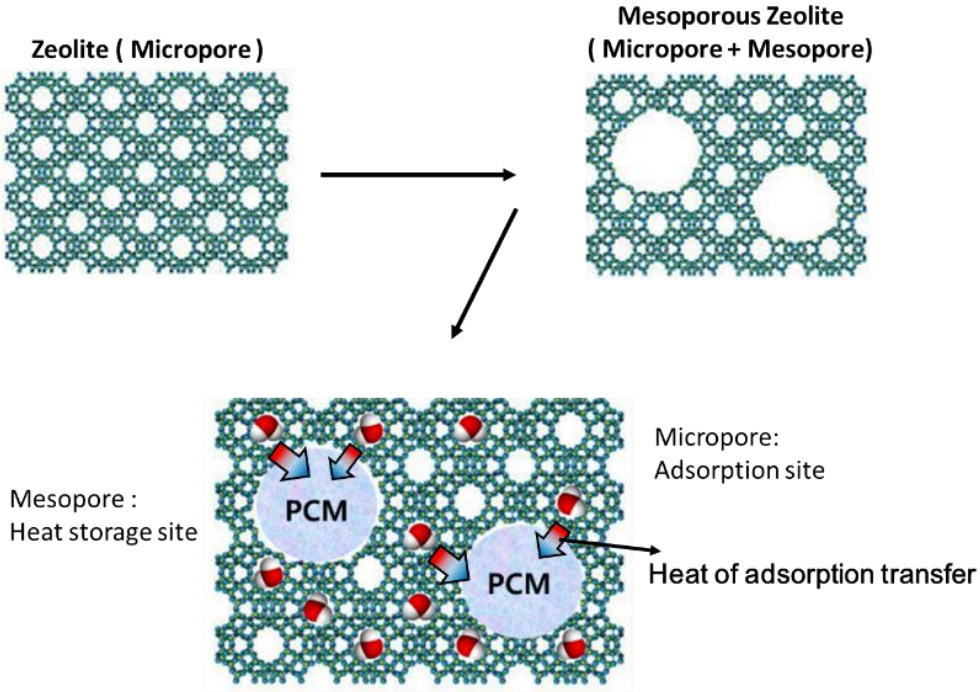

Figure 69. Schematic illustration of PCM-inserted MSSZ-13.

3.4.2 Experimental – preparation of PCM-inserted MSSZ-13

3.4.2.1 Preparation of MSSZ-13

As for the preparation method of MSSZ-13, fluoride etching by using NH_4F solution via ultrasonic treatment was carried out. To etch SSZ-13 by using NH_4F solution, first, ion-exchange from Na^+ to NH_4^+ was done. Specifically, 5 g of Na^+-SSZ-13 (SiO_2/Al_2O_3=17.7) zeolite was added in 100 g of 0.5 M of NH_4Cl solution. Then, the mixed solution was kept in 60 ℃ oven for 2 hours. After 2 hours, the mixed solution was filtered. The obtained zeolite powder was added in to new 100 g of 0.5 M of NH_4Cl solution and maintained at 60 ℃ in oven for 2 hours. Repeated this process once again, then filtered the mixed solution. The obtained solid material was washed with 500 ml of DI water, subsequently dried at 60 ℃ for overnight. Prepared sample was characterized by N_2 adsorption, XRD and SEM.

For developing PCM-inserted MSSZ-13, preparation of MSSZ-13 with optimized condition was necessary. To make MSSZ-13 works as both heat storage material and adsorbent, achievement of following conditions were necessary.

1. Large mesopore diameter(d> 7 nm)
2. High mesopore volume(> 3-5 times larger)
3. High micropore volume(=Small decrease in micropore volume)
4. No structure change before and after treatment of preparing MSSZ-13

Hence, fluoride etching of NH_4^+-SSZ-13 by using NH_4F solution via ultrasonic(US) treatment was carried out in various condition, to figure out best conditions for achieving necessary condition. Specifically, 40 g of 40 wt% NH_4F solution was prepared. Then, 1 g of NH_4^+-SSZ-13 zeolite was added in to the solution, and, the solution was put into 40 ℃ of pre-heated US bath. Subsequently, US treatment was carried out for several minutes. Detail experimental conditions are described in table below. The temperature of US bath was maintained at initial temperature by using ice. After US treatment, the mixed solution was filtered, and thoroughly washed with 60 ℃, 500 ml of DI water. The obtained solid was dried at oven for

overnight. The prepared samples were characterized by N_2 adsorption, XRD and SEM.

Table 11. Fluoride etching treatment conditions.

Treatment	Temperature [℃]	Time [min]	Denoted Sample Name
Ultrasonic	40	60	US40-1H
	40	120	US40-2H
	40	180	US40-3H

3.4.2.2 Preparation of PCM-inserted MSSZ-13

As for the host adsorbent, MSSZ-13 is used. As for the PCM, paraffin (C22, Docosane) was inserted into MSSZ-13 via vapor transportation. The detail procedures of vapor transportation are described in chapter 2.2.4. The porous structures of SSZ-13, MSSZ-13, and paraffin-inserted MSSZ-13 are characterized by N_2 adsorption. In addition, the water-vapor adsorption isotherms of SSZ-13 and PCM-inserted MSSZ-13, are measured to identify that adsorption site is still remained, before and after inserting PCM. The water-vapor adsorption is also measured at 3 different temperature to investigate a temperature dependence on the isotherms of both SSZ-13, and PCM-inserted MSSZ-13. From the result of water vapor adsorption isotherms, the isosteric heat of adsorption of water on each adsorbent, is calculated. Moreover, the melting properties of inserted paraffin, i.e. phase change temperature and the enthalpy of fusion, is characterized by DSC. DSC measurement is repeat for 5 times to investigate that inserted PCM is leaked or not, from the mesoporous space, with repeated thermal treatment.

3.4.3 Theoretical evaluation

3.4.3.1 Governing equation

In the theoretical study, I assumed to neglect the temperature profiles in the PCM-inserted adsorbent pellet. Hence, since there are no differences in the mass- and energy- balances between the concepts of PCM-inserted adsorbent. Therefore, the mathematical model of fixed-bed adsorption was same to that used in chapter 3.2.2.1, which referenced from several previous works[4,76–78]. The energy- balance and mass- balances of two types of adsorbent, i.e. SSZ-13, and PCM-inserted MSSZ-13, are governed as follows:

Type 1. SSZ-13

Overall mass balance : $\frac{\partial C}{\partial t} + u\frac{\partial C}{\partial x} + \frac{\rho_B}{\varepsilon}\frac{dq}{dt} = 0$ (Eq.32)

Adsorption rate : $\rho_B \frac{dq}{dt} = K_{LDF}\,(q^* - q)$ (Eq.33)

Energy balances for fluid : $c_{p,F}\rho_F \frac{\partial T_F}{\partial t} + c_{p,F}\rho_F u\frac{\partial T_F}{\partial x} - h_1 a_1 \frac{(1-\varepsilon)}{\varepsilon}(T_p - T_F) = 0$ (Eq.34)

Energy balances for pellet : $c_{p,p}\rho_p \frac{\partial T_p}{\partial t} + h_1 a_1 (T_p - T_F) - Q_{st}\rho_p \frac{dq}{dt} = 0$ (Eq.35)

Type 2. PCM-inserted MSSZ-13

Overall mass balance: $\frac{\partial C}{\partial t} + u\frac{\partial C}{\partial x} + \frac{\rho_B}{\varepsilon}\frac{dq}{dt} = 0$ (Eq.36)

Adsorption rate : $\rho_B \frac{dq}{dt} = K_{LDF}\,(q^* - q)$ (Eq.37)

Energy balances for fluid : $c_{p,F}\rho_F \frac{\partial T_F}{\partial t} + c_{p,F}\rho_f u\frac{\partial T_F}{\partial x} - h_1 a_1 \frac{(1-\varepsilon)}{\varepsilon}(T_p - T_F) = 0$ (Eq.38)

Energy balances for pellet :

$c_{p,p}\rho_p \frac{\partial T_p}{\partial t} + h_1 a_1 (T_p - T_F) - Q_{st}\rho_p \frac{dq}{dt} + \rho_{pcm}\frac{\partial H(T)}{\partial t} = 0$ (Eq.39)

Also, the initial conditions, boundary conditions are same to that used in chapter 3.2.2.1. In the calculation, all equations are changed in form of dimensionless parameters. The equations are discretized by the explicit method for the calculations. And equations are solve computationally using Excel/VBA.

3.4.3.2 Estimation of model parameters

Once again, most of estimated parameters used in this study, such as saturation pressure of water vapor, diffusion coefficients, and heat transfer coefficients, were calculated as same method, used in chapter 3.2.2.2.

The LDF overall mass transfer coefficient for SSZ-13, K_{LDF}, was also calculated from same equation, Eq.19, in chapter 3.2.2.2.

$$\frac{1}{K_{LDF}} = \frac{R_p}{3k_F}\frac{q^*\rho_s}{C} + \frac{{R_p}^2}{15\varepsilon_s D_{eff}}\frac{q^*\rho_s}{C} + \frac{{R_s}^2}{15D_s} \quad \text{(Eq.40)}$$

However, in case of SSZ-13, the last term of this equation was calculated from the knudsen diffusion in the micropores of zeolite crystal. Also, in case of PCM-inserted MSSZ-13, K_{LDF} is calculated by same the equation used in Eq.40, not Eq.20, because in this concept, the microporous space is remained owing to the size difference between the micropore diameter and the PCM molecular size, thereby, diffusion inside micropores was considered.

The Specific value of parameters used in the calculations used in the simulation of dehumidifying fixed-bed adsorption is shown in Table 12. In addition to the estimated parameters described above, basic parameters related to the column, such as column length, column diameter, void fraction, inlet temperature, concentration of water vapor at the inlet, and superficial flow velocity are assumed parameters in this study. The size of adsorbent pellet and the value of void fraction inside the pellet, ε_{macro}, are also assumed values.

On the other hand, heat capacity and density of pellet is calculated values from the bulk mesoporous silica or paraffin parameters. Those bulk parameter values are referenced from the various previous works or data sheets[81,82].

Finally, the ratio of PCM inserted in adsorbent, the phase change temperature of PCM inside the mesopores, and the enthalpy of fusion of PCM are measured values during experimentally prepared. The isosteric heat of adsorption is calculated from the water vapor adsorption isotherms measure at different temperatures.

Table 12. Parameters used in the simulation.

column	
Column length, L	0.6 m
Column diameter, d_c	0.06 m
Void fraction, ε	0.4
Inlet temperature, $T_{F,in}$	308 K
Relative concentration of water vapor at the inlet	50 %
Concentration of water vapor at the inlet, C_{in}	1.097 mol/m^3
Superficial flow velocity, u_0	0.6 m/s
Adsorbent (Type1. SSZ-13)	
Pellet density, ρ_p	370 kg/m^3
Diameter of a pellet, d_p	0.002 m
Heat capacity of a pellet, $C_{p,p}$	730 J/kg·K
Isosteric heat of adsorption, Q_{st}	42.0 KJ/mol
Macropore porosity of a particle, ε_{macro}	0.48
Adsorbent (Type2. PCM-inserted MSSZ-13)	
Pellet density, ρ_p	458 kg/m^3
Diameter of a pellet, d_p	0.002 m
Heat capacity of a pellet, $C_{p,p}$	880 J/kg·K
Isosteric heat of adsorption, Q_{st}	44 KJ/mol
Macropore porosity of a particle, ε_{macro}	0.48
Ratio of PCM in the adsorbent, w_1	0.24 g-PCM/g-SBA-15
Phase change start temperature, T_{start}	308 K
Phase change end temperature, T_{end}	319 K
Enthalpy of fusion, H	156.3 J/g-PCM

3.4.4 Results and discussion

3.4.4.1 Preparation of MSSZ-13

Ion exchange of zeolite from Na^+ to NH_4^+ was carried out. To investigate the structural change before and after the ion-exchange treatment, both Na^+-SSZ-13 and NH_4^+-SSZ-13 was characterized by XRD, N_2 adsorption, and SEM. As you can notice from Figure 70, both samples showed same patterns of XRD, whether the cation of zeolite is Na^+ or NH_4^+. Therefore, it can be considered that there is no structure change resulted from ion-exchange treatment. N_2 adsorption-desorption isotherm and pore size distribution is shown in Figure 71. Also, the porous characteristics calculated from the nitrogen adsorption isotherm are shown in Table 13.

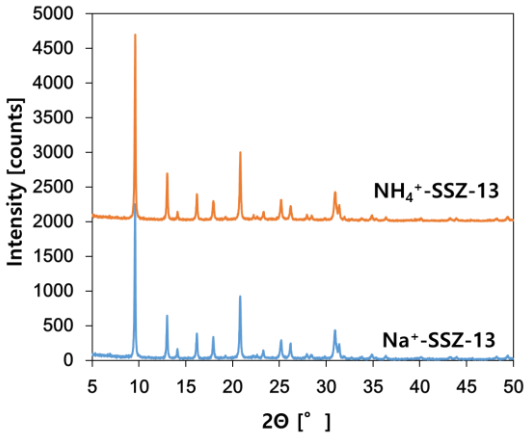

Figure 70. XRD patterns of SSZ-13 and ammonium ion-exchanged SSZ-13.

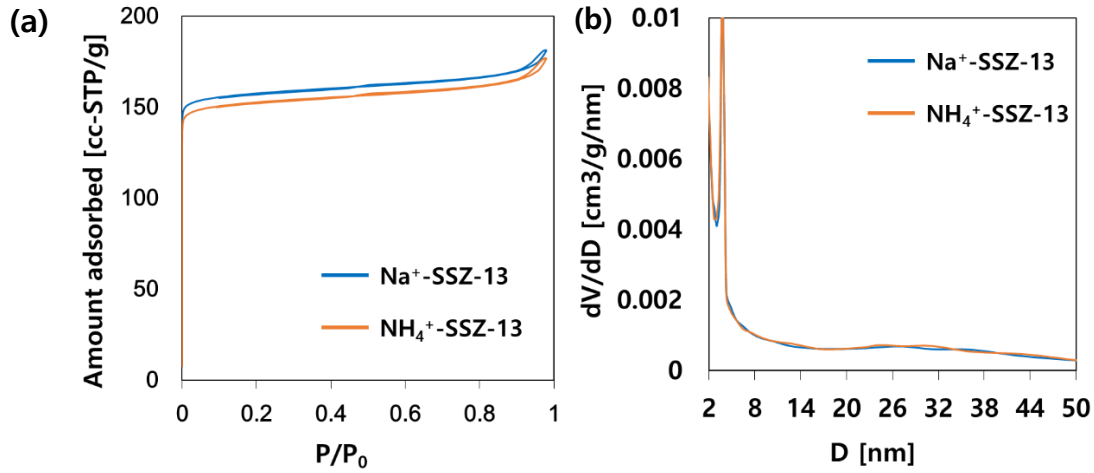

Figure 71. (a) N_2 adsorption-desorption isotherm, and (b) pore size distribution.

Table13. Porous characteristics of samples.

Sample	S_{BET} [m^2/g]	V_{meso}* [cm^3/g]	V_{micro}* [cm^3/g]	V_{total} [cm^3/g]	D_{meso}* [nm]
Na^+-SSZ-13	646	0.053	0.223	0.276	6.69
NH_4^+-SSZ-13	624	0.054	0.215	0.269	6.63

* V_{micro} is measured by t-plot method.
* V_{meso} is calculated by V_{total} - $V_{micro.}$
* D_{meso} is measured by BJH method.

The N_2 adsorption-desorption and the pore size distributions of Na^+-SSZ-13 and NH_4^+-SSZ-13, which depicted in Figure 71, were almost overlapped. Also, in Table 13, both Na^+-SSZ-13 and NH_4^+-SSZ-13 showed almost the same value of porous characteristics, such as BET surface and pore volume. From these results, porous characteristics also didn't changed before and after an ion-exchange treatment. Moreover, SEM images of Na^+-SSZ-13 and NH_4^+-SSZ-13 are shown in Fig.72

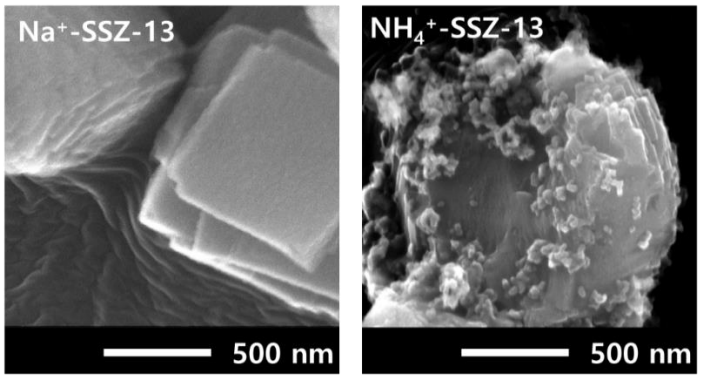

Figure 72. SEM images of Na^+-SSZ-13 (left), and NH_4^+-SSZ-13 (right)

The pure Na^+-SSZ-13 crystal showed rectangular domains and morphologies with clean surface. The ion-exchanged NH_4^+-SSZ-13 showed quite small, surrounded particles near SSZ-13 crystal, but, both samples showed rectangular domains, similar size, and same morphology. Therefore, the crystal domains and morphologies are not changed via ion-exchange.

Subsequently, to prepare the MSSZ-13, fluoride etching of NH_4^+-SSZ-13 crystal by ultrasonic(US) treatment using NH_4F solution, was carried out. In the preparation, to achieve higher mesopore volume, severe conditions were chosen.

Specific conditions are described in chapter 3.4.2.1. Samples are denoted by the treatment method and treated temperature-treated time, i.e. US40-1H, US40-2H, and US40-3H. The prepared samples are characterized by XRD, as shown in Figure 73. In the results of XRD, crystallinity of each sample was calculated by following equation:

$$\text{crystallinity} = \frac{\text{intensity of sample}}{\text{intensity of reference sample}(NH_4^+ - SSZ - 13)}$$

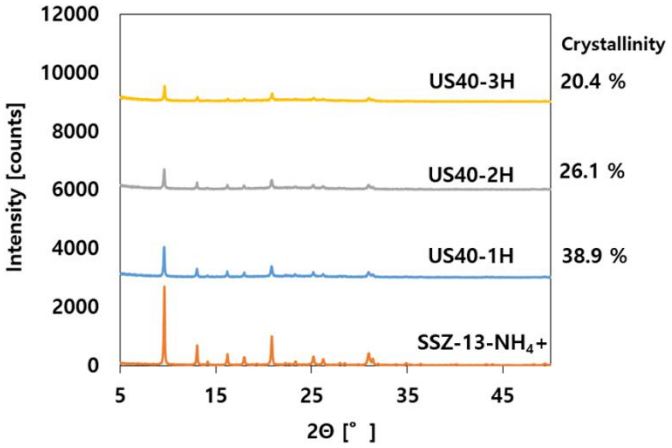

Figure 73. XRD patterns of SSZ-13 and prepared MSSZ-13, which are US40-1H, US40-2H, and US40-3H.

As you can notice from Figure 73, the crystallinities of prepared samples decreased with increase of treatment time. However, XRD pattern of crystals does not changed before and after fluoride etching. Therefore, with dissolving of crystals using NH_4F, crystallinity was subsequently decreased, but, microporous crystalline structure derived from SSZ-13 was still remained.

Also, N_2 adsorption-desorption isotherms and pore size distribution are shown in Figure 74. And, the porous characteristics calculated from N_2 adsorption isotherm were listed in Table 14. BET surface area and micropore volume were decreased with increase of treatment time. Besides, mesopore volume was increased with increase of treatment time until 60 min, then decreased with increase of treatment time. This might be due to forming macropores or destruction of crystal, owing to the severe level of etching treatment. This study aims to preparing MSSZ-13 with large micropore volume, large mesopore volume and large mesopore diameter. Therefore, in terms of optimized condition, US40-1H is most adequate sample for

used as host adsorbent, in the concept of PCM-inserted MSSZ-13.

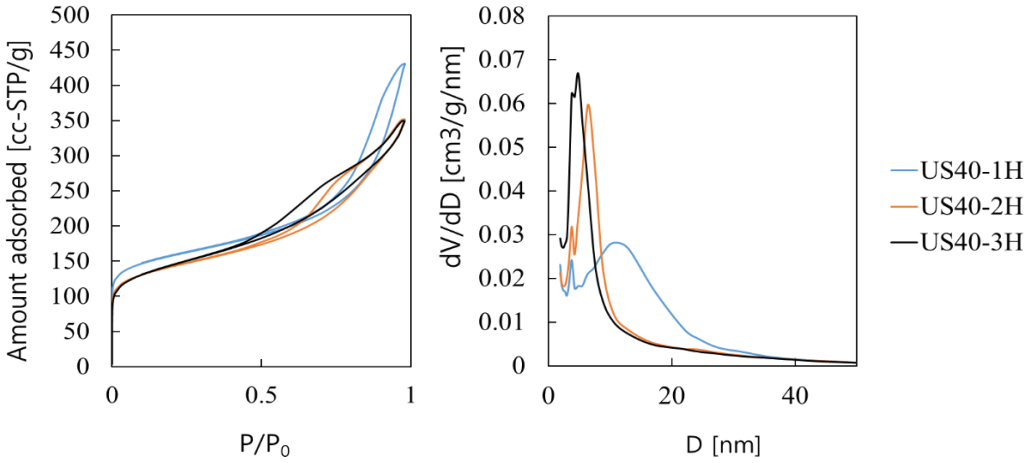

Figure 74. N_2 adsorption-desorption isotherm and pore size distribution of US40-1H, US40-2H, and US40-3H.

Table 14. Porous characteristics of samples.

Sample	Treatment Time [min]	S_{BET} [m^2/g]	V_{meso}* [cm^3/g]	V_{micro}* [cm^3/g]	V_{total} [cm^3/g]	D_{meso}* [nm]
NH_4^+-SSZ-13	-	624	0.054	0.215	0.269	6.63
US40-1H	60	555	0.512	0.132	0.644	9.18
US40-2H	120	495	0.424	0.105	0.529	6.93
US40-3H	180	484	0.439	0.087	0.526	5.93

* V_{micro} is measured by t-plot method.
* V_{meso} is calculated by V_{total} - V_{micro}.
* D_{meso} is measured by BJH method.

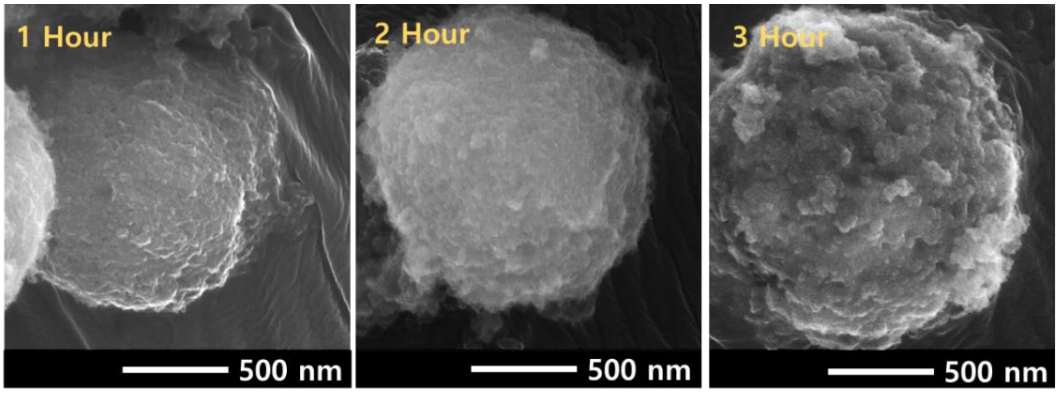

Figure 75. SEM images of US40-1H, US40-2H and US40-3H.

SEM images of each sample are shown in Figure 75. The morphology of each sample showed more round shape, rather than original sharp rectangular shape, due to the fluoride etching. However, still rectangular domains of SSZ-13 crystal and morphology of SSZ-13 was observed. This result agrees with the result of XRD, in Figure 73.

As a results, NH_4F solution dissolve both silica and alumina, and successfully formed mesopores inside of SSZ-13. For the optimize condition for preparing PCM-inserted MSSZ-13, sample US40-1H is considered as most suitable material, owing to their 4-5 times higher mesopore volume compared to micropore volume, high crystallinity, high micropore volume and large mesopore diameter. Therefore, the surface of US40-1H crystal is measured by SEM to clarify the mesoporous structure of US40-1H on the surface, as shown in Figure 76.

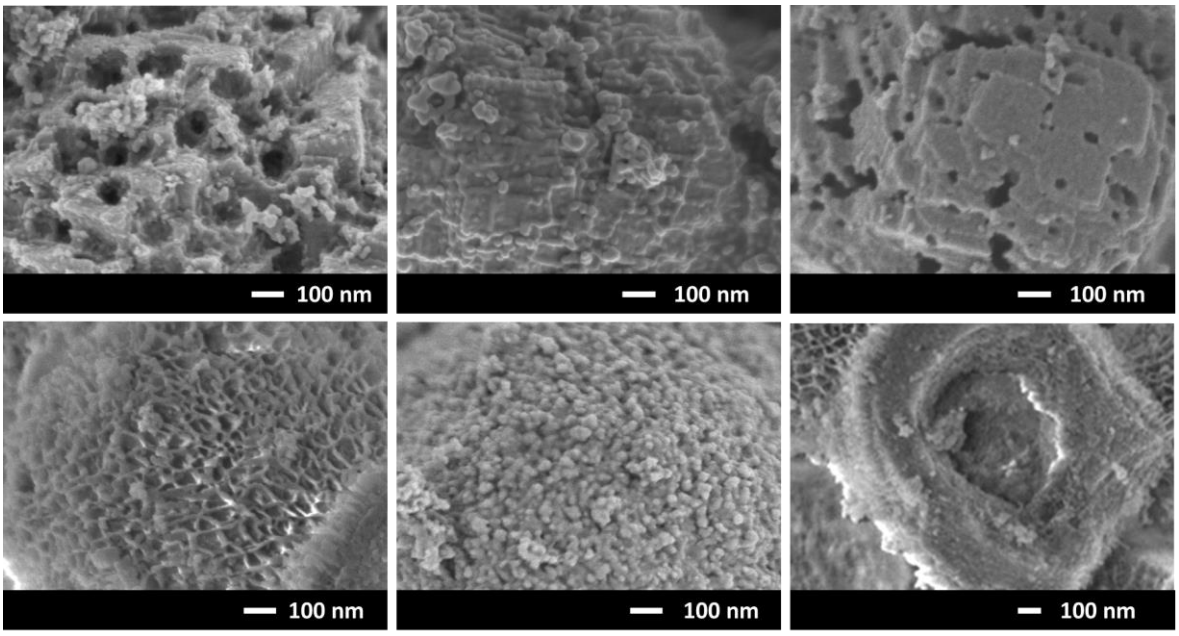

Figure 76. Surface of the mesoporous SSZ-13 (US40-1H) crystal.

As you can notice form the Figure 76, there are various types of surface with various size and shape of hole are observed in SEM images. Hole-like meso-macropores, crater-like macropores, and honeycomb-like meso-macropores are observed. From this results, it can be considered that the mesopores are not orderly introduced in the crystal of zeolite SSZ-13. However, it can be also concluded that, meso- and macro-size of pores are successfully introduced in the crystal of zeolite SSZ-13.

3.4.4.2 Characterization of PCM-inserted MSSZ-13

In the concept of PCM-inserted MSSZ-13, PCM molecules must be larger than the micropore diameter of MSSZ-13, to utilize the microporous space as adsorption site. Therefore, first, nitrogen adsorption of SSZ-13 and paraffin-inserted SSZ-13, not MSSZ-13, was measured, to investigate that paraffin can be used as PCM, as shown in Figure 77.

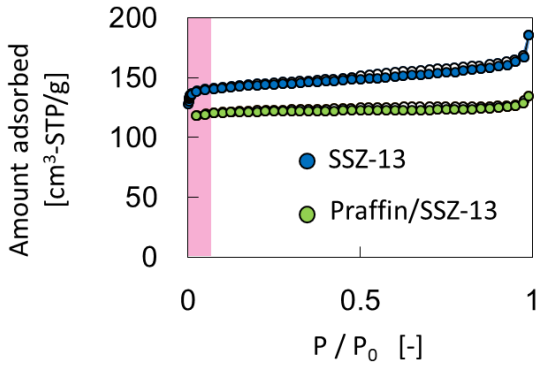

Figure 77. Nitrogen adsorption isotherms of SSZ-13 and paraffin-inserted SSZ-13.

As depicted in Figure 77, there was no difference in the amount of adsorbed nitrogen, especially at the low pressure range (pink colored range). This uptake of amount adsorbed nitrogen at the low pressure range, is derived from the amount of adsorbed nitrogen on microporous space. If paraffin can access to the micropore, microporous space would be occupied by inserted paraffin, and this uptake will not observed. Hence, from this result, it is confirmed that paraffin cannot access to the micropores of SSZ-13, and identified that paraffin can be used as PCM.

For the host adsorbent, US40-1H, which is prepared in chapter 3.4.4.1, is used as MSSZ-13 in this study. Subsequently, paraffin was inserted into the MSSZ-13 via vapor transportation method. To investigate the porous characteristics of PCM-inserted MSSZ-13, nitrogen adsorption-desorption isotherms of SSZ-13, MSSZ-13 and PCM-inserted MSSZ-13 were measured, as shown in Figure 78. Also, mesoporous and microporous volume of each sample, calculated from nitrogen adsorption isotherm, are listed in Table 15. Owing to the fluoride treatment, the mesoporous volume of MSSZ-13 is significantly increased compared to SSZ-13. However, possibly due to the severe etching treatment, micropore volume of MSSZ-13 is decreased compared to SSZ-13. On the other hand, by inserting PCM

into MSSZ-13, the mesopore volume is significantly decreased compared to MSSZ-13. This indicates that PCM was successfully inserted only into the mesopores of SSZ-13. However, nearly 40 % of the micropore volume of MSSZ-13 is decreased by inserting PCM. As identified in Figure 78, PCM cannot access to the micropore of SSZ-13. Hence, PCM is occupying the microporous space is not the reason of decrease in micropore volume by inserting PCM. This is because, the diffusion route for nitrogen becomes dead-end by inserting PCM. Major diffusion route for nitrogen is mesoporous space, and mesoporous space is occupied by PCM. Therefore, nitrogen molecules cannot access to the some parts of micropore, and this is why the micropore volume was decreased with inserting PCM. Also, for this reason, even though the micropore volume is decreased, but still, a separation of adsorption site for nitrogen, and heat storage site for paraffin, was achieved.

The melting property and the stability of PCM-inserted in MSSZ-13, was characterized by repeated DSC measurement. The phase-change peak of inserted paraffin in MSSZ-13 was observed as shown in Figure 79, and did not changed with repeated measurement. This indicates that the inserted PCM did not leak from the mesoporous space of MSSZ-13, during the repeated thermal treatments. Melting point of inserted paraffin was 42.6 ℃, and the enthalpy of fusion was 155.8 J/g-PCM. These value of the melting point and the enthalpy of fusion are slightly lower than that of bulk PCM, i.e. 43 ℃ and 236.5 J/g-PCM, respectively.

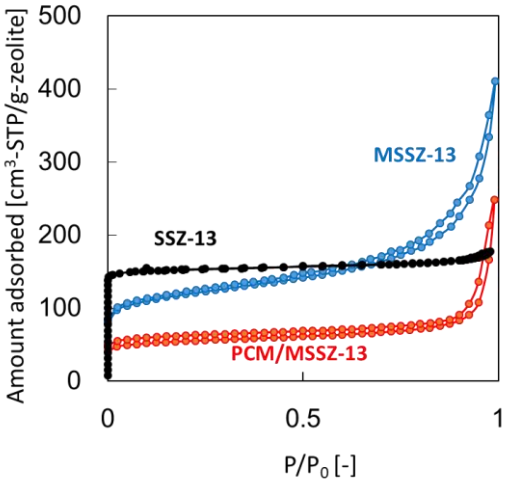

Figure 78. Nitrogen adsorption-desorption isotherms of SSZ-13, MSSZ-13 and PCM-inserted MSSZ-13.

Table 15. Mesoporous and microporous volume of SSZ-13, MSSZ-13 and PCM-inserted MSSZ-13.

	SSZ-13	MSSZ-13	PCM-inserted MSSZ-13
V_{micro} (cc/g-zeolite)	0.215	0.115	0.066*
V_{meso} (cc/g-zeolite)	0.053	0.420	0.317

* 57% of MSSZ-13, 30 % of SSZ-13

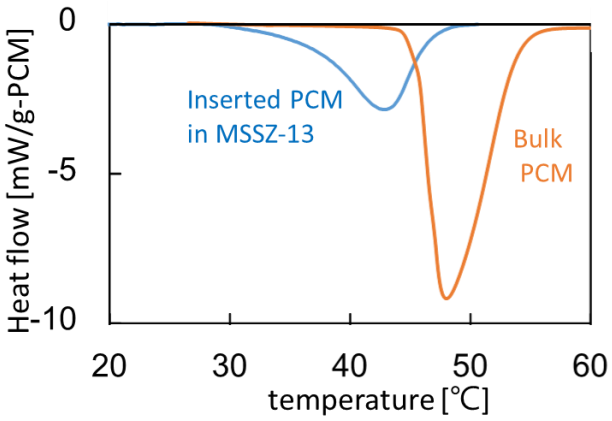

Figure 79. DSC curves of paraffin inserted in MSSZ-13 and bulk paraffin as reference.

The water adsorption isotherms of SSZ-13 at three different temperature is shown in Figure 78. As you can notice from Figure 80, among 30 ℃, 35 ℃, and 40 ℃, there was no temperature dependency on the water vapor isotherm, when the x-axis is the P/P_0. As for the another reference, the water adsorption isotherms of SSZ-13 (SiO_2/Al_2O_3=10), which is reported in the literature of Luo[83], is shown in Figure 81 also showed no temperature dependency, when the x-axis is the P/P_0, at large temperature range, which is from 20 ℃ to 79 ℃, Hence, the temperature dependency is considered to be possibly neglected when the x-axis is the P/P_0. Also, the isosteric heat of adsorption of SSZ-13 calculated from the result of Figure 80. Consequently, there was no temperature dependency on the water vapor adsorption isotherm, and this isotherm can be expressed as a function of P/P_0.

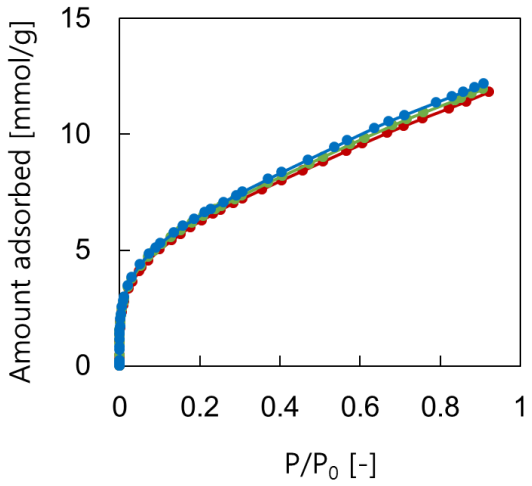

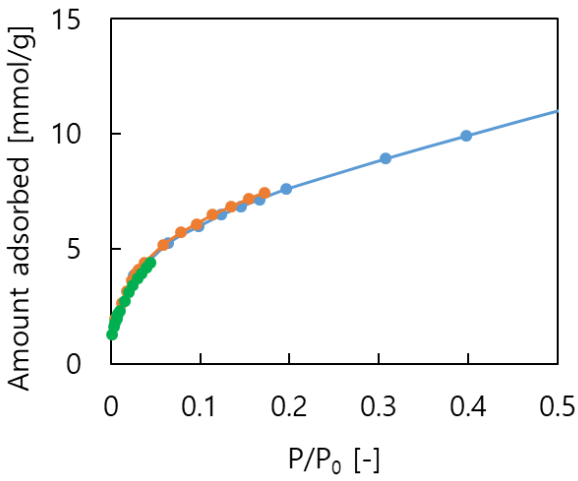

(Left)Figure 80. Water vapor adsorption isotherm of SSZ-13 used in this study, at three different temperature. Blue line 30 ℃, green line 35 ℃, and red line 40 ℃.
(Right)Figure 81. Water vapor adsorption isotherm of reference SSZ-13 from the work of Luo[83] at three different temperature. Blue line 20 ℃, orange line 50 ℃, green line 79 ℃.

Subsequently, the water vapor isotherm of prepared, PCM-inserted MSSZ-13 was measured at 6 different temperature, and shown in Figure 82. As you can notice from Figure 82, also, there was no temperature dependency on the water vapor adsorption isotherms after inserting PCM. Therefore, the water vapor adsorption isotherm of PCM-inserted MSSZ-13 also can be considered as a function of P/P_0. Also, the isosteric heat of adsorption of PCM-inserted SSZ-13 calculated from the result of Figure 82.

Since there was no temperature dependency on the each of water vapor isotherms of SSZ-13 and PCM-inserted MSSZ-13, water vapor isotherm of SSZ-13 and PCM-inserted MSSZ-13 is shown in Figure 83, to compare the adsorbed amount of nitrogen at each of adsorbent. In Figure 83, the amount of adsorbed nitrogen on PCM-inserted MSSZ-13 was decreased compared to that on SSZ-13. This is because, as already discussed in Figure 78 and Table 15, some of the micropores, which is space for the adsorption, are not able to access owing to the existence of PCM. Even though there was a decrease in the amount of adsorbed, but still, the water vapor successfully adsorbed on PCM-inserted MSSZ-13.

In summary, from the results above, the PCM-inserted MSSZ-13 that simultaneously function as both heat storage material and also adsorbent, is successfully prepared.

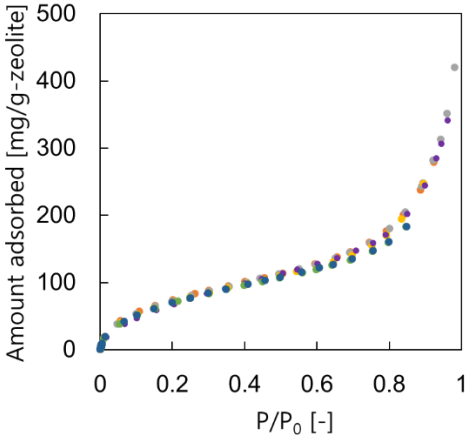

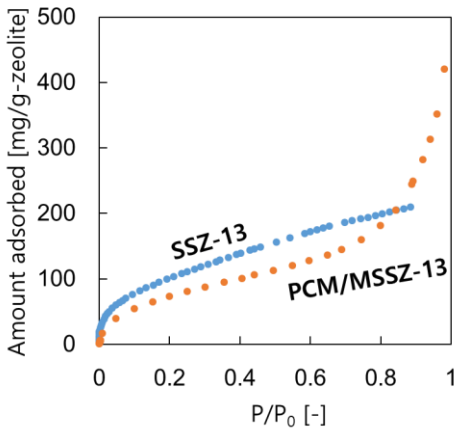

(Left) Figure 82. Water vapor adsorption isotherms of PCM-inserted MSSZ-13 at 6 different temperatures. 20 ℃ (orange line), 25 ℃ (gray line), 30 ℃ (yellow line), 35 ℃ (purple line), 40 ℃ (green line), and 45 ℃ (gray line).

(Right) Figure 83. Adsorption isotherms of SSZ-13 and PCM-inserted MSSZ-13.

3.4.4.3 Theoretical evaluation of PCM-inserted MSSZ-13

The simulations of dehumidifying fixed-bed adsorption process with SSZ-13 and PCM-inserted MSSZ-13, were performed under adiabatic condition. For each adsorbent, the fluid temperature at the outlet (Fig. 84 (a)), the amount of water-vapor adsorbed in whole fixed-bed (Fig.84 (b)), and the relative amount of adsorbed to the equilibrium amount (Fig.84 (c)), with time changing, were calculated during the initial 20 minutes.

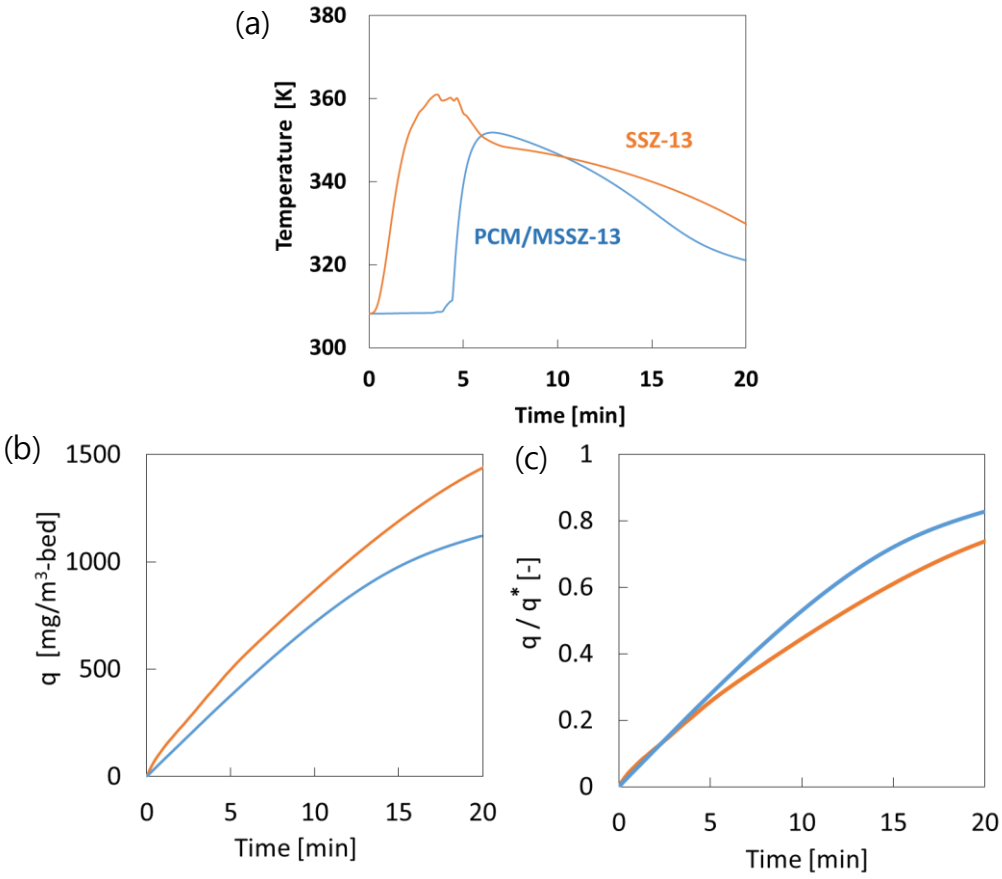

Figure 84. (a) The temperature of fluid at the outlet, (b) the amount of adsorbed water vapor, and (c) the relative amount of adsorbed water to equilibrium amount, as a function of time.

As shown in Figure 84 (a), PMC-inserted MSSZ-13 showed isothermal behaviors during the initial 5 minutes of adsorption process, owing to the latent-heat storage through PCM. Also, the increase of fluid temperature was slightly suppressed due to the sensible and latent heat storage through PCM. However, despite of the latent-heat storage through PCM, the amount of adsorbed water vapor on PCM-inserted MSSZ-13, was smaller, compared to the amount adsorbed on SSZ-13, in all the time as shown in Figure 84 (b). On the other hand, in terms of the relative amount of adsorbed to the equilibrium amount, q / q^* of PCM-inserted MSSZ-13 was larger than that of SSZ-13, during the initial 2 - 3 minutes, as shown in Figure 84 (c). This larger relative amount of adsorbed is obtained, due to the latent-heat storage through PCM. However, after 2 - 3 minutes, q / q^* of PCM-inserted MSSZ-13 became smaller than that of SSZ-13. These results suggest that PCM-inserted

MSSZ-13 successfully worked as heat-storage material, but, the effect of heat recovery on the adsorption performance was not significant. This becomes more distinct, when it compared to the results of PCM-inserted SBA-15 in chapter 3.2.4.2.

In the results of Figure 54, the adsorption performance of PCM-inserted SBA-15 was increased due to the heat-storage through PCM, during initial 7 minutes, despite of a smaller amount of q^*. Also, in Figure 84, q / q^* of PCM-inserted SBA-15 was significantly larger than that of SBA-15. On the contrary, in case of PCM-inserted MSSZ-13, the adsorption performance was not increased even though inserted PCM was successfully worked as heat-storage material. This suggests that there is a factor that emerging the difference on the adsorption process of between SBA-15 and SSZ-13. This factor is considered as water-vapor adsorption isotherm. The water-vapor adsorption isotherms of SBA-15, SSZ-13, PCM-inserted SBA-15 and PCM-inserted MSSZ-13 is depicted in Figure 85. In Figure 85, the amounts of adsorbed water vapor on SBA-15 and PCM-inserted SBA-15 are linearly increase with changes of P/P_0, which follows the Henry equation. On the other hand, the amounts of adsorbed water vapor on SSZ-13 and PCM-inserted SSZ-13 are dramatically increased at low range of P/P_0, then, increased moderately, which follows the Langmuir equation. In the simulation of dehumidifying fixed-bed adsorption, the fluid temperature was increased nearly 40 - 50 ℃ higher, as shown in Figure 84 (a). With increase of temperature, the relative pressure P/P_0 changes from initial condition 0.5 to approximately 0.05. Subsequently, with the changes of P/P_0, the equilibrium amount of adsorbed water, q^*, changes from q^*_1 to q^*_2, as listed in Table 16. q^*_1 is the amount of adsorbed water vapor when the relative pressure is 0.5, and q^*_2 is the amount of adsorbed water vapor when the relative pressure is 0.05. As you can notice from Table 16, the equilibrium amount of adsorbed water on SBA-15 and PCM-inserted SBA-15 changes much more significantly with change of the temperature, compared to that on SSZ-13 and PCM-inserted MSSZ-13. This suggests that the adsorption performance of SBA-15 is more affected to the temperature changes, which resulted from the heat of adsorption, compared to the case of SSZ-13.

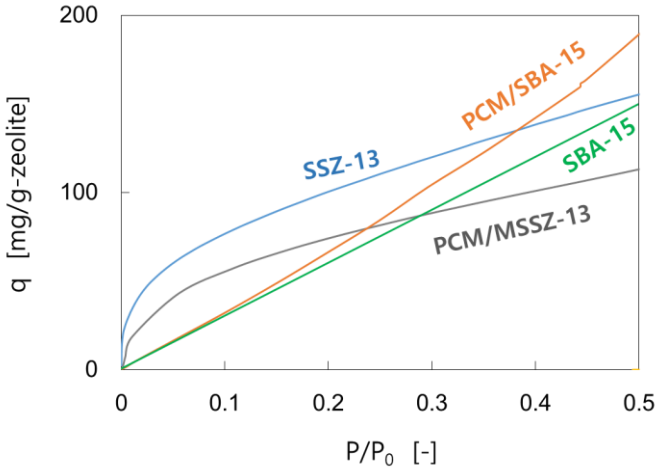

Figure 85. Water vapor adsorption isotherms of SBA-15, PCM-inserted SBA-15, SSZ-13, and PCM-inserted MSSZ-13.

Table 16. The changes of $q^*$with the changes of P/P_0.

	q^*_1 [mg/g-zeolite] (when P/P_0=0.5)	q^*_2 [mg/g-zeolite] (when P/P_0=0.05)	q^*_2 / q^*_1 [%]
SBA-15	190	15	8 %
PCM-inserted SBA-15	150	15	10%
SSZ-13	150	60	40%
PCM-inserted SSZ-13	110	40	36 %

In conclude, the PCM-inserted MSSZ-13 is proposed for a new concept of PCM-inserted adsorbent. PCM-inserted MSSZ-13 with having both heat storage site and adsorption site, was successfully prepared. To evaluate the effectiveness of PCM-inserted MSSZ-13, the simulation of dehumidifying fixed-bed adsorption process was run. However, the PCM-inserted MSSZ-13 showed decreased adsorption performance, even though PCM successfully worked as the heat storage material. The reason why the performance improvement of PCM-inserted MSSZ-13 was not achieved is because, the adsorption performance of SSZ-13 is not significantly affected by the temperature changes. Therefore, as for the concept of PCM-inserted adsorbent, PCM-inserted MSSZ-13 is not suitable concept to improve the adsorption performance. To develop this concept further, using zeolite of which more sensitive to the temperature changes than SSZ-13, such as SAPO-34, can be considered as future plan[8].

3.4.5 Conclusion

To realize the PCM-inserted adsorbent, it is necessary to separate the PCM-existing site and the adsorbate-existing site inside one material. Therefore, three different concepts of PCM-inserted adsorbent is proposed in this chapter, i.e. PCM-inserted SBA-15, PCM-inserted CNT and PCM-inserted MSSZ-13. Also, the effectiveness of each proposed concept on adsorption performance is evaluated through the simulation of dehumidifying fixed-bed adsorption process. The fluid temperature changes when the packed adsorbent is PCM-inserted SBA-15, PCM-inserted CNT, and PCM-inserted MSSZ-13, are summarized in Figure 86. Subsequently, the adsorbed amounts of water vapor in the whole bed of PCM-inserted SBA-15, PCM-inserted CNT, and PCM-inserted MSSZ-13, with changes of time, are summarized in Figure 87.

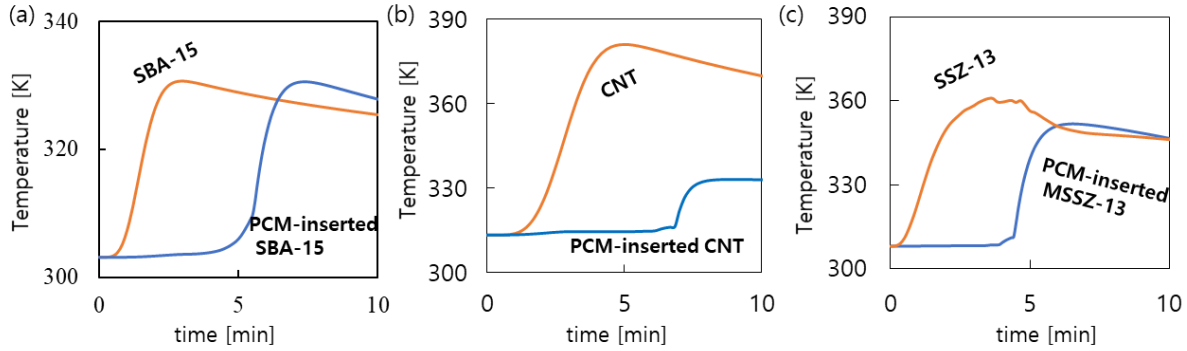

Figure 86. The fluid temperature when packed adsorbent was (a) PCM-inserted SBA-15, (b) PCM-inserted CNT, and (c) PCM-inserted MSSZ-13.

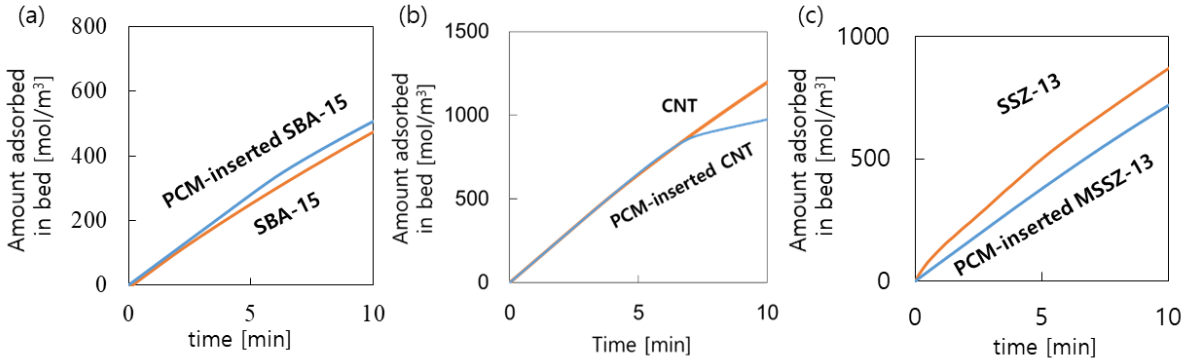

Figure 87. The adsorbed amount of water vapor in the whole bed of (a) PCM-inserted SBA-15, (b) PCM-inserted CNT, and (c) PCM-inserted MSSZ-13.

As for the reference, the changes of the fluid temperature and the amount of adsorbed in bed, without PCM, are also showed in Figure 86 and Figure 87.

In Figure 86, all of the proposed concepts of PCM-inserted adsorbent showed isothermal behavior during initial several minutes, and suppressed temperature increase, owing to the heat recovery of PCM. However, in the result of Figure 87, there is a difference in the adsorption performance between each concept. With inserting of PCM, PCM-inserted SBA-15 showed most improved adsorption process. With inserting of PCM, the adsorption performance of PCM-inserted CNT was very slightly increased, and the adsorption performance of PCM-inserted MSSZ-13 was decreased, not increased. These results indicates that, the effect of heat recovery through PCM on adsorption performance, can be differed by changes of some other parameters. As for other parameters the shape of adsorption isotherm branch, the degree of decreasing q^* with inserting PCM can be considered.

Once again, PCM-inserted SBA-15 stored the released heat of adsorption, and this heat recovery through PCM successfully resulted in the improvement of adsorption process. Consequently, among three concepts, PCM-inserted SBA-15 can be considered as most adequate concept for the PCM-inserted adsorbent.

From the summarized results, the presence of heat-storage function inside the adsorbent was not enough to achieve high adsorption performance. It is clarified that adequate condition is required to achieve the enhancement of adsorption performance through the heat-recovery. Hence, optimization of PCM-inserted SBA-15, through the parametric study, is necessary to effectively use the PCM-inserted SBA-15 as adsorbent.

Chapter 4. Optimization of PCM-inserted SBA-15 through parametric study

4.1 Introduction

Adsorption and desorption is an exothermic and endothermic phenomenon, respectively. In the process of adsorption, the generated heat during adsorption increases the temperature of the system and affects the apparent rate of adsorption, resulting in significant degrading of the performance of the process. Therefore, the removal of the heat of adsorption is important requirement in the adsorption process[71,72]. Theoretically, the highest performance of adsorption process is achieved through realization of an isothermal adsorption process under entirely adiabatic condition. Thus, realizing isothermal-adiabatic condition can be considered as an ultimate objective to upgrading adsorption performance.

As a method for the removal of the generated heat of adsorption, heat exchanger is one of the most representative examples[9]. Providing metal voids and internal fins[10], and using expandable graphite[11] are also reported as methods for the removal of the heat of adsorption, with improved the thermal conductivity. Those methods utilize sensible heat to remove the heat of adsorption. On the other hand, there is a heat-recovery method by using latent heat of phase change material (PCM)[13]. PCM in adsorption processes, absorbs the released heat of adsorption, and changes from solid to liquid. This latent heat storage through PCM has an advantage that it can store a high density of thermal energy within a small temperature range[84].

As mentioned in previous chapter 3.1, rubber spheres[73], metal voids[52], and polymer capsules[15] are reported as a container of PCM. However, these reported containers are having problems, such as difficulty for handling, heterogeneous distribution, and slow heat-transfer. Therefore, in the previous chapter 3, dual-functional PCM-inserted adsorbent[85] is proposed as a new concept to suppress and recover the released heat of adsorption. In this concept, by inserting the PCM directly into the void space of adsorbent, the generation of the heat of adsorption and the recovery of the heat by the PCM occur simultaneously in one material.

This concept has an advantage such that rapid heat-transfer, homogenous distribution, and less leakage problem. And, in chapter 3, as a specific concept of the PCM-inserted adsorbent, PCM-inserted SBA-15, PCM-inserted CNT, and PCM-inserted MSSZ-13 was prepared. Also, to understand the effectiveness of each PCM-inserted adsorbents as for the both adsorbent and the heat storage material, simulation of fixed-bed dehumidifying adsorption process with the prepared PCM-inserted SBA-15 was run. As a result, each adsorbent showed isothermal behavior under adiabatic condition during an initial few minutes, but among them, PCM-inserted SBA-15 showed most improved performance. This result suggests that the heat of adsorption was successfully recovered, and also, this new concept is demonstrated as effective method to improve the performance of adsorption.

However, desirable conditions for the fabrication of PCM-inserted adsorbent and effective conditions for applying PCM-inserted SBA-15 is yet unknown. Thus, understanding of the key parameter is still required for modeling the PCM-inserted SBA-15 with high performance. This chapter aims to figure out the desirable conditions for the high performance of PCM-inserted adsorbent. To investigate key parameters for modeling PCM-inserted adsorbent, parametric studies of PCM-inserted SBA-15 in adsorption process were carried out. As an example of adsorption process, once again, fixed-bed dehumidifying adsorption process with PCM-inserted SBA-15 was simulated. The enthalpy of fusion of inserted PCM, the amount of inserted PCM, and the temperature of the fluid at the inlet were investigated as key parameters. The simulations were run under adiabatic condition. The desirable condition for PCM-inserted SBA-15 was evaluated from the effectiveness of fixed-bed dehumidifying adsorption process; which is, the amount of water adsorbed on SBA-15 in the initial few minutes of adsorption process.

4.2 Theoretical evaluation of PCM-inserted SBA-15 under various conditions

4.2.1 Mathematical modeling

A fixed-bed dehumidifying adsorption process was simulated under adiabatic conditions with PCM-inserted SBA-15. As an experimentally prepared PCM-inserted SBA-15, the sample prepared in chapter 3.2 was used. Also, SBA-15 without PCM was simulated as a reference. Since this parametric study uses adsorbent as PCM-inserted SBA-15 and everything is exactly same, except the value of key parameters, the details of mathematical models and assumptions for the calculations are exactly same to that used in chapter 3.2.

4.2.2 Selection of key parameters and calculation conditions

In the result of experimentally prepared PCM-inserted SBA-15, 0.655 g of paraffin was inserted in 1 g of SBA-15, and the measured enthalpy of fusion of the inserted paraffin was 53.3 J/g-PCM. This value corresponds to 23% of that of bulk. The decrease of apparent enthalpy of fusion of the inserted PCM inside the mesopore is already discussed in chapter 2. The phase change of the inserted paraffin from solid to liquid started at 304 K and ended at 317 K, which was also largely shifted from the phase change temperature of bulk, i.e. 317 and 327 K, respectively.

To increase the heat-storage efficiency, increase of the latent-heat-storage capacity can be considered. Heat storage capacity is determined by the enthalpy of fusion of the inserted PCM, H, and the amount of the inserted PCM, w_1. Therefore, these two parameters are considered as the key parameters for modeling high functional PCM-inserted SBA-15, as adsorbent fabricating parameters. On the other hand, as a key parameter for operating PCM-inserted adsorbent in adsorption process, the temperature of fluid at inlet, $T_{F,in}$, was studied. In this parametric study, to neglect the effect of changes in relative humidity at the inlet, relative humidity of water vapors at the inlet is fixed at 50%, as listed in Table 6. Therefore, the concentration of water vapors at the inlet is

determined by only $T_{F,in}$. For this reason, as an effective condition parameter in adsorption process, $T_{F,in}$ was also considered a key parameter. Basically, for the each parameter, the experimentally prepared values of H , w_1 , and $T_{F,in}$, were used, which were 53.3 J/g , 0.66 g/g, and 303 K, respectively, in the calculations. And in the study of each key parameters, the values of the selected parameters used are listed in Table 17.

Table 17. Selected key parameters and the studied values.

Study 1. Key parameter : Enthalpy of fusion of the inserted PCM, H (J/g-PCM)	
Temperature of fluid at inlet, $T_{F,in}$ (K)	303
Enthalpy of fusion of the inserted PCM, H (J/g-PCM)	53.3*, 118.3, 236.5
Ratio of the inserted PCM in SBA-15, w_1 (g-PCM/g-SBA-15)	0.66*
Study 2. Key parameter : Ratio of the inserted PCM in SBA-15, w_1 (g-PCM/g-SBA-15)	
Temperature of fluid at inlet, $T_{F,in}$ (K)	303
Enthalpy of fusion of the inserted PCM, H (J/g-PCM)	53.3*
Ratio of the inserted PCM in SBA-15, w_1 (g-PCM/g-SBA-15)	0.66*, 0.85, 1.05
Study 3. Key parameter : Temperature of fluid at inlet, $T_{F,in}$ (K)	
Temperature of fluid at inlet, $T_{F,in}$ (K)	303, 318, 333
Enthalpy of fusion of the inserted PCM, H (J/g-PCM)	53.3*
Ratio of the inserted PCM in SBA-15, w_1 (g-PCM/g-SBA-15)	0.66*

*values that experimentally prepared PCM-inserted SBA-15.

The pellet density and the heat capacity of the pellet are changes in the parametric study of the ratio of the inserted PCM in SBA-15, w_1.. The corresponding values of the pellet density and the heat capacity of the pellet to the change in w_1 are summarized in Table 18.

Table 18. Correspondingly changed values with the changes of w_1.

Ratio of the inserted PCM in SBA-15, w_1	0.66	0.85	1.05
Pellet density, ρ_p (kg/m^3)	551	616	682
Heat capacity of a pellet, $C_{p,p}$ (J/kg·K)	1037	1087	1128

On the other hand, the phase-change temperature of PCM should be higher than the fluid temperature at inlet, $T_{F,in}$, to observe the latent-heat storage effect in adsorption performance. As listed in Table 18, basically, the phase change of the inserted PCM started at 304 K and ended at 317 K. However, these temperatures were lower than $T_{F,in}$, which listed in Table 3, 318 and 333 K. Therefore, with the changes of $T_{F,in}$, the phase-change temperature of PCM must be changed. The changed phase-change temperature, on purpose, is listed in Table 19. In all other parametric studies, $T_{F,in}$ was fixed at 303 K, and also both T_{start} and T_{end} were fixed at 304 and 317 K, respectively.

Table 19. Values of changed parameters with the change in inlet temperature

Temperature of fluid at inlet, $T_{F,in}$ (K)	303	318	333
Phase-change-start temperature, T_{start} (K)	304	319	334
Phase-change-end temperature, T_{end} (K)	317	332	347

The values of other parameters, which are not studied as key parameters, are used as exactly same parameters used in chapter 3.2. These values are fixed in all the simulations performed in this study.

4.3 Results and discussion

4.3.1 Study 1. The enthalpy of fusion of inserted PCM

According to the changes of the enthalpy of fusion of inserted PCM, *H*, the changes in the amount of water vapor adsorbed in total fixed-bed (Fig.88 (a)), the changes in the fluid temperature at the outlet (Fig.88 (b)), and changes in the ratio of stored latent-heat to the enthalpy of fusion, χ, (Fig.88 (c)), were calculated and showed as a function of time, within initial 20 minutes. In Figure 88 (a), there was no difference in the amount of adsorbed water between the various enthalpy of fusion during initial 5 minutes. After that, the amount of adsorbed water-vapor was getting larger with increase of the value of *H*. In Figure 88 (b), the fluid temperature at the outlet depicted isothermal behavior during the initial several minutes, due to the latent-heat storage effect of PCM. Hence, this suggests that PCM completely absorbed the released heat of adsorption during initial stage and successfully worked as latent-heat storage material. Also, the latent-heat storage capacity increase with the increase of *H*. Therefore, the isothermal behavior was observed for longer time, which indicates that the heat storage through PCM lasted for longer time, with the increase of *H*. This result can be also suggested from the result Figure 88 (c). In Figure 88 (c), the time required for the value of χ reaching to 100%, getting longer with increase of *H*. The increase of fluid temperature (Fig.88 (b)) was observed after χ reached to 100% (Fig.88 (c)), which indicates, after heat storage through PCM completed. In this time, PCM works as only sensible-heat storage material, hence, increase of the temperature affects to the apparent rate of adsorption, and causing degradation of the adsorption performance after χ reached to 100% (Fig.88 (a)). Therefore, inserted PCM with a higher value of the enthalpy of fusion stored the larger amount of thermal energy, resulting in a longer time latent-heat storage, a more suppression to the increase in temperature, and the higher performance on the adsorption process.

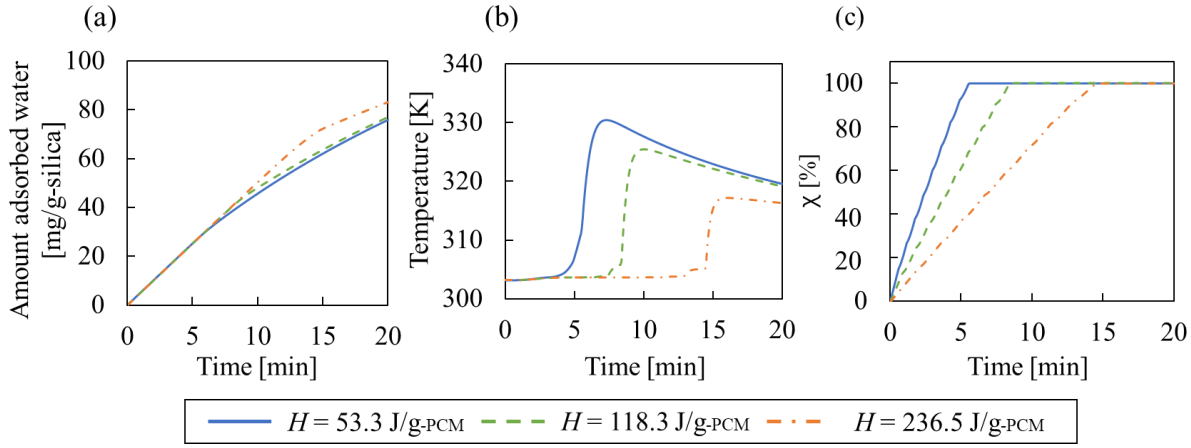

Figure 88. Time courses of (a) the amount of adsorbed water vapor, (b) temperature change of the fluid at the outlet, and (c) the ratio of amount of stored heat through PCM to the enthalpy of fusion, with different value of the enthalpy of fusion of inserted PCM.

As a result, the enthalpy of fusion of inserted PCM significantly affected on the heat-storage capacity. And, the increase of heat-storage capacity effected to the adsorption performance, in the sense of high-performance maintaining time. The experimentally prepared value of enthalpy of fusion of paraffin was 23% of the bulk. To increase the enthalpy of fusion, it is already confirmed that the increase of pore diameter is necessary, in chapter 2. Hence, PCM-inserted adsorbent with a larger pore-size is required for the realization of more enhanced adsorption performance. According to the previous researches done by Kruk[86], and Galarneau[87], the expansion of mesopore of SBA-15 can be realized by using a swelling agent[86], or changing the aging temperature[87]. However, the method for expanding mesopore diameter of SBA-15, larger than approx.20 nm, is not reported. Hence, to using host adsorbent with large mesopore diameter more than approx. 20 nm, mesoporous silica with ultra-large mesopore such as MCF, not SBA-15, can be considered as an alternative method. However, in any case, other parameters such as density, adsorption equilibrium will subsequently change with the change of mesopore diameter, thereby, further consideration should be required. Also, selection of PCM molecule with higher enthalpy of fusion compared to paraffin can be an additional method for achieving much higher performance.

But, the limitation is that, there is not that much materials, which possessing higher enthalpy of fusion but similar melting-point range compared to paraffin.

4.3.2 Study 2. The amount of inserted PCM

According to the changes of the ratio of inserted PCM, the changes in the amount of water-vapor adsorbed in whole fixed-bed (Fig.89 (a)), and the changes in the temperature of fluid at the outlet (Fig.89 (b)), and the ratio of the stored heat to the enthalpy of fusion, χ, (Fig.89 (c)) were calculated and depicted as a function of the time. With increase of the ratio of inserted amount of PCM, w_1, the adsorbed amount of water vapor was slightly increased as shown in Figure 89 (a). Also, in Figure 89 (b), with the increase of w_1, the fluid temperature at the outlet depicted an isothermal behavior for longer time, and the increase of fluid temperature was more suppressed. This suggests that PCM completely absorbs the released heat during the time for isothermal behavior in adsorption process. Moreover, with increase of w_1, the longer time was required for χ reaching to 100%. This indicates that the latent-heat storage occurred for a longer time. This is because, with the increase of w_1, the latent-heat storage capacity also increased. With the increase of heat-storage efficiency, the fluid temperature was more suppressed and latent heat storage occurred for longer time, which resulted in performance upgrading.

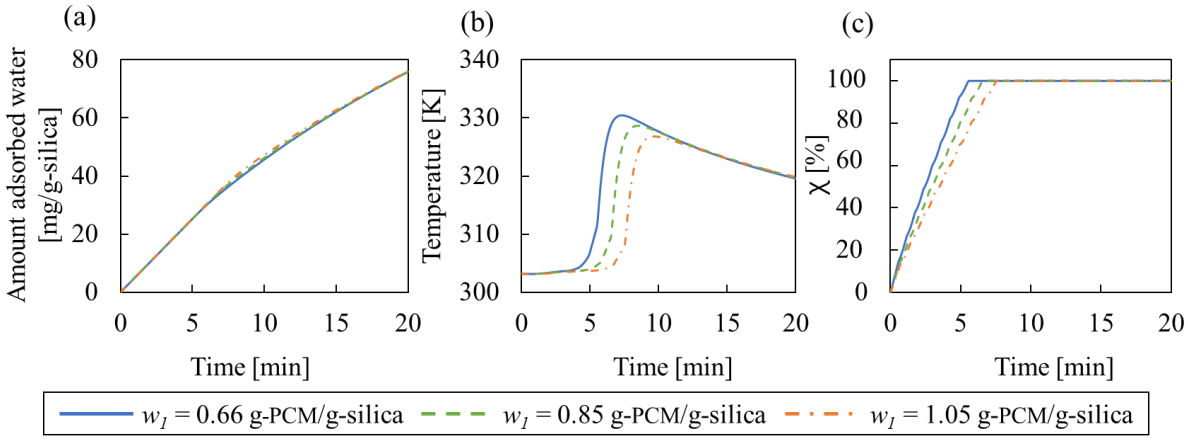

Figure 89. Time courses of (a) the amount of adsorbed water vapor, (b) temperature changes of the fluid at the outlet, and (c) the ratio of amount of stored heat through PCM to the enthalpy of fusion, with different amount of inserted PCM in SBA-15.

As a result, the amount of inserted PCM inside adsorbent, affected to the adsorption performance. Inserting PCM with larger w_1 is desirable to improve the g adsorption performance, owing to the increase of heat-storage capacity. To inserting larger PCM in adsorbent, larger mesopore volume of host SBA-15 is required. Again, it is already confirmed that larger mesopore volume of SBA-15 can be achieved by expanding pore diameter, in chapter 2. And, the mesopore diameter can be increased by using swelling agent[86] and changing aging temperature[87], as discussed in chapter 4.3.1. Also, as an alternative method for inserting PCM in the adsorbent pellet, addition to the mesoporous space, utilization of the secondary-structure space, such as intergranular spaces is necessary. To inserting PCM into secondary-structure space, the inserting method 'liquid impregnation', discussed in chapter 2, can be considered.

4.3.3 Study 3. The inlet temperature

According to the changes in the fluid temperature at the inlet, $T_{f,in}$, the changes in the amount of water-vapor adsorbed in whole fixed-bed (Fig.90 (a)), the changes in $T_{f,out}$ - $T_{f,in}$ (Fig.90 (b)), and the changes in ratio of the stored heat to the enthalpy of fusion, χ, (Fig.90 (c)) were calculated and depicted as a function of time. In Figure 90 (a), the inlet temperature, 333 K showed the highest amount of adsorbed water as shown among the various $T_{f,in}$. Also, in Figure 90 (a), with the increase of $T_{f,in}$, the amount adsorbed of water significantly increased in the very initial few minutes. Next, as shown in Figure 90 (b), the temperature of fluid at the outlet showed an isothermal behavior for initial few minutes. However, unlike other key parameters, the increase of $T_{f,in}$ resulted in shorter time of the isothermal behavior and larger increase of the temperature of fluid passing through the bed. Moreover, with increase of $T_{f,in}$, the time for χ reaching to 100% became shorter (Fig.90 (c)). Since χ reached to 100%, and the temperature of fluid passing through the bed showed isothermal behavior during the initial stage, it can be considered that PCM successfully worked as latent-heat storage material.

In this calculation, only the inlet temperature changed as a key parameter. Hence, the heat-storage capacity of PCM was the same under each $T_{f,in}$. Therefore, the isothermal behavior for shorter time indicates that larger amount of the heat of adsorption was released per time. Releasing larger amount of the heat per time suggests that the rate of adsorption increased. This also agreed with the rapid increase of the adsorbed amount of water in Figure 90 (a). The gradient in Fig.90 (a) corresponds to the rate of adsorption. The rate of adsorption is increased with the change of the inlet temperature, which also changes the concentration of water vapor at the inlet. Since relative humidity at the inlet was fixed as 50%, with the increase of $T_{f,in}$ from 303 to 318 to 333 K, the concentration of water vapor at the inlet increased from 0.84 to 1.81 to 3.60 mol/m^3, respectively. In the mathematical model equations governed in this study, the rate of adsorption is calculated from the Eq.5. In this equation, the rate of adsorption is determined by the difference between q^* and q. Therefore, with the increase of $T_{f,in}$, the water-vapor concentration increase and the difference between q^* and q also increase, resulted in the adsorption of a larger amount of water on PCM-inserted SBA-15 in the same period of time.

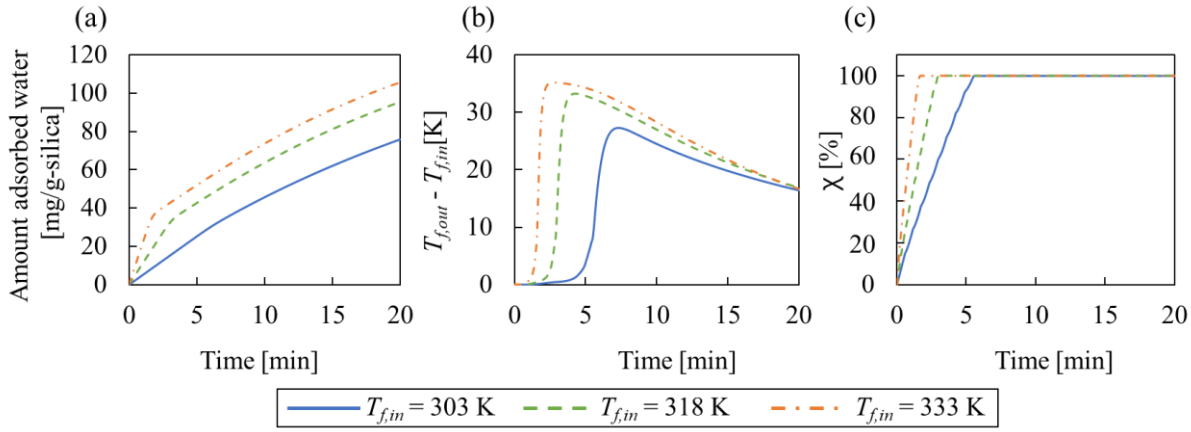

Figure 90. Time courses of (a) the amount of adsorbed water vapor, (b) the difference of the fluid temperature between at the inlet and at the outlet, and (c) the ratio of amount of stored heat through PCM to the enthalpy of fusion, with different fluid temperature at the inlet.

Compared to the other key parameters (Fig.88 (a) and Fig.89 (a)), $T_{f,in}$ significantly affect to the adsorption performance (Fig.90 (a)). From this result, it can be considered that PCM-inserted adsorbent can be more effectively used for the recovery of heat of adsorption, by fastening the rate of adsorption. Therefore, when relative humidity of fluid at the inlet is fixed, higher fluid temperature at the inlet is more adequate for the operating condition of PCM-inserted SBA-15. With increase of $T_{f,in}$, the phase change temperature of PCM was intentionally changed as shown in Table 19. To increase the phase change temperature of PCM in real, selection of longer carbon chain paraffin as PCM, or selection of PCMs with functional group, such as fatty acids are considerable. Furthermore, other conditions that rapid adsorption can be achieved, such as high concentration, short diffusion route, and rapid diffusion coefficient would be desirable condition.

4.3.4 Most adequate conditions proposed through parametric studies

The dehumidifying fixed-bed adsorption process with PCM-inserted SBA-15 with the most adequate parameter values used in this study (H = 236.5 J/g-PCM, w_1 = 1.05 g-PCM/g-silica, and $T_{f,in}$ = 333 K) was simulated. And, as a reference, SBA-15 without PCM ($T_{f,in}$ = 303 K), PCM-inserted SBA-15 with experimentally prepared (H = 53.3 J/g-PCM, w_1 = 0.66 g-PCM/g-silica, and $T_{f,in}$ = 303 K) [85], were also simulated. For each adsorbent, the changes of the adsorbed amount of water-vapor in whole fixed-bed (Fig.91 (a)), the the changes in $T_{f,out}$ - $T_{f,in}$ (Fig.91 (b)), and the ratio of the stored heat through to the enthalpy of fusion, χ, (Fig.91 (c)) were calculated as a function of time. As shown in Figure 91 (a), experimentally prepared PCM-inserted SBA-15 showed a slightly larger amount of adsorbed water compared to SBA-15 without PCM. However, by employing the most adequate parameter values proposed in this study to the PCM-inserted SBA-15, the adsorbed amount of water increased dramatically, for nearly 4 times larger amount, during initial several minutes (Fig.91 (a)). However, in case of PCM-inserted SBA-15 with most adequate parameters, the temperature of fluid passing through the bed, shown in Figure 91 (b), depicted an isothermal behavior for 1

minutes owing to the huge amount of released heat of adsorption during same period. After 1 minute, the fluid temperature increased about 30 K from inlet to outlet, which does not suppressed compared to other adsorbent (Fig.91 (b)). Also, from the result of Figure 91 (c), it is suggested that PCM successfully worked as latent-heat storage material. In conclusion, the performances of adsorption and heat-storage are significantly improved through the modeling of PCM-inserted SBA-15 with the adequate parameter values. This improvement can be achieved by the increase of both heat storage capacity of PCM and the rate of adsorption at the same time by combining the most adequate individual key parameters.

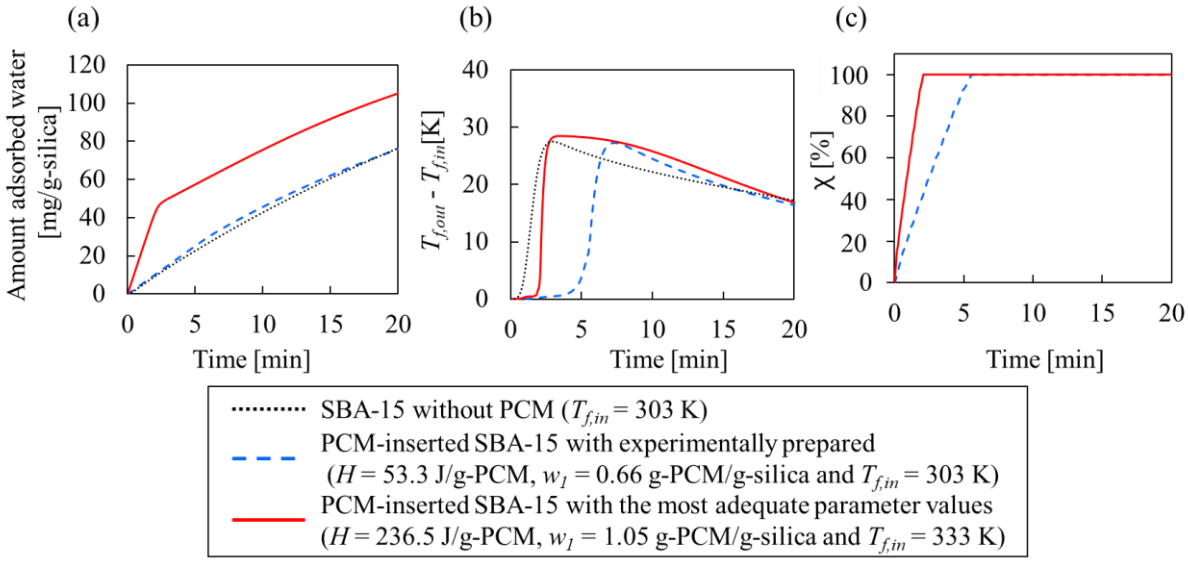

Figure 91. Time courses of (a) the amount of adsorbed water vapor; (b) the difference of the fluid temperature between at the inlet and at the outlet; (c) the ratio of amount of stored heat through PCM to the enthalpy of fusion with SBA-15 (black dotted line), PCM-inserted SBA-15 with experimentally prepared (blue dashed line), and PCM-inserted SBA-15 with most adequate parameters used in this study (red solid line).

4.4 Conclusions

Understanding of key parameters for fabrication and operating condition of PCM-inserted SBA-15 is necessary to optimize the performance of PCM-inserted SBA-15. In this study, the enthalpy of fusion of the inserted PCM, the ratio of inserted amount of PCM, and the temperature of fluid at the inlet, were investigated as key parameters. As for a parametric studies for each key parameters, the simulation of fixed-bed dehumidifying adsorption process was performed. As a result, the increase of both the enthalpy of fusion and the amount of inserted PCM increased the heat storage efficiency of PCM, resulted in the improvement of adsorption performance. The increase of fluid temperature at the inlet affected to the apparent rate of adsorption, resulted in drastic improvement of the performance of adsorption process. Based on these individual parametric studies, PCM-inserted SBA-15 with the most adequate parameter values was modeled. The modeled adsorbent achieved high performance in the fixed-bed dehumidifying adsorption process, which was 4 times improved performance, at the initial few minutes. Accordingly, PCM-inserted SBA-15 could applied on dehumidifying adsorption process with enhanced performance. Also, PCM-inserted SBA-15 have a potential to be used in highly exothermic and rapid adsorption process, where the inserted PCM is expected to work more effectively for the recovery of the heat of adsorption.

Chapter 5. Experimental evaluation of PCM-inserted adsorbent

5.1 Introduction

As described in chapter 3, PCM-inserted adsorbent is proposed as a new method for the recovery of the heat of adsorption in this study. By inserting PCM directly into the adsorbent itself, the generation of the heat of adsorption and removal of the heat of adsorption can be completed inside one material. Therefore, the apparently isothermal adsorption system under adiabatic condition is expected to be achieved by developing PCM-inserted adsorbent. Ultimately, performance of adsorption performance is expected to be highly improved via developing PCM-inserted adsorbent. However, to substantiate the idea of PCM-inserted adsorbent, separation of the space for existing adsorbate and the PCM inside the adsorbent, is necessary. Hence, as a more specific concept of PCM-inserted adsorbent, three different concepts of PCM-inserted adsorbent are proposed, i.e. PCM-inserted SBA-15, PCM-inserted CNT and PCM-inserted MSSZ-13, in chapter 3. Specific explanations about each concept of PCM-inserted adsorbent were discussed in the chapter 3.2, 3.3, and 3.3 respectively. Also, each concept of PCM-inserted adsorbent was successfully prepared in chapter 3.

The heat recovery efficiency of the prepared each concept of PCM-inserted adsorbent was theoretically evaluated through a dehumidifying fixed-bed adsorption process. From the theoretical evaluation results, PCM-inserted SBA-15 showed improved adsorption performance owing to the heat recovery through PCM. However, it is revealed that just having the heat-storage site inside the adsorbent was not enough to achieve high adsorption performance. It is clarified that adequate condition is required to achieve the enhancement of adsorption performance through the heat-recovery. Therefore, parametric studies for optimizing PCM-inserted SBA-15 were also done by the simulation of dehumidifying fixed-bed adsorption process, in chapter 4.

Simulation has many advantages such that, short time-consuming, low cost, easy to change parameters, and possible to consider non-realistic conditions. This advantages of simulation enables us to understand qualitative characteristics, deeply. Theoretical evaluation was essential to understand the key parameters, effectiveness, and requirements, for developing and optimizing the PCM-inserted adsorbent. However, simulation have limitations compared to the experiment, such as the lack of the validity of mathematical model and assumptions used in simulation, and accuracy of coding. In actual, to simplify the mathematical model used in chapter 3 and chapter 4, many assumptions are made. In terms of experiment, these things are non-necessary because experiment is realistic result.

For this reason, the experimental evaluation of the effectiveness of PCM-inserted adsorbent is necessary. In this chapter, evaluation of PCM-inserted adsorbent through the experiment of dehumidifying fixed-bed adsorption process was performed. To experiment the dehumidifying fixed-bed adsorption process, adsorption process was built-up by using TCD detector. Gas flow including water vapor was supplied by bubbling the liquid water. As for the PCM-inserted adsorbents, prepared PCM-inserted SBA-15 and PCM-inserted MSSZ-13 in chapter 3, were used.

5.2 Experimental

The dehumidifying fixed-bed adsorption process was built-up by using TCD detector. Schematic image of dehumidifying fixed-bed adsorption process is depicted in Figure 92.

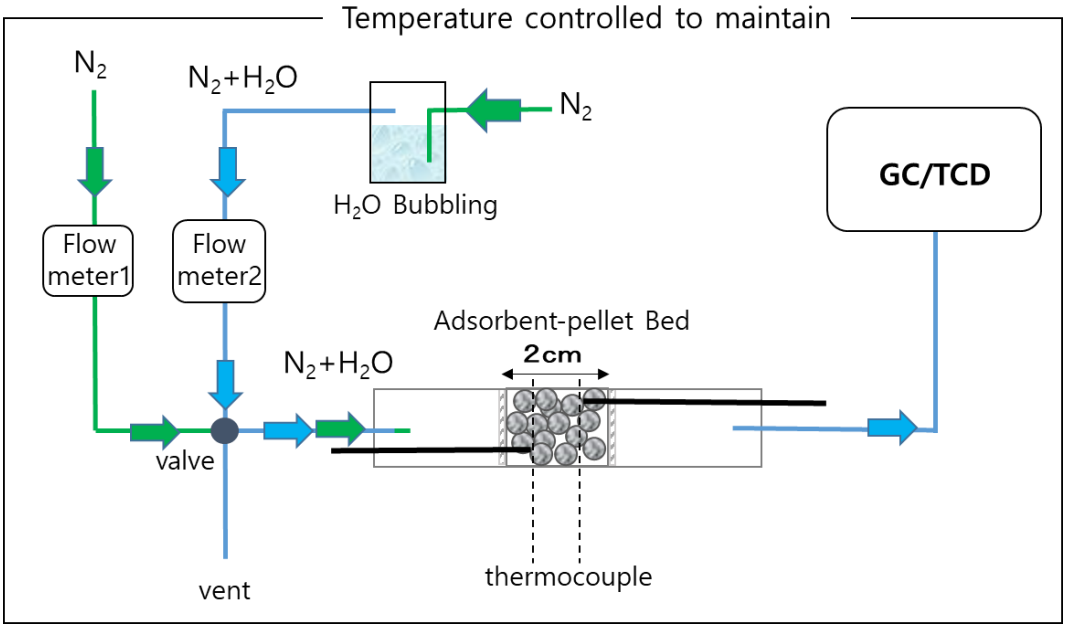

Figure 92. Schematic image of dehumidifying fixed-bed adsorption process.

Nitrogen gas was supplied in two different line. One line is directly connected to the column of the adsorbent, and the other nitrogen line is connected to the hot water bath(80 – 90 ℃), for containing water vapor. Then the mixed gas of nitrogen and water vapor was cool down until reach temperature set in adsorption process. One line of flow is containing pure nitrogen only, and the other line of flow is containing saturated water vapor with nitrogen. Then, the water-containing nitrogen line was connected to the column of adsorbent bed, or vent. The flow rate of each line was controlled by flowmeter. The flow rate used in the simulation in chapter 3 and 4, was fast flow rate, which was bed-length per second. This is because, PCM-inserted adsorbent was proposed in the purpose of applying in short-time rapid adsorption process, such as PSA, as mentioned in chapter 1 and

3. For the experimental evaluation, using same condition of that used in simulation is preferable to obtain the validity of the simulation results. However, the generation of water vapor could not catch up the fast flow rate, resulted in un-sustainable supplement of water vapor in the experiment of adsorption process. Therefore, flow rate of both line was fixed at 100 ml/min in all the experiment. Relative humidity at inlet was fixed at 50 % in all the experiment. In the experiment, the temperature of the system of adsorption process, which is shown in black box in Figure 92, was controlled to maintain set temperature. The setting temperature of system was 29.5 ℃ in case of PCM-inserted SBA-15, and 34.5 ℃ in case of PCM-inserted MSSZ-13. The column of the adsorbent bed was surrounded by styrofoams to make the adiabatic condition in the adsorbent bed. The temperature of adsorbent bed was measured at two point, by using thermocouple. One is near the inlet and the other is near the outlet. The length of adsorbent bed was 2 cm and the diameter of the radius direction of bed was 1 cm. The pelletized adsorbent was sieved in the range of 2 mm - 4 mm, then packed in the bed. The supplied gas flow at the inlet, passed through the adsorbent bed, then detected by TCD. The concentration of water vapor was detected, and with the change of concentration, the amount of adsorbed water was calculated.

5.3 Result and Discussion

5.3.1 Experimental evaluation of PCM-inserted SBA-15

The dehumidifying fixed-bed adsorption process with prepared PCM-inserted SBA-15 in chapter 3, was carried out. Characteristics of prepared PCM-inserted SBA-15, such as melting point, enthalpy of fusion, porous properties, and water-vapor adsorption isotherms, are described in chapter 3.2. The fluid temperatures measured by thermocouples at the inlet and at the outlet are depicted in Figure 93 (a) and (b), respectively. Also, the amount of water-vapor adsorbed in the whole fixed-bed, which was calculated from the changes of concentration measured by TCD, is depicted in Figure 93 (c). Subsequently, the relative amount of adsorbed water vapor to equilibrium amount, which is q/q^*, is depicted in Figure 93 (d).

As shown in Figure 93 (a) and (b), the increase of fluid temperature was suppressed in all the time, whether at the inlet or at the outlet, by using PMC-inserted SBA-15. In Figure 93 (c), according to this heat recovery effect through PCM, the amount of adsorbed water vapor on PCM-inserted SBA-15, was almost same during initial 3 minutes, compared to SBA-15, despite of a smaller amount of q^*. The same amount of adsorbed water between SBA-15 and PCM-inserted SBA-15 during initial 3 minutes, indicates that, same amount of heat was released from the adsorbent between SBA-15 and PCM-inserted SBA-15 during initial 3 minutes. Therefore, the suppression of the fluid temperature of PCM-inserted SBA-15 during initial 3 minutes in Figure 93 (a) and (b), obviously suggests that, inserted PCM was successfully worked as both the sensible-heat storage material and latent-heat storage material. However, the fluid temperature of PCM-inserted SBA-15 did not show isothermal behavior. In simulation, the fluid temperature of PCM-inserted SBA-15 showed isothermal behavior during latent-heat storage through PCM occurs. From this result, to increase the accuracy of the simulation, it can be considered that further consideration is required, such as the melting speed of PCM. Even though PCM succeed to recover the heat of adsorption, the

amount of adsorbed water vapor did not increased, as shown in Figure 93 (c). It is already known that the effect of heat recovery through PCM on adsorption performance can be differed by changes of some other parameters. Therefore, the reason why performance improvement was not observed is because, the conditions used in experiment, such as flow rate, bed length, pellet size and so on, were different from that used in the simulation. Also, in experiment, the fixed-bed was not entirely adiabatic, and the heat transfer along the radial direction was not able to neglect, since the bed length was not long enough than bed diameter. These are also can be considered as the reason for that the improvement of adsorption process was not observed. On the other hand, the value of q/q^* of PCM-inserted SBA-15 was higher than that of SBA-15, during initial 8 minutes. With existence of PCM, the value of q/q^* was increased during initial 8 minutes. This suggest that PCM-inserted SBA-15 was successfully recovered the heat of adsorption, and resulted in the increase of apparent rate of adsorption, during initial 8 minutes.

To investigate the reproducibility of the experimental results depicted in Fig.93, dehumidifying fixed-bed adsorption using SBA-15 was repeated for 3 times. The fluid temperatures at the inlet and at the outlet are depicted in Figure 94 (a) and (b), respectively. The amount of water-vapor adsorbed in whole fixed-bed is depicted in Figure 94 (c). As you can notice from Fig.94, the temperature and the amount of adsorbed were almost overlapped, between 3 times of repeated measurements. Therefore, the experimental results depicted in Fig.93 is considered to be reliable.

In summary, from the results above, PCM-inserted SBA-15 successfully worked as both heat storage material and adsorbent at the same time in the experiment. This results suggests that PCM-inserted SBA-15 is proved as an effective concept for the PCM-inserted adsorbent as proposed in this dissertation. However, the improvement of adsorption performance by using PCM-inserted SBA-15 was not observed. The improvement of adsorption performance might be achieved by preparing the optimized PCM-inserted SBA-15, with adequate parameters used in chapter 4.

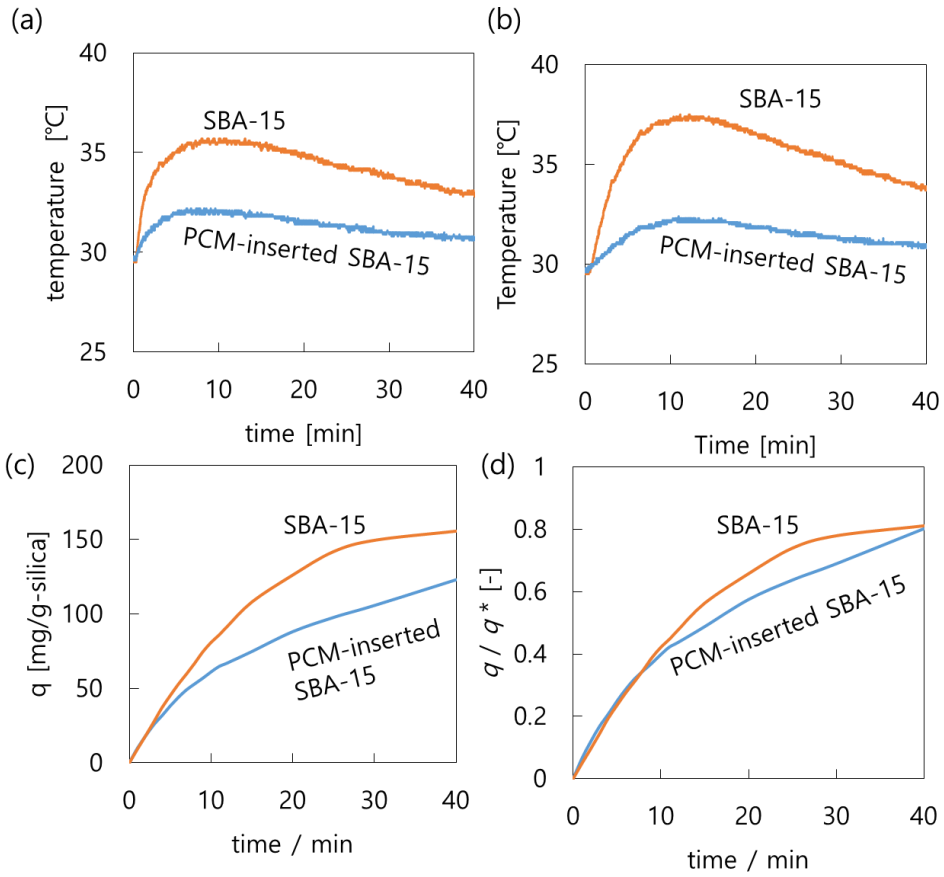

Figure 93. Time course of (a) fluid temperature at inlet, (b) fluid temperature at outlet, (c) the amount of adsorbed water vapor in whole fixed-bed, and (d) the relative amount of adsorbed water vapor to equilibrium amount.

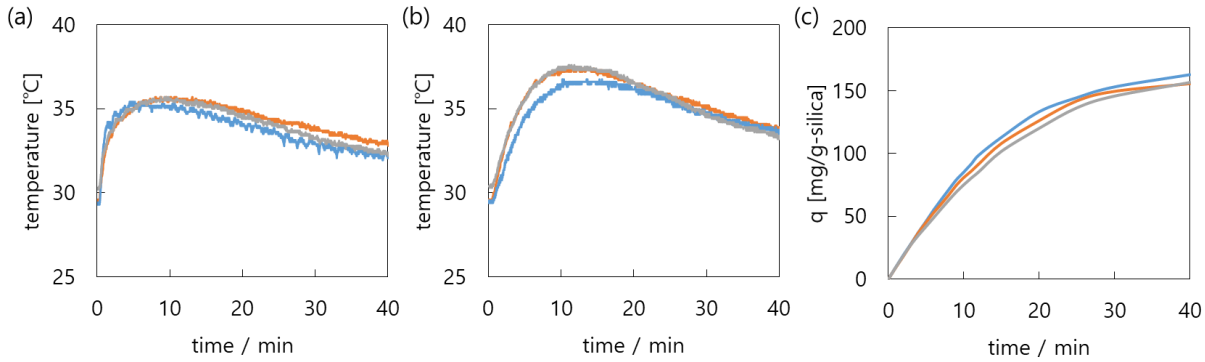

Figure 94. Time course of (a) fluid temperature at inlet, (b) fluid temperature at outlet, and (c) the amount of adsorbed water vapor in whole fixed-bed with repeated measurement. (orange line: first measurement, blue line: second measurement, gray line: third measurement).

5.3.2 Experimental evaluation of PCM-inserted MSSZ-13

The dehumidifying fixed-bed adsorption process with prepared PCM-inserted MSSZ-13 in chapter 3, was experimented. Characteristics of prepared PCM-inserted MSSZ-13 are described in chapter 3.4. The fluid temperatures measured at the inlet and at the outlet, are shown in Figure 95 (a) and (b), respectively. Also, the amount of water-vapor adsorbed in the whole fixed-bed, which was calculated from the changes of concentration detected by TCD, is depicted in Figure 95 (c). Subsequently, the relative amount of adsorbed water vapor to equilibrium amount, which is q/q^*, is depicted in Figure 95 (d).

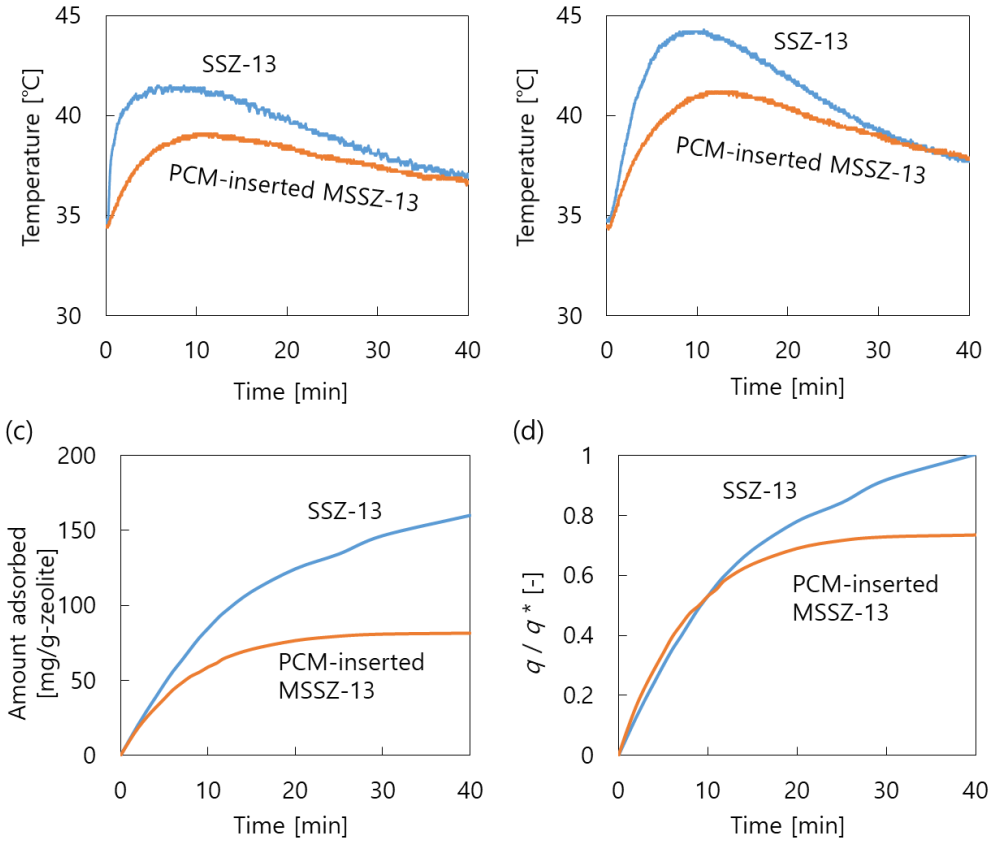

Figure 95. Time course of (a) fluid temperature at inlet, (b) fluid temperature at outlet, (c) the amount of adsorbed water vapor in whole fixed-bed, and (d) the relative amount of adsorbed water vapor to equilibrium amount.

The results shown in Figure 95 is on the almost same tendency of the results of PCM-inserted SBA-15. As shown in Figure 95 (a) and (b), the increase of fluid temperature was suppressed in all the time, whether at the inlet or at the outlet, by using PMC-inserted MSSZ-13. This suggests that, inserted PCM was successfully worked as a heat storage material in the adsorbent. However, in Figure 95 (c), even though the successful heat recovery through PCM, the amount of adsorbed water vapor on PCM-inserted MSSZ-13, was smaller compared to SSZ-13. This might be because, as already described in previous chapter 3.4, the decrease of q^* was severe with inserting PCM and the SSZ-13 is not very sensitive adsorbent at temperature changes. On the other hand, the value of q/q^* of PCM-inserted MSSZ-13 was higher than that of SSZ-13, during initial 10 minutes. This suggest that PCM-inserted SBA-15 was successfully recovered the heat of adsorption, and resulted in the increase of apparent rate of adsorption.

In summary, from the results above, PCM-inserted MSSZ-13 also successfully worked as both heat storage material and adsorbent at the same time in the experiment. This results suggests that PCM-inserted MSSZ-13 is proved as an effective concept for the PCM-inserted adsorbent as proposed in this dissertation. However, the improvement of adsorption performance by using PCM-inserted MSSZ-13 was not observed. As already discuss in the chapter 3.4, PCM-inserted MSSZ-13 is not a suitable concept for the improvement of adsorption performance. Further consideration and optimization of this concept is required to achieve performance improvement in adsorption process.

5.4 Conclusion

In this chapter, I experimentally evaluated two different prepared PCM-inserted adsorbent in chapter 3, i.e. PCM-inserted SBA-15 and PCM-inserted MSSZ-13, through dehumidifying fixed-bed adsorption process. The experimental results of PCM-inserted SBA-15 and PCM-inserted MSSZ-13 showed that suppressed fluid temperature, and increased value of q/q^*. This suggest that inserted PCM in both adsorbents are successfully worked as heat storage material, and owing to the temperature changes, the apparent rate of adsorption was increased. From this results, PCM-inserted SBA-15 and PCM-inserted MSSZ-13 are proved as an effective concept for the PCM-inserted adsorbent, as proposed in this chapter. However, in the experiment, each of PCM-inserted adsorbent did not showed improved adsorption performance, which is adsorbing larger amount at the same period of time. In the theoretical evaluation in chapter 3, PCM-inserted SBA-15 showed improved adsorption performance. Therefore, the degraded adsorption performance of PCM-inserted SBA-15 in the experiment, is considered as resulted from the differences between the conditions and assumptions used in experiment and that used in simulation. To achieve higher performance in the adsorption process, realization of the optimized PCM-inserted SBA-15 with adequate parameters, used in chapter 4 is considered to be required. Also, in case of PCM-inserted MSSZ-13, even though the concept itself is proved as an effective concept, it is already known that PCM-inserted MSSZ-13 is not a suitable concept for the improvement of adsorption performance, in chapter 3.4. However, through the further consideration and optimization of this concept, achievement of improved performance in adsorption process might be achieved.

Chapter 6. General conclusions

6.1 Conclusions

In this dissertation, as a new concept for the recovery of the heat of adsorption using phase change material (PCM), several types of PCM-inserted adsorbent are proposed, prepared, and evaluated. The PCM-inserted adsorbent is a concept that inserting PCM directly into the pores of adsorbent. Rapid latent-heat storage and its recovery through the PCM is the advantage of PCM-inserted adsorbent. To develop the PCM-inserted adsorbent, following steps are required, thereby, I have discussed throughout this dissertation.

(1) Understanding of phase change behavior of PCM in the mesoporous space

(2) Proposal and theoretical evaluation of specific concept for the PCM-inserted adsorbent

(3) Optimization of PCM-inserted adsorbent through parametric studies

(4) Experimental evaluation of the effectiveness of the proposed system

The ultimate goal of the PCM-inserted adsorbent is improvement of adsorption performance by recovery of the heat of adsorption. Therefore, the effectiveness of proposed and prepared PCM-inserted adsorbent was evaluated by the degree of improvement in adsorption performance. Details of the main results obtained in this thesis are summarized as follows:

First, the changes in the enthalpy of fusion and melting point of organic PCMs confined in the mesopores are investigated. Mesopore diameter, functional groups of PCM molecules, and functional groups of the wall of the host material were investigated as affecting parameters on the melting behavior of confined PCMs. When the pore diameter decreases, the values of the enthalpy of fusion and melting point of PCM were decreased. Also, when the interaction between PCM molecules and the surrounding wall of the host is strong, the enthalpy of fusion and melting point of PCM were decreased. For the development of PCM-inserted adsorbent, high enthalpy of fusion is required. By selecting the host materials with large mesopores (e.g. 10–20 nm) and PCM molecules with a functional group

having weak interaction with the host material such as paraffin, the high enthalpy of fusion of confined PCM, which is greater than 50% of the value of the bulk, can be achieved.

Second, three different specific concepts are proposed and evaluated for the PCM-inserted adsorbent realizing the separation of the space for existing adsorbate and the PCM inside the adsorbent. Through the conceptual studies, PCM-inserted mesoporous silica SBA-15 was considered as the most effective concept for the PCM-inserted adsorbent. The PCM-inserted SBA-15 successfully recovered the heat of adsorption and showed improved performance.

Third, to optimize the performance of the PCM-inserted SBA-15, parametric studies of the key parameters for the fabrication and the operating condition of PCM-inserted SBA-15 are performed. The enthalpy of fusion of the inserted PCM, the ratio of inserted amount of PCM, and the temperature of fluid at the inlet, were investigated as key parameters. Based on these individual parametric studies, PCM-inserted SBA-15 was modeled with the most adequate parameter values performed in this thesis. The modeled adsorbent achieved high performance in a fixed-bed dehumidifying adsorption process, which was 4 times improved performance, during the initial stage. This significant improvement can be achieved by the rapid heat recovery through PCM under adequate conditions, hence, PCM-inserted SBA-15 can be considered as an effective new method for the heat recovery in such adsorption processes.

Finally, the effectiveness of PCM-inserted SBA-15 is experimentally evaluated. The experimental results of PCM-inserted SBA-15 and PCM-inserted mesopore-created zeolite SSZ-13 revealed suppressed fluid temperature, and increased value of q/q^*. This suggests that inserted PCM in both adsorbents successfully work as the heat storage material. Owing to the temperature suppression, the apparent rate of adsorption was increased. From these results, PCM-inserted SBA-15 is proved as an effective conceptual material for the PCM-inserted adsorbent, as proposed in this dissertation. However, in the experiment, the PCM-inserted SBA-15 did not showed improved adsorption performance, which adsorbs a larger amount of water at the same period of time than SBA-15 without PCM.

6.2 Future perspectives

As described in the conclusions, the concept of 'PCM-inserted adsorbent' is concluded as an effective method for the recovery of heat of adsorption. The most impressive effectiveness of the 'PCM-inserted adsorbent' is a rapid removal of heat of adsorption by shortening the heat transfer distance compared to the other previous researches, described in the chapter 1.

In addition, through this thesis, the limitation of 'PCM-inserted adsorbent is also revealed, which is the adsorption performance is not significantly improved even though inserting PCM. This might be caused by two reasons. One is that the equilibrium amount of adsorbed water vapor decreases with inserting PCM. Another is that the latent heat storage capacity of inserted PCM is restricted by the physical properties of PCM, and this latent heat storage capacity of PCM is much smaller than compared to the released heat of adsorption. However, these limitations can be solved by applying PCM-inserted adsorbent in the short-time adsorption process. The most of short-time adsorption process, for instance PSA, is terminated before it reaches to the adsorption equilibrium state. Therefore, PCM-inserted adsorbent can be more effectively used when it applied on short-time process with highly exothermic adsorptive-adsorbent combination system.

As an example of short-time adsorption process, hydrogen storage tank applied in the fuel-cell vehicle was described in the introduction, chapter 1.1.3.2. Figure 96 shows the volume and the weight of hydrogen storage tank for the fuel-cell vehicle. Lighter and smaller hydrogen storage tank is easier to be applied in the vehicle. Therefore, a research target area for the hydrogen storage tank is near the origin, which showed as yellow square area in the Figure 96. By using adsorption in the hydrogen storage, the hydrogen tank is expected to be get closer to the target area, as shown in red line in Figure 96. However, when it comes to consider hydrogen charging at the hydrogen station, the hydrogen storage tank using adsorption cannot be lighter or smaller owing to the drastic increase of the amount of heat exchanger with the increase of exothermic heat by adsorption. As a result, the hydrogen storage tank cannot approach to the target area even after

using adsorption, as shown in the green line in the Figure 96. However, as shown in the pink line in Figure 96, hydrogen storage tank can approach to the target area with using PCM-inserted adsorbent. This calculation result is based on several assumptions. First, a decrease of amount of adsorbed hydrogen with inserting PCM was neglected. Also, the amount of inserted PCM was assumed as equal amount of PCM-inserted SBA-15 prepared in chapter 3.1. An increase of specific heat through inserting PCM was neglected. And the degree of increased temperature during the hydrogen charging assumed as 60 ℃. The weight of heat exchanger was calculated as a proportional value to the removed amount of heat. However, following those assumptions, the roughly estimated hydrogen storage tank showed the possibility of a realization of hydrogen storage tank with PCM-inserted adsorbent by get closer to the target.

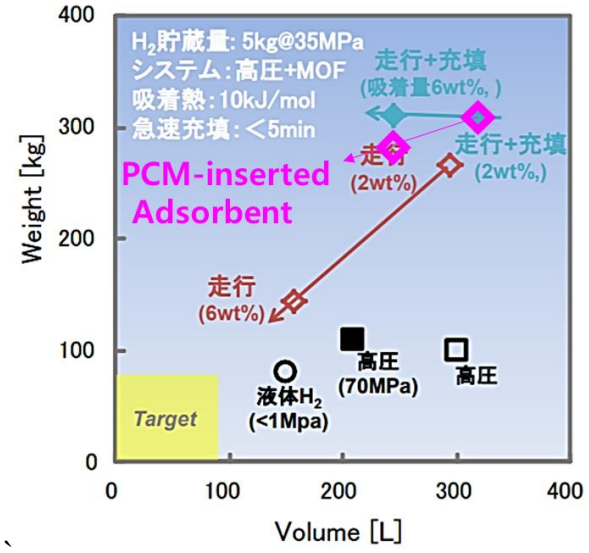

Figure 96. The weight and volume of the hydrogen storage tank[96].

Consequently, based on my results, I can further improve the adsorption performance by optimizing the PCM-inserted adsorbent. Details of my future prospects are discussed below:

First, the PCM-inserted adsorbent can be improved with realization of the adequate parameters, which is the higher enthalpy of fusion of the inserted PCM and the larger amount of inserted amount of PCM. This can be obtained by preparing the PCM-inserted SBA-15 with a larger mesopore diameter. According

to the works by Kruk[35], and Galarneau[36], a large mesopore diameter of SBA-15 can be realized by using a swelling agent[35], or changing the aging temperature[36]. Also, selecting a PCM molecule having higher enthalpy of fusion compared with that of paraffin can be an additional method. Moreover, it might be considerable to utilize not only the mesoporous space inside the pores, but also the one in the secondary structure, such as the intergranular spaces. To insert PCM into both mesopores and a certain part of secondary structure, the PCM-inserting method called 'liquid impregnation' can be used. It is already known that two different phase changes, i.e. solid-liquid phase change of PCM inserted inside mesopores, and the one inside the secondary structure, were observed by inserting PCM via liquid impregnation[22]. However, further consideration is required, because other parameters such as density, adsorption equilibrium, and diffusion rate will be subsequently changed with the changes in mesopore diameters or filling secondary structure.

Second, developing a new concept of the PCM-inserted adsorbent by using a temperature-sensitive adsorbent, can be considered to improve the adsorption performance of adsorbent. Instead of SSZ-13, there is silicoaluminophosphate (SAPO), which has the same structure as SSZ-13, but slightly a different component. SAPO-type zeolite possesses P atom in the structure, and shows sensitivity to the temperature change during adsorption. Since the structure of SAPO-type zeolite is the same to SSZ-13, the separation of PCM molecules (paraffin) and the adsorbate (water) can be realized. However, unlike SSZ-13, the adsorption performance of SAPO-type zeolite is significantly decreased with increase of temperature. Therefore, development of a new concept of PCM-inserted adsorbent by using a SAPO-type zeolite can improve the adsorption performance.

Third, the effectiveness of PCM-inserted adsorbent was increased with fastening the apparent adsorption rate found in this dissertation. Therefore, by applying the PCM-inserted adsorbent into not only the dehumidifying fixed-bed adsorption, but also highly exothermic and short adsorption processes, such as separation of natural gas, storage of hydrogen, and PSA, the adsorption performance will be significantly improved.

Reference

1 B. A. Fil, M. Korkmaz and G. Özmetin, *J. Chil. Chem. Soc.*, 2014, **59**, 2686–2691.

2 D. Zhou, Z. Xu, Y. Wang, J. Wang, D. Hou and S. Dong, *Environ. Sci. Pollut. Res.*, 2015, **22**, 3794–3802.

3 K. Chihara and M. Suzuki, *J. Chem. Eng. Japan*, 1983, **16**, 53–61.

4 J. F. Horstmeier, A. Gomez Lopez and D. W. Agar, *Int. J. Greenh. Gas Control*, 2016, **47**, 364–375.

5 M. J. Sinicropi, T. M. Aaron, F. W. Leavitt, H. R. Schaub and J. Smolarek, U.S. Patent, No.5453112, 1995.

6 H. Demir, M. Mobedi and S. Ülkü, *Renew. Sustain. Energy Rev.*, 2008, **12**, 2381–2403.

7 M. Hamdy, A. A. Askalany, K. Harby and N. Kora, *Renew. Sustain. Energy Rev.*, 2015, **51**, 1223–1234.

8 L. Calabrese, L. Bonaccorsi, P. Bruzzaniti, A. Frazzica, A. Freni and E. Proverbio, *Mater. Renew. Sustain. Energy*, 2018, **7**, 1–13.

9 K. C. Furman and N. V. Sahinidis, *Ind. Eng. Chem. Res.*, 2002, **41**, 2335–2370.

10 A. Rezk, S. Mahmoud and A. Elsayed, *Appl. Therm. Eng.*, 2013, **53**, 278–284.

11 T. Eun, H. Song, J. Hun Han, K. Lee and J. Kim, *Int. J. Refrig.*, 2000, **23**, 64–73.

12 D. Zhou, C. Y. Zhao and Y. Tian, *Appl. Energy*, 2012, **92**, 593–605.

13 M. M. Farid, A. M. Khudhair, S. A. K. Razack and S. Al-Hallaj, *Energy Convers. Manag.*, 2004, **45**, 1597–1615.

14 X. Li and Y. Li, *adsorption*, 2015, **21**, 383–389.

15 M. A. Rady, A. S. Huzayyin, E. Arquis, P. Monneyron, C. Lebot and E. Palomo, *Renew. Energy*, 2009, **34**, 718–726.

16 T. Kadoono and M. Ogura, *Phys. Chem. Chem. Phys.*, 2014, **16**, 5495–8.

17 E. Oró, A. De Gracia, A. Castell, M. M. Farid and L. F. Cabeza, *Appl. Energy*, 2012, **99**, 513–533.

18 P. Schossig, H.-M. Henning, S. Gschwander and T. Haussmann, *Sol. Energy Mater. Sol. Cells*, 2005, **89**, 297–306.

19 H. K. Christenson, *J. Phys. Condens. Matter*, 2001, **13**, R95–R133.

20 C. L. Jackson and G. B. McKenna, *J. Chem. Phys.*, 1990, **93**, 9002.

21 S. Kittaka, S. Takahara, H. Matsumoto and Y. Wada, *J. Chem. Phys.*, 2013, **138**, 204714.

22 R. A. Mitran, D. Berger, C. Munteanu and C. Matei, *J. Phys. Chem. C*, 2015, **119**, 15177–15184.

23 M. Moshoeshoe, M. S. Nadiye-Tabbiruka and V. Obuseng, *Am. J. Mater. Sci.*, 2017, **7**,

191–221.

24 N. J. Robert J., Argauer, Kensington, Md., George R., Landolt, Audubon, U.S. Patent. 3702886 A, 1972.

25 N. E. R. Zimmermann and M. Haranczyk, *Cryst. Growth Des.*, 2016, **16**, 3043–3048.

26 B. M. Weckhuysen and J. Yu, *Chem. Soc. Rev.*, 2015, **44**, 7022–7024.

27 V. Valtchev and S. Mintova, *MRS Bull.*, 2016, **41**, 689–693.

28 X. Chen, A. Vicente, Z. Qin, V. Ruaux, J. P. Gilson and V. Valtchev, *Chem. Commun.*, 2016, **52**, 3512–3515.

29 M. Ogura, S. Y. Shinomiya, J. Tateno, Y. Nara, E. Kikuchi and M. Matsukata, *Chem. Lett.*, 2000, **29**, 882–883.

30 E. Koohsaryan and M. Anbia, *Chinese J. Catal.*, 2016, **37**, 447–467.

31 T. Yanagisawa, T. Shimizu, K. Kuroda and C. Kato, *Bull. Chem. Soc. Jpn.*, 1990, **63**, 988–992.

32 D. DZhao, J. Feng, Q. Huo, N. Melosh, G. Fredrickson, B. Chmelka and G. Stucky, *Science*, 1998, **279**, 548–552.

33 J. S. Beck, J. C. Vartuli, W. J. Roth, M. E. Leonowicz, C. T. Kresge, K. D. Schmitt, C. T.-W. Chu, D. H. Olson, E. W. Sheppard, S. B. McCullen, J. B. Higgins and J. L. Schlenker, *J. Am. Chem. Soc*, 1992, **114**, 10834–10843.

34 X. Bao, X. S. Zhao, X. Li and J. Li, *Appl. Surf. Sci.*, 2004, **237**, 380–386.

35 M. Kruk, *Acc. Chem. Res.*, 2012, **45**, 1678–1687.

36 A. Galarneau, H. Cambon, F. Di Renzo and F. Fajula, *Langmuir*, 2001, **17**, 8328–8335.

37 H. J. Shin, R. Ryoo, M. Kruk and M. Jaroniec, *Chem. Commun.*, 2001, **1**, 349–350.

38 T. Ma, L. Liu and Z. Yuan, *Chem. Soc. Rev.*, 2013, **42**, 3977–4003.

39 C. H. Tessmer, R. D. Vidic and L. I. Uranowski, *Environ. Sci. Technol.*, 1997, **31**, 1872–1878.

40 H. P. Boehm, E. Diehl, W. Heck and R. Sappok, *Angew. Chemie Int. Ed. English*, 1964, **3**, 669–677.

41 T. Ramanathan, F. T. Fisher, R. S. Ruoff and L. C. Brinson, *Chem. Mater.*, 2005, **17**, 1290–1295.

42 D. B. Mawhinney, V. Naumenko, A. Kuznetsova, J. T. Yates, J. Liu and R. E. Smalley, *J. Am. Chem. Soc.*, 2000, **122**, 2383–2384.

43 J. Wang, *Electroanalysis*, 2005, **17**, 7–14.

44 P. Chen, X. Wu, J. Lin and K. L. Tan, *Science*, 1999, **285**, 91–3.

45 J. Kong, M. G. Chapline and H. Dai, *Adv. Mater.*, 2001, **13**, 1384–1386.

46 C. Liu, Y. Y. Fan, M. Liu, H. T. Cong, H. M. Cheng and M. S. Dresselhaus, *Science*, 1999, **286**, 1127–1129.

47 A. M. Cassell, J. A. Raymakers, J. Kong and D. Hongjie, *J. Phys. Chem. B*, 1999, **103**, 6484–6492.

48 M. Kumar and Y. Ando, *J. Nanosci. Nanotechnol.*, 2010, **10**, 3739–3758.

49 I. Dincer, S. Dost and X. Li, 1997, **21**, 1157–1171.

50 M. Aihara, T. Nagai, J. Matsushita, Y. Negishi and H. Ohya, 2001, **69**, 225–238.

51 L. Feng, W. Zhao, J. Zheng, S. Frisco, P. Song and X. Li, *Sol. Energy Mater. Sol. Cells*, 2011, **95**, 3550–3556.

52 X. Li and Y. Li, *Adsorption*, 2015, **21**, 383–389.

53 S. Mondal, *Appl. Therm. Eng.*, 2008, **28**, 1536–1550.

54 A. Sari, *Energy Convers. Manag.*, 2004, **45**, 2033–2042.

55 A. Sari, C. Alkan and C. Bilgin, *Appl. Energy*, 2014, **136**, 217–227.

56 J. Wang, M. Yang, Y. Lu, Z. Jin, L. Tan, H. Gao, S. Fan, W. Dong and G. Wang, *Nano Energy*, 2016, **19**, 78–87.

57 K. Morishige and H. Iwasaki, 2003, 2808–2811.

58 M. Miyahara and K. E. Gubbins, *J. Chem. Phys.*, 1997, **106**, 2865.

59 X. Min, M. Fang, Z. Huang, Y. Liu, Y. Huang, R. Wen, T. Qian and X. Wu, *Sci. Rep.*, 2015, **5**, 12964.

60 T. Nomura, C. Zhu, N. Sheng, K. Tabuchi and A. Sagara, *Sol. Energy Mater. Sol. Cells*, 2015, **143**, 424–429.

61 S. Valange, R. Palacio, A. Charmot, J. Barrault, A. Louati and Z. Gabelica, *J. Mol. Catal. A Chem.*, 2009, **305**, 24–33.

62 W. Libbrecht, F. Deruyck, H. Poelman, A. Verberckmoes, J. Thybaut, J. De Clercq, P. Van and D. Voort, *Chem. Eng. Journa*, 2015, **259**, 126–134.

63 B. Scheibe, E. Borowiak-palen and R. J. Kalenczuk, *Mater. Charact.*, 2009, **61**, 185–191.

64 M. Barczak, *New J. Chem.*, 2018, **42**, 4182–4191.

65 A. Schreiber, I. Ketelsen and G. H. Findenegg, *Phys. Chem. Chem. Phys.*, 2001, **3**, 1185–1195.

66 J. L. Zeng, Z. Cao, D. W. Yang, F. Xu, L. X. Sun, L. Zhang and X. F. Zhang, *J. Therm. Anal. Calorim.*, 2009, **95**, 501–505.

67 K. Morishige, K. Kawano and T. Hayashigi, *J. Phys. Chem. B*, 2000, **104**, 10298–10303.

68 H. Tanaka, T. Hiratsuka, N. Nishiyama, K. Mori and M. T. Miyahara, *Adsorption*,

2013, **19**, 631–641.

69 N. V Churaev, S. A. Bardasov and V. D. Sobolev, *Colloids Surfaces A Physicochem. Eng. Asp.*, 1993, **79**, 11–24.

70 S. Farooq, M. M. Hassan and D. M. Ruthven, *Chem. Eng. Sci.*, 1988, **43**, 1017–1031.

71 N. Ben Amar, L. M. Sun and F. Meunier, *Appl. Therm. Eng.*, 1996, **16**, 405–418.

72 R. Z. Wang, *Int. J. Refrig.*, 2001, **24**, 602–611.

73 M. Toledo, C. Rojas, E. Montes, J. Veloso and A. Sáez, *Appl. Therm. Eng.*, 2013, **51**, 512–519.

74 J. F. Horstmeier, A. Gomez Lopez and D. W. Agar, *Int. J. Greenh. Gas Control*, 2016, **47**, 364–375.

75 S. Karthikeyan and R. Velraj, *Int. J. Therm. Sci.*, 2012, **60**, 153–160.

76 K. Hwang, J. Jun and W. Lee, *Chem. Eng. Sci.*, 1995, **50**, 813–825.

77 S. Karthikeyan, G. Ravikumar Solomon, V. Kumaresan and R. Velraj, *Energy Convers. Manag.*, 2014, **78**, 74–80.

78 M. Simo, S. Sivashanmugam, C. J. Brown and V. Hlavacek, *Ind. Eng. Chem. Res.*, 2009, **48**, 9247–9260.

79 L. Usón, M. G. Colmenares, J. L. Hueso, V. Sebastián, F. Balas, M. Arruebo and J. Santamaría, *Catal. Today*, 2014, **227**, 179–186.

80 N. R. Pradhan, H. Duan, J. Liang and G. S. Iannacchione, *Nanotechnology*, 2009, **20**, 245705.

81 L. Meng, X. Zhu and E. J. M. Hensen, *ACS Catal.*, 2017, **7**, 2709–2719.

82 L. Qiu, V. Murashov and M. A. White, *Solid State Sci.*, 2000, **2**, 841–846.

83 Y. Luo, H. H. Funke, J. L. Falconer and R. D. Noble, *Ind. Eng. Chem. Res.*, 2016, **55**, 9749–9757.

84 S. M. Hasnain, *Energy Convers. Manag.*, 1998, **39**, 1127–1138.

85 J. Choi, K. Yoshie, T. Moteki and M. Ogura, *Ind. Eng. Chem. Res.*, 2019, **58**, 10114–10118.

86 M. Kruk, *Acc. Chem. Res.*, 2012, **45**, 1678−1687.

87 A. Galarneau, H. Cambon, F. Di Renzo, R. Ryoo, M. Choi and F. Fajula, *New J. Chem.*, 2002, **27**, 73–79.

88 CNT Technology Overview, http://www.nanoscience.com/applications/education/overview/cnt-technology-overview

89 Carbon nanotube composites, http://coecs.ou.edu/Brian.P.Grady/nanotube.html

90 DSC, https://www.netzsch-thermal-analysis.com/us/products-solutions/differential-scanning-calorimetry/dsc-214-polyma

91 Fixed-bed reactor, http://www.cchem.berkeley.edu/molsim/teaching/spring2013/CCS/Group8/packed.html

92 PSA, https://en.wikipedia.org/wiki/Pressure_swing_adsorption

93 窪川清一,「技術ハイライト、新吸着材ＡＱＳＯＡ®を適用した製品開発」, Adsorption News, Vol.25, No.4

94 Food container, http://www.sofrigam.com.

95 Hand warmer, https://en.wikipedia.org/wiki/File:Handwaermer12.jpg

96 本田技術研究所(Honda),「自動車技術から見た水素貯蔵材料 に関して期待するもの」

97 Silica density and heat capacity https://www.azom.com/properties.aspx?ArticleID=1114

98 Carbon nantobue density, https://en.wikipedia.org/wiki/Carbon_nanotube

99 PCM capsule, https://www.alibaba.com/product-detail/Micro-phase-change-material-thermal-regulating_1522572666.html

Appendix

Notation

a	Atomic radius [m]
a_1	Specific surface area of pellet [m^2/m^3] (=$6/d_p$)
a_2	Specific surface area of PCM capsule [m^2/m^3] (=$6/d_{cap}$)
C	Concentration [mol/m^3]
$c_{p,cap}$	Heat capacity of PCM capsule [J/Kg · K]
$c_{p,F}$	Heat capacity of fluid [J/Kg · K]
$c_{p,p}$	Heat capacity of pellet [J/Kg · K]
D	Molecular diffusion coefficient [m^2/s]
d_c	Diameter of column [m]
d_{cap}	Diameter of column [m]
D_{eff}	Effective diffusion coefficient [m^2/s]
D_k	Knudsen diffusion coefficient [m^2/s]
d_p	Pellet diameter [m]
D_s	Diffusion coefficient in particle of SBA-15 [m^2/s]
H	Enthalpy of fusion [J/Kg-PCM]
h_1	Heat transfer coefficient between fluid and pellet [W/$m^2 \cdot K$]
H_2	Heat transfer coefficient between fluid and PCM capsule [W/$m^2 \cdot K$]
k	Thermal diffusion coefficient[W/m · K]]
k_b	Boltzmann constant
k_F	Mass transfer coefficient in boundary film [m/s]
K_{LDF}	LDF mass transfer coefficient [s^{-1}]
L	Column length [m]
M	Molecule molar weight[Kg/mol]
p	Pressure [Pa]
p_0	Saturated pressure [pa]
q	Amount adsorbed in bed [mol/m^3]
q^*	Amount adsorbed in bed at equilibrium state [mol/m^3]
Q_{st}	Isosteric heat of adsorption [J/mol]
R	Gas constant [J/mol · K]
R_p	Radius of pellet [m]
r_{pore}	Radius of pore [m]
R_s	Radius of particle [m]
t	Time
T_{cap}	Temperature of PCM capsule [K]
T_{end}	Phase change end temperature [K]
T_F	Temperature of fluid [K]
T_p	Temperature of pellet [K]
T_{start}	Phase change start temperature [K]
u	Superficial flow velocity[m/s]
w_1	Ratio of PCM in PCM-inserted adsorbent [$g_{-PCM}/g_{-SBA-15}$]
w_2	Ratio of PCM in PCM capsule [$g_{-PCM}/g_{-capsule}$]
x	Axial distance coordinate [m]

Greek Symbols

ρ_B	Density of adsorbent in bed [kg $/m^3$]
ρ_F	Density of fluid [kg $/m^3$]
ρ_{cap}	Density of PCM capsule [kg $/m^3$]
ρ_p	Density of pellet [kg $/m^3$]
ρ_{pcm}	Density of PCM in pellet or in capsule [kg $/m^3$]
ε_{cap}	Fraction of PCM capsule in bed
ε_{macro}	Macropore porosity in pellet
ε_{meso}	Mesopore porosity in SBA-15 particle
ε_p	Fraction of pellet in bed
ε_s	Porosity in SBA-15 pellet
ε	Void fraction in bed
μ	Viscosity [Pa · S]
μ_F	Viscosity of fluid [Pa · S]
τ	Tortuosity
χ	Ratio of the adsorbed heat to the enthalpy of fusion of PCM

Subscripts

0	initial condition
ads	absorbent, SBA-15
B	Bed
F	Fluid
in	parameters at inlet
out	parameters at outlet
p	pellet
pcm	PCM
s	solid, particle

Acknowledgement

First and foremost, I would like to express deep respect and gratitude to my supervisor, Professor Masaru Ogura. He always supported me throughout the thesis and the life in doctoral course. I learned many knowledges, experienced variety environments, and realized a philosophy as a researcher, through his guidance and mentorship. This dissertation would not have been possible without his heartfelt and enthusiastic instruction. Once again, I sincerely appreciate to my supervisor professor.

I would like to express respect and appreciation to Professor Akiyoshi Sakoda and Associate professor Hirotaka Fujita, for their hearty mentorship and everything to promote my research at the beginning of this study. This dissertation also would not have been possible without their mentoring.

I would like to express my gratitude to Professor Kenichi Yoshie, for all of his supports and instructions in the research of adsorption process. He provided me with valuable comments and teach me useful techniques for proceeding this work.

I am deeply appreciate to Associate Professor Takahiko Moteki, for all the support in my experiment, valuable comments, and fruitful discussions in thesis.

I sincerely appreciate to Professor Akihiko Matsumoto and Associate Professor Hiromitsu Ito, for their insightful comments and supports in all the studies and experimental techniques.

I sincerely grateful to Professor Valentin Valtchev, for his support and instructions in the research of a preparation of mesoporous zeolite SSZ-13.

I would like to thank Professor Yasuyuki Sakai, Associate Professor Tichi Ito, Associate Professor Hirokazu Sugiyama, Associate Professor Toru Wakihara, and Professor Akihiko Matsumoto for their insightful comments and advices as members of the thesis defense committee.

I would like to express my gratitude for kind support from all the members in Ogura laboratory. It was a great pleasure for me to join in this laboratory and having an opportunity to work with the members. I always learn from their intelligence, encouragement, and skill. In particular, I sincerely thanks to Mrs.

Junko Torii, for the continuous assistance and support in the official work. Also, I would like to thank all of colleagues: Dr. Sibel Sogukkanli, Mr. Takeshi Ohnishi, Mr. Kiyoyuki Yamazaki, Mr. Yusuke Ohata, Ms. Aisa Kawano, Mr. Tomohiro Imaseki, Mr. Naoto Tominaga, Mr. Tomohiro Sei.

I would like to acknowledge financial support from MERIT (Material Education program for the future leaders in Research, Industry, and Techonology) and UTEC.

Finally, I express special gratitude to my family, Gi-hwan Choi, Jong-ye Oh, Jae-wang Choi and In-gi Kim. Their encouraging and supporting on me made this dissertation possible.

List of publication

1. Jihye Choi, Hirotaka Fujita, Masaru Ogura, Akiyoshi Sakoda, 'Confinement effect on enthalpy of fusion and melting point of organic phase change materials in cylindrical nanospace of mesoporous silica and carbon'. *Adsorption*, **2018**, 24, 345–55

2. Jihye Choi, Kenichi Yoshie, Takahiko Moteki, Masaru Ogura. 'Theoretical Evaluation of an Organic Phase Change Material (PCM)-Inserted Dual-Functional Adsorbent for the Recovery of Heat of Adsorption', *Ind. Eng. Chem. Res.*, **2019**, 58, 10114–8

3. Jihye Choi, Kenichi Yoshie, Takahiko Moteki, Masaru Ogura, 'Parametric studies on fixed-bed dehumidifying adsorption process using PCM-inserted adsorbent for effective recovery of the heat of adsorption', *J. Chem. Eng, Jpn.*, submitted